TECHNISCHE UNIVERSITÄT MÜNCHEN

Department Chemie
Lehrstuhl für Biotechnologie

Mechanism of the Molecular Chaperone Hsp90

Martin Josef Heßling

Vollständiger Abdruck der von der Fakultät für Chemie der Technischen Universität München zur Erlangung des akademischen Grades eines Doktors der Naturwissenschaften genehmigten Dissertation.

Vorsitzender:	Univ.-Prof. Dr. Christian F.W. Becker
Prüfer der Dissertation:	1. Univ.-Prof. Dr. Johannes Buchner
	2. Univ.-Prof. Dr. Thomas Kiefhaber
	3. Univ.-Prof. Dr. Thorsten Hugel

Die Dissertation wurde am 28.01.09 bei der Technischen Universität München

eingereicht

und durch die Fakultät für Chemie am 30.03.09 angenommen.

1 Introduction

1.1 Protein folding

Proteins are the most versatile biological macromolecules. In proteins, twenty amino acids are connected via peptide bonds in genetically coded order. The sequence of each protein is the information passed from genetic ancestor molecules like DNA and RNA which is sufficient for its structure and function and to manage its fate in the cell (Anfinsen, 1973; Anfinsen et al, 1961). After synthesis at the ribosome the nascent polypeptide chain is released from the last t-RNA molecule which carried the last amino acid attached to the polypeptide chain (McQuillen et al, 1959). The proteins then adopt their specific three dimensional structures. This process is called folding presumably due to the analogy to a sheet of paper, as in both cases parts of sheet or protein chain which are far apart might get in direct contact to each other (Fersht and Daggett, 2002; Dobson and Karplus, 1999). The process can occur spontaneously as no information other than the sequence of amino acids is needed. Because of the chemical properties of the peptide bond, some strain reduces chain motility of an unfolded protein that is due to the resonance-stabilised amid bond (imid for proline). The description of the main chain conformation of a protein breaks down to a series of two torsion angels for each amino acid that describe the orientation of a plane in which the amino group of the respective and the carboxy-function of the proceeding amino acid lies and a plane with the Carboxy group of the respective and the amino group of the succeeding amino acid is aligned. These angels are termed Φ and Ψ. Steric hindrance due to the bulkiness of the side chain explains certain propensities for each amino acid (Ramachandran and Sasisekharan, 1968). For secondary structural elements like the alpha helix or the beta-sheet defined values for Φ and Ψ are assignable. Therefore certain propensities to find a specific amino acid in defined structural elements like alpha-helix or beta-sheet can be explained by the requirement of certain torsion angels that define the backbone conformation. Steric strain and a sum of a large number of weak interactions define the native state of proteins (Vendruscolo and Dobson, 2005). These are van der

Waals forces, induced dipole interactions, dipole-dipole interactions, salt bridges and hydrogen bonds. In addition the hydrophobic effect favours folding by extrusion of water from the unfolded protein chain. Native structure is fine tuned by the optimisation of all possible interactions that are directly related to the conformation of the protein. Hydrogen bonds are sterically the most demanding in this respect. Now having an idea of what defines the native state of a protein, the question remains how does it get there and how is that accomplished in a reasonable time? Random scanning of all possible conformational states of can be neglected due to the fact that it takes too long to find the correct fold just by sampling all possible conformations (Dill and Chan, 1997; Levinthal, 1968). Therefore it has been proposed and also shown experimentally that proteins fold via pathways to their native states. This means that gain of a defined conformation is coupled to a reduction of free enthalpy providing directionality to the process. Metaphorically speaking, the process can be compared to a ball that is rolling on a more or less steep surface form a higher level in to a sink which represents the native state. This model is represented by the folding funnel that simplifies this view (**Figure 1**). The process starts form a randomly structured ensemble of unfolded protein molecules. Structure formation is coupled to reduction of free enthalpy and directs the ensemble to more defined intermediate conformations. These intermediates can guide proteins to their native conformation and thus accelerate the folding of proteins (Wagner and Kiefhaber, 1999). The intermediate structures are only partially folded and therefore expose a certain hydrophobic surface to the solvent. These surfaces tend to associate because of the hydrophobic effect

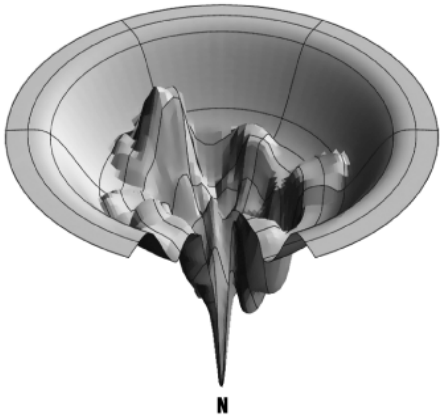

Figure 1: Folding funnel model. Energy landscape of protein conformations shows minima besides the native state (N) implying that protein folding intermediates exists (Dill and Chan, 1997).

(Kiefhaber et al, 1991). Therefore intermediate structures reduce the efficiency of protein folding by unspecific association processes termed aggregation.

1.1.1 Protein folding in the cell

In the cell individual proteins are not alone. The protein concentration in the cytoplasm reaches values of 200 mg/mL (Parsell and Lindquist, 1994). In addition, other macromolecules and cell organelles contribute to the crowding. Protein-protein interactions take place all the time. Protein folding in such a dense solution of sticky surfaces needs guidance to prevent protein aggregation and protein misfolding which is toxic to the cell (Bukau et al, 2000; Buchner, 1996). Neurodegenerative diseases and autoimmune responses, among others, are triggered by protein misfolding and aggregation (Bossy-Wetzel et al, 2004; Buxbaum, 2004; Lucking and Brice, 2000; Prusiner, 1996).

Thus, in the cell protein synthesis and folding is a controlled pathway starting at the exit tunnel of the ribosome, where nascent chains get in contact with proteins called chaperones that guard them in the non-native state (Hartl and Hayer-Hartl, 2002; Lindquist and Craig, 1988). In the bacterial cytosol, trigger factor fullfils this task (Ferbitz et al, 2004). In eukaryotes trigger factor is replaced by a protein complex with similar functions called ribosome-associated complex (RAC) (Gautschi et al, 2001). The binding of trigger factor near the exit tunnel of the ribosome, exposes a surface to which the newly synthesised polypeptide chains bind through hydrophobic interactions (Patzelt et al, 2001). As the chain grows, trigger factor guides the growing polypeptide away from the ribosome, preventing aggregation through interaction with hydrophobic surfaces of the polypetide (Kaiser et al, 2006; Scholz et al, 1997). After these initial binding events the newly synthesised protein matures and forms already compact intermediates. It is then transferred to downstream chaperones for further maturation. Which chaperone pathways are used for individual protein folds is a matter of debate and much detail remains uncharted (Kerner et al, 2005; Blagosklonny, 2002; Nathan et al, 1997). Often targeting to organelles is coupled to protein folding or even to the synthesis of the protein

(Blobel, 2000; Hartl et al, 1989). Here chaperones take over and guide the polypeptides which have an address coded in a signal sequence to the specific organelle. Transport processes into chloroplast and mitochondria require unfolded polypeptides that are in complexes with chaperones (Young et al, 2003; Funfschilling and Rospert, 1999; Komiya et al, 1997). Proteins targeted to the endoplasmatic reticulum (ER) are synthesized into the lumen by a mechanism which requires an N-terminal export signal that recruits an export factor (signal recognition particle (SRP)) which stalls translation and directs the synthesizing ribosome to the ER membrane (Lakkaraju et al, 2008; Walter and Blobel, 1982). There it doks to a translocation channel through which the polypeptide chain is synthesized.

1.2 Catalysed protein folding

Protein folding catalysts do not confer to directionality to the conformational changes they influence. They catalyse conformational transitions of high energy barrier, like the isomerisation of peptidyl-proly bonds or the formation and shuffling of disulfide bonds. Proline is the only proteinogenic imino acid in nature and has a propensity to form cis-peptidly prolyl bonds in the unfolded protein chain. In addition, cis-proline bonds are also found in the native state of proteins like the immunoglobulins (Feige et al, 2004; Thies et al, 1999; Matsushima et al, 1978). The cis-proline moiety is found in subtypes of beta-turn. Its special structural features are used in the cell for various regulation processes (Nelson et al, 2006; Ranganathan et al, 1997; Sawada et al, 1987). This slow cis-trans isomerisation is catalyse by a specific group of protein folding catalysts, the PPIases (Fischer et al, 1989). Three structural distinct classes of PPIases are known. These are the cyclophilins, the FKBPs and the parvuline-type PPIases (Fischer and Aumuller, 2003). The mechanism of catalysis is still debated for the different classes and substrate specificity is difficult to predict. However, for efficient catalysis the partial double bond character of the resonance-stabilized imide bond needs to be abrogated in the transition sate (Golbik et al, 2005). Through accelerating this slow process, which has an activation energy of 20 kcal mol^{-1}, protein folding is accelerated and more efficient due to the lower accumulation of

intermediate states which could lead to aggregation during folding (Kiefhaber et al, 1991).

Proteins destined for export and some mitochondrial proteins do contain disulfide bonds in their native state (Reddehase et al, 2009; Gruber et al, 2006; Mesecke et al, 2005; Grauschopf et al, 2003). The disulfide bridge has a stabilizing effect due to a reduction of conformational freedom in the unfolded state (Feige and Buchner., 2009). The oxidation and the shuffling of non-native disulfide bonds is accelerated by the enzyme protein disulfide isomerases (PDI) in the ER (Freedman et al, 1989; Anfinsen et al, 1961). In prokaryotic organisms, oxidation of disulfide bonds occurs in a first step by an unspecific, strongly oxidizing protein (Jonda et al, 1999). Then disulfide shuffling is catalysed by a reduced protein DsbC (Gleiter and Bardwell, 2008). In eukaryotes this sharp distinction between functions is not found. Here multiple copies of PDI proteins, which make up more then 1% of the total protein exist, that are involved in oxidizing and shuffling of disulfide bonds (Appenzeller-Herzog and Ellgaard, 2008). The thioredoxin (THR) motif including the active site CXYC is preserved in all these proteins (Gruber et al, 2006). The mechanism of PDI involves the formation of mixed disulfides with substrate (Darby et al, 1994). Beside its strict catalytic activities of PDI it has a chaperone activity (Winter et al, 2002; Klappa et al, 1997).

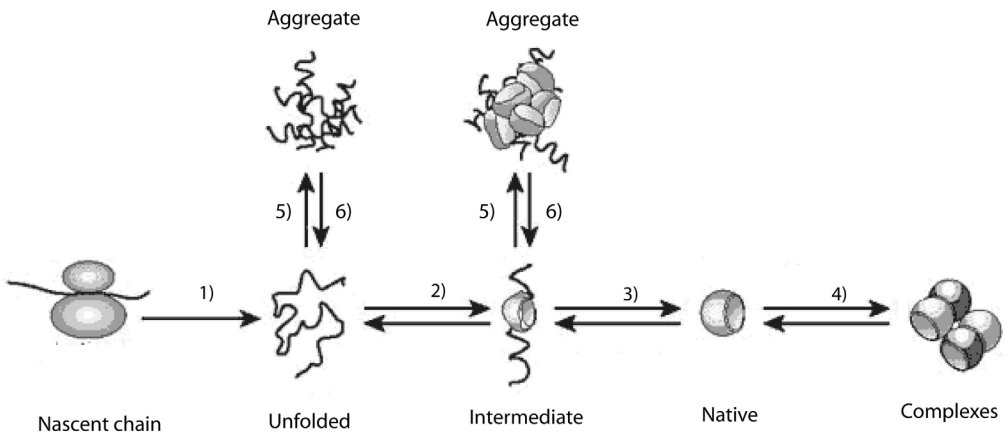

Figure 2: Protein conformations. Dependent on the maturity of the polypeptide, different sets of chaperones interact. Through reversible interactions, distraction from the pathway is prevented. 1) Nascent chains at the ribosomal exit tunnel interact with trigger factor or Hsp70 proteins. In eukaryotic cells a complex called RAC including Hsp70 activity associates with the ribosome and the emerging nascent chains. 2) The released polypeptide still interacts with trigger factor and Hsp70 proteins. 2-3) Matured intermediates with higher structural integrity interact with Hsp60 and Hsp90 molecular chaperones. 4) Hsp90 was described to constantly scan native proteins and is involved in complex assembly reactions in the cell. 5) sHsps bind aggregating proteins tightly and require additional factors to trigger the release. 6) Hsp100 proteins act on aggregates in concert with Hsp70 to pull out unfolded polypeptides and redirect them for productive folding. An equal mechanism is thought to take place for sHsp-bound proteins. Figure modified from Dobson, 2003.

1.3 Chaperone-assisted folding

In the crowded cytosol, the conformation of proteins is constantly guarded by chaperones. The pool of chaperone-bound partially folded proteins are feed not only by protein synthesis as mentioned previously, but proteins unfold spontaneously and are bound by chaperones (Albanese et al, 2006; Bukau et al, 2006). In addition, complex assembly processes in the eukaryotic cell require guidance of chaperones (McClellan et al, 2007). Import into the mitochondria and chloroplast depend on chaperones (Baker et al, 2007; Young et al, 2003; Truscott et al, 2003). The functional principle of chaperones is founded in the reversible binding to unfolded or partially folded polypeptide chains which would otherwise aggregate quickly and therefore be removed and distracted from a productive folding pathway. In contrast

to protein folding catalysts chaperone-assisted folding is not accelerated. The intermediate binding blocks aggregation due to a reduction of the concentration of free aggregation-prone conformations. Some chaperones interact with nascent or nascent-like chains which are fully expanded polypeptides (**Figure 2**). This task, as mentioned previously, is taken by trigger factor or, if trigger factor function is absent, it can be substituted by Hsp70 proteins (Deuerling et al, 2003). Nascent chain binding seems to be essential for bacterial protein expression (Genevaux et al, 2004). As the protein matures, more compact intermediates form which are not bound by trigger factor or Hsp70 proteins. At this maturity stage, other chaperones capable to interact with more native-like protein folding intermediates. Hsp60 proteins are large complexes out of fourteen subunits in bacteria that form a folding chamber in which folding intermediates become trapped (Spiess et al, 2004; Lorimer, 1996; Braig et al, 1994a). Inside the chamber hydrophobic surfaces are in a dynamic exchange with hydrophilic surfaces that are exposed toward substrates. This process enables binding and release of the substrates inside the chamber. The interchange of hydrophilic and hydrophobic surfaces through conformational changes is driven by ATP hydrolysis of Hsp60 and the binding of the co-chaperone Hsp10 (**Figure 2**). Inside this chamber, folding can take place without interference the hydrophobic surfaces of other proteins that would be required for aggregation (Fenton and Horwich, 2003). The substrate is able to fold efficiently. The homolog CCT in eukaryotes lakes the Hsp10 co-chaperone but requires assistance of another co-chaperone, prefoldin (Siegert et al, 2000; Vainberg et al, 1998). Hsp90 is another player which interacts with specific proteins and assists them in their folding (see below). Also, aggregates can be redirected to a productive folding pathway. This requires their dissociation which is performed by Hsp100 motors (Lee et al, 2003). These hexameric rings pull out single polypeptide chains form aggregates and thread them through a central pore (Lum et al, 2008; Lum et al, 2004; Parsell et al, 1994). A nascent-like state is achieved after release form the chaperone machine which resets the initially failed folding reaction. In this pathway, Hsp70 helps pulling out polypeptides from the aggregate and assists in the refolding after release from Hsp100 (Glover and Lindquist, 1998; Sanchez et al, 1993). Small heat shock proteins very efficiently

prevent aggregation (Haslbeck et al, 2005a; Jakob et al, 1993). Unfolded proteins become sequestered into these oligomeric proteins in stable substrate complexes. Substrates are released and refolded by Hsp70 and Hsp100 molecular chaperones (Cashikar et al, 2005; Haslbeck et al, 2005b; Lee and Vierling, 2000). The pathway, in this respect, is related to the fate of protein aggregates. sHsps seem to fulfill a buffering role and prevent exposure of toxic protein folding intermediates to the cytosolic environment.

1.4 Hsp90

1.4.1 Regulation of Hsp90 expression

Hsp90 expression is strongly induced under heat shock conditions (Finkelstein et al, 1982). In eukaryotes this regulation is based on a feedback regulation loop including the heat shock factor (Hsf) (Rabindran et al, 1991). Interaction of heat shock factor with the promoters of heat shock genes activates their transcription (Mathew and Morimoto, 1998). In vertebrates four different heat shock factors have been identified (Nakai et al, 1997; Sarge et al, 1994). However, the main heat shock factor 1 is responsible for the regulation of heat shock genes to physiological and environmental stresses (Zou et al, 1998b; Sarge et al, 1993). Hsf is bound by Hsp90 and presumably other factors as a monomer in the unstressed cell. Aggregation-prone protein folding intermediates are capable to compete with Hsf for Hsp90 binding (Zou et al, 1998a). Then, when released form Hsp90, Hsf becomes phoshorylated by Map-Kinases and is imported into the nucleus were it binds as a trimer to Hsf responsive elements and activates the expression of various heat shock proteins like

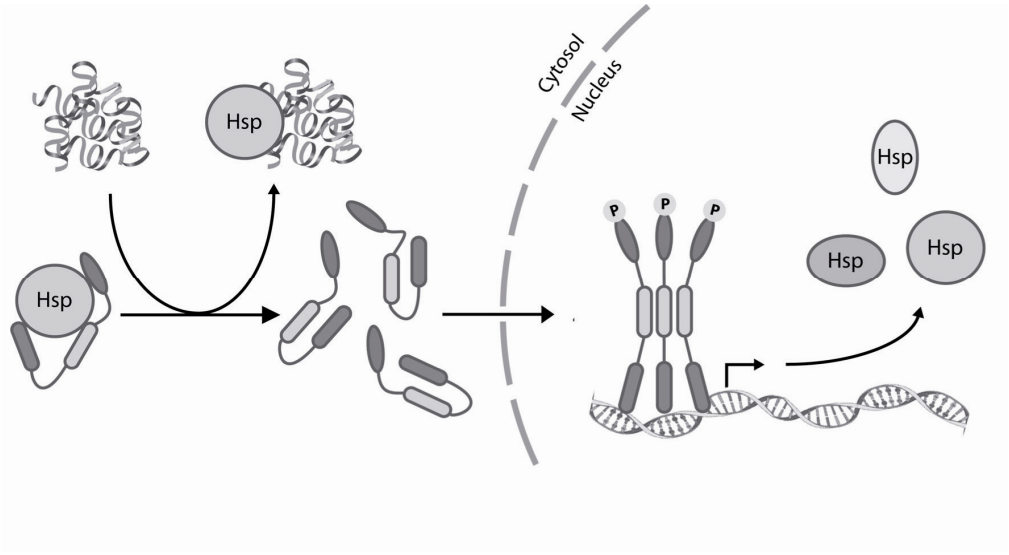

Figure 3: Principle of Hsf1-based transcriptional activation of Heat shock genes. Hsf1 in the unstressed cytosol is bound to Hsp90. After release form Hsp90, Hsf can be transported to the nucleus, becomes phosphorylated and binds as a trimer to Hsf response elements and activates the transcription of heat shock proteins. Modified from (Pockley, 2003).

Hsp70, Hsp60 homologs and Hsp90 (Fukunaga and Hunter, 2004; Kim et al, 1997; Knauf et al, 1996). By generating more Hsp90 activity due to the activated transcription, Hsf becomes sequestered in the cytosol as a monomer and transcriptional activation decreases (**Figure 3**) (Bharadwaj et al, 1999). Interestingly, a similar principle of the heat shock response is found in bacteria. Here the transcriptional machinery is dependent on specific sigma factors. Sigma32 is the factor responsible to induce the transcription of heat shock operons in bacteria (Yura, 1996). This protein is bound to DnaK (the *E. coli* homolog of Hsp70) and DnaJ (the *E. coli* Hsp40) and a very similar negative feedback loop applies as in eukaryontes in which sigma32 is released from the chaperone as competing unfolded proteins accumulate due to heat stress (Rodriguez et al, 2008).

1.4.2 Hsp90 isotypes

In eubacteria there is only one Hsp90 gene and normally none in archea (Bardwell and Craig, 1987). In eukaryotes the Hsp90 function is essential (Panaretou et al, 1998; Obermann et al, 1998). But interestingly, the unstressed cell copes with a 20 times reduction in the Hsp90 level (Picard et al, 1990). In *Saccaromyces cerevisiae* and in *homo sapiens,* two isotypes are found in the cytosol (Hsc82 and Hsp82 in *Saccaromyces cerevisiae* and Hsp90alpha and Hsp90beta in *Homo sapiens*) (Borkovich et al, 1989). Differing functions in the cell are currently debated in the literature although the isotypes have high sequence similarity. Hsc82 in yeast is the constantly expressed version of the protein while Hsp82 is strongly induceable by heat shock. In addition there are paralogs in the mitochondria and in the ER (not in yeast), TRAP1 and GRP94 respectively (Felts et al, 2000; Gupta, 1995).

1.4.3 Biochemistry of Hsp90

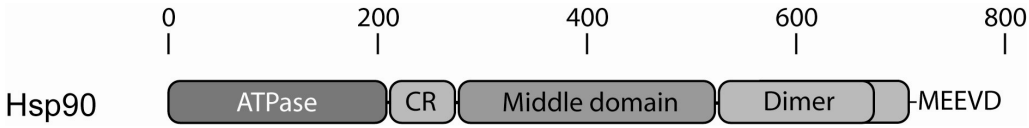

Figure 4: Domain topology of the Hsp90 molecular chaperone from *saccaromyces cerevisiae*. Amino acid (aa) 1- 210 compose the N-terminal domain, aa 210-262 form a charged region that links N-terminal and middle domain which ranges from aa 262 to app. 530. The C-terminal dimerisation domain including the C-terminal MEEVD sequence is made up form aa 530 to 709.

The chaperone machine Hsp90 is associated in the de novo folding processes of only a specific subset of signalling proteins (Richter et al, 2005; Nathan et al, 1997). It binds partial folded protein folding intermediates and near-native proteins (Picard, 2006a; Nathan et al, 1997; Jakob et al, 1995). In addition, it seems to be involved in the assembly and regulation of multiprotein complexes (Zhao et al, 2005). In vitro it has a passive holdase function that enables improved refolding after stresses that cause unfolding of substrates (Jakob et al, 1995; Wiech et al, 1992). Knowledge about substrates that specifically depend on Hsp90 assisted activation in the cell is still growing. Among the identified candidates are, among others, kinases and transcription factors (Caplan et al, 2007; Pratt et al, 2006; Nathan and Lindquist, 1995).Thus, Hsp90 is a potential drug target for cancer chaperoning important signal transducers in the cell (Chiosis and Tao, 2006; Whitesell and Lindquist, 2005; Chiosis et al, 2001).

Hsp90 is a member of the GHKL ATPases which are generally comprised of 2 subunits that are associated tail to tail via C-terminal dimerisation domains (Dutta and Inouye, 2000). The ATPase function depends on complex conformational changes that lead intermediately to a dimerised form of the N-terminal domains

which harbour the site for ATP binding and form together with the middle domain the active site of the ATPase (Meyer et al, 2004; Richter et al, 2001; Prodromou et al, 1997b). The Hsp90 protomer consists of 3 domains; the N-terminal ATP binding domain, a middle domain partially contributing to active site formation and sites for substrate interaction and the C-terminal domain which mediates dimerisation and TPR co-chaperone association (**Figure 4**) (Muller et al, 2004; Meyer et al, 2003; Richter et al, 2001; Scheufler et al, 2000; Minami et al, 1994). With the exception of the charged linker region located between the N-terminal domain and the middle domain, Hsp90 seems to be conserved form *Escherichia coli* to *Homo sapiens* (Richter et al, 2005). The hydrolysis rate of 1 min^{-1} for yeast Hsp90 is very slow compared to other ATP-driven motors. This observation led to the assumption that conformational changes prior to hydrolysis are key bottlenecks for the reaction (Maruya et al, 1999; Grenert et al, 1997). Some regions like the ATP-lid in the N-terminal domain seem to be inhibitory elements (Richter et al, 2006). Interestingly, if the lid-region is deleted, Hsp90 becomes hydrolysis inactive, however when heterodimers with wt protein are analysed, the lidless-protomer acts as a potent activator of the wt ATPase activity (Richter et al, 2006). In addition mutations leading to stronger interaction between the N-terminal domains led to an activated ATPase activity (Prodromou et al, 2000). Therefore it was assumed that the intermediately formed N-terminal dimerized Hsp90 is a key conformation in each ATP hydrolysis cycle (Siligardi et al, 2004). In addition, structures of the isolated domains and recently published full-length structures in different conformations of the chaperone revealed a high flexibility between the domains (**Figure 5**) (Shiau et al, 2006; Ali et al, 2006).

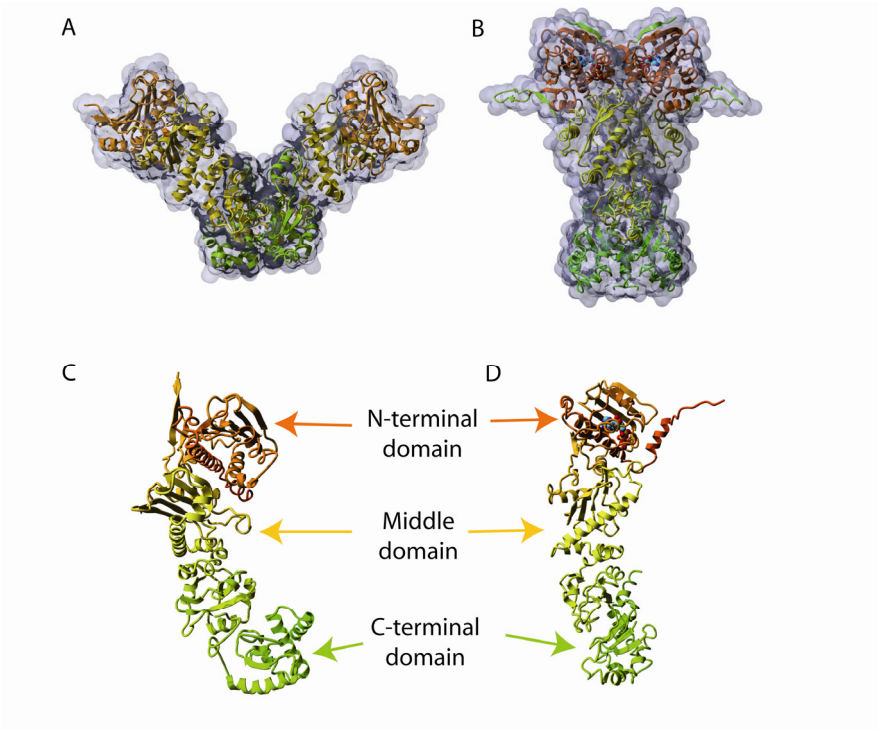

Figure 5: Crystal structures of Hsp90 in the apo and the closed state. Depicted in red is the N-terminal ATP binding domain, in yellow the middle domain and in green the C-terminal dimerisation domain as indicated in C and D. A) Structure of the E. coli homolog of Hsp90 in its nucleotide-free state. B) Yeast Hsp90 in its closed N-terminal dimerised state in complex

Large conformational changes take place in the cycle driven by ATP hydrolysis (**Figure 5 A and B).** The crystal structure of the closed state is stabilized by the non-hydrolysable ATP analogue AMP-PNP. In addition, flexible parts in the charged region need replacement to obtain diffracting crystals (Ali et al, 2006). Also the above mentioned mutant increasing the propensity for N-terminal dimerisation and activating the ATPase activity was used for crystallisation (Ali et al, 2006). p23, a co-chaperone of Hsp90 that interacts exclusively with the closed state, was further more used to stabilize this particular closed conformation. Biochemical studies guided structure determination and emphasised that Hsp90 is a highly dynamic and flexible molecule.

1.5 Hsp90 co-chaperones

In the eukaryotic cell, Hsp90 function is supported by co-chaperones which have not been found in bacteria. Most co-chaperones have been identified in complex with intracellular steroid hormone receptors. These proteins bind to steroid hormones with a ligand binding domain which is located at the C-terminal part of these transcription factors. The ligand binding domains posses a deep hydrophobic cleft to which the

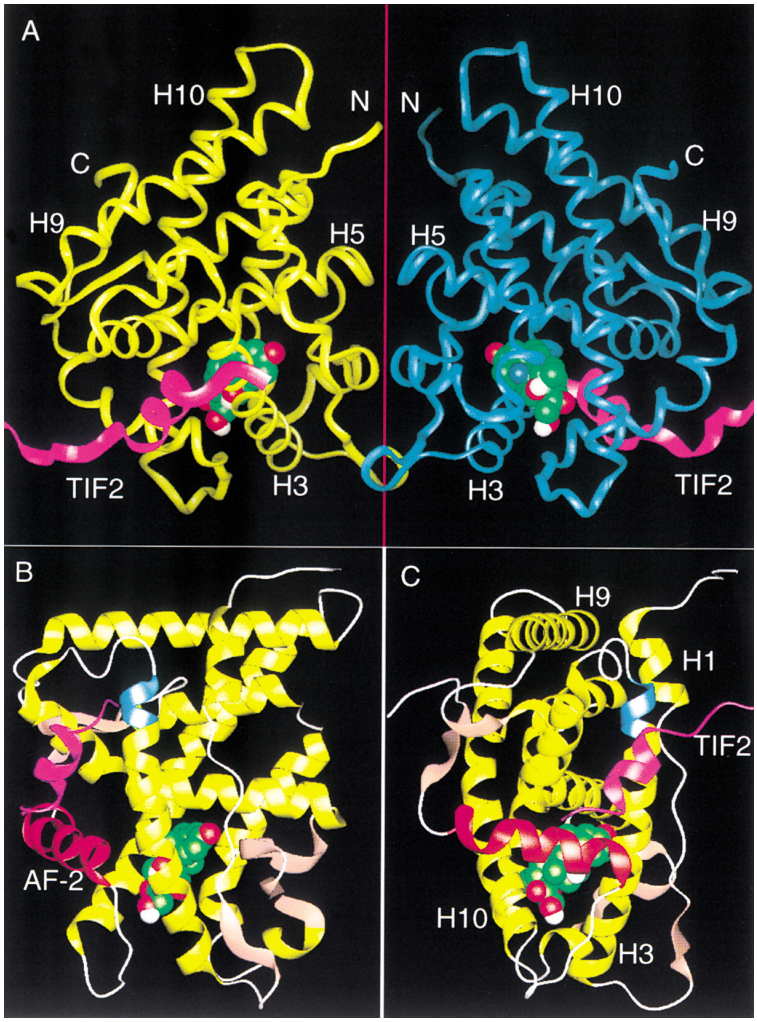

Figure 6: Crystal structure of the Glucocorticoid (GR) receptor ligand binding domain (LBD). (A) Overall arrangement of the GR LBD dimer including the co-activator peptides TIF2. The two LBDs are shown in yellow and blue worms; the two TIF2 peptides are in purple ribbon; and the two dexamethasone molecules are in space-filling representation with carbon, oxygen, and hydrogen colored in green, red, and white, respectively. The C2 symmetry axis is shown in red. (B and C) Two 90-degree views of the GR/Dex/TIF2 monomer complex, where helices are colored in yellow and β-strands are in gold. The AF-2 helix is in red and the lysine residue from helix 3 that forms the charge clamp is in blue. The TIF2 peptides are shown in purple (1M2Z). Figure taken from Bledsoe et al, 2002.

hormone binds (Pratt et al, 2006) (**Figure 6**). Hsp90 is required to activate the protein for hormone binding. Afterwards a lid helix (AF2 for the GR) in the ligand binding domain moves above the bound steroid, thereby generating a new interaction surface for co-activator binding and dimerisation of the receptor which is required for transcriptional activation and DNA binding (Bledsoe et al, 2002).

In vitro, different Hsp90-associated conformations of steroid hormone receptors could be identified (**Figure 7**). The associated co-chaperones are different in these complexes. In an early maturation stage, Hsp70 and a co-chaperone called Hop were found (Chen et al, 1996). Later on an adaptor function was assigned to Hop which co-localises Hsp70 and Hsp90 to improve substrate transfer between them (Chen and Smith, 1998; Johnson et al, 1998). Form the analysis of another factor called Hip which is involved in glucocorticoid receptor activation, it had been reasoned that Hip, and also Hop, function to activate the receptor by regulating Hsp70 (Prapapanich et al, 1998). However, expression of human Hip in yeast boosts the GR activity in yeast cells, by a mechanism that is not dependent on a Hsp70-Hip interaction (Nelson et al, 2004). The steroid receptor molecules in Hop-, Hip- and Hsp70- containing complexes are inactive in ligand binding (Smith, 1993). In addition, transfer to Hsp90 requires an Hsp70 co-chaperone called Hsp40 (Cintron and Toft, 2006). When the substrate maturation proceeds an exchange of co-chaperones takes place (Johnson and Toft, 1994; Smith, 1993). The incoming factors are FKBP51, FKBP52 or Cyp40 and the small acidic p23 co-chaperone (Ward et al, 1999; Johnson and Toft, 1995c; Smith et al, 1990).

The FKBPs are both chaperones and protein folding catalysts. They have PPIase activity (Pirkl and Buchner, 2001). In addition they can bind and prevent the aggregation of protein folding intermediates (Bose et al, 1996; Freeman et al, 1996). p23 has a unstructured C-terminal tail exhibiting chaperone function (Weikl et al, 1999; Johnson and Toft, 1995b).

In this complex, steroid hormone receptors can bind ligand (Smith, 1993). To analyse the complexes of the maturing intracellular receptors a lot of effort was required because of its dynamic nature (Smith and Toft, 2008). After hormone associates, the SHR substrate is released from the complex and the Hsp90 system is free to enter

another cycle. Most of the insights described above on the components of the Hsp90 system were investigated using cell lysates. Factors required only in catalytic amounts were therefore difficult to analyse in this assay (**Figure 7**).

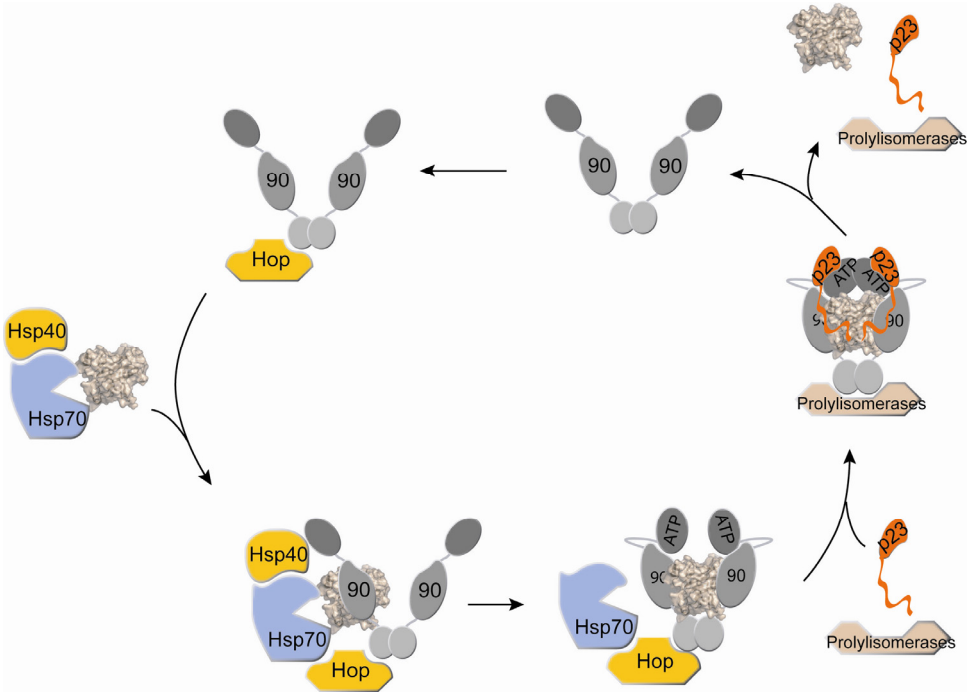

Figure 7: Proposed activation pathway for steroid hormone receptors (SHRs). Substrate becomes activated by Hsp70 for Hsp90 binding. Hop acts as an adaptor protein co-localising Hsp70 and Hsp90. ATP hydrolysis is required for efficient folding of substrate by Hsp70 and Hsp90. Upon maturation of substrate Hop and Hsp70 are exchanged by Prolylisomerases and p23. In that complex SHRs are binding competent and are released after hormone binding form the chaperone system.

Other substrate classes of Hsp90 exist for which not much detail about the activation pathway has been accumulated (www.picard.ch/DP/Hsp90interactors.pdf). Kinases constitute another huge group of Hsp90-dependent client proteins. Their activation and folding depends on Hsp90 but they require a different co-chaperone which is called Cdc37. Kinase binding to Hsp90 has been suggested to be catalysed and stabilized by Cdc37. The large list of co-chaperones can be classified by their

binding site to Hsp90. Most co-chaperones identified to date interact via a Tetratricopetide Repeat (TPR) domain with the very C-terminal part of Hsp90 and especially the last MEEVD motif found in all eukaryotic variants of Hsp90 (Carrello et al, 1999). The other group interacts with other parts of Hsp90. In the following characteristic structures of Hsp90 co-chaperones will be introduced.

1.5.1 TPR co-chaperones

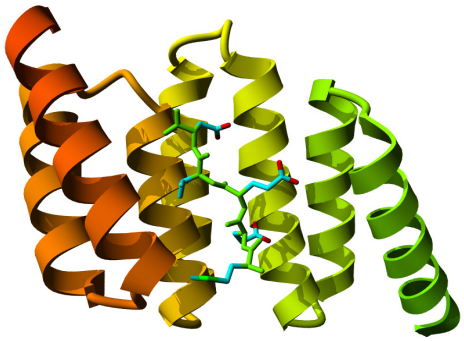

Figure 8: Crystal structure of the TPR2a domain of Hop (1ELR). The protein is coloured with a gradient form Red to green form N- to C-terminus. First two TPR motifs form the first four helices. The extended peptide in the structure corresponds to the C-terminal MEEVD motif found in Hsp90.

The Tetratricopeptide repeat is a characteristic motif found in Hsp70 and Hsp90 interacting proteins (Scheufler et al, 2000; Carrello et al, 1999; Ratajczak and Carrello, 1996). It is a weak conserved stretch of 34 amino acids which forms two or three alpha helices (Goebl and Yanagida, 1991). Three TPR motifs can form a TPR-domain (**Figure 8**). Hsp90 co-chaperones usually have a TPR-domain with 7 alpha helices that form a cleft capable to interact with extended peptide stretches found at the C-terminus of Hsp70 and Hsp90. Only very few specific amino acids are required to define the specificity. Affinities for this interaction with Hsp90 rank in the low nanomolar range (Brinker et al, 2002). The TPR domain is fused to co-chaperones in modular way with other domains. In the case of FKBP51/52, Cyp40 (Cpr6 and Cpr7 in yeast) a PPiase domain is linked to the TPR domain (Pirkl and Buchner, 2001) and a phosphatase domain in the case of PP5 (Ppt1p in yeast) (Wandinger et al, 2006; Jeong et al, 2003). Chip, an ubiquitin ligase involved in tagging of proteins for degradation, also interacts with Hsp90 via a TPR domain

(Zhang et al, 2005; Ballinger et al, 1999). Besides enzymatic activities other functions can be combined with the TPR domain.

Hop was shown to act as an adaptor by binding Hsp70 and Hsp90 through two TPR domains simultaneously (Wegele et al, 2006). In addition, it has a strong inhibitory function on the Hsp90 ATPase activity (Richter et al, 2003).

CNS1, another co-chaperone, which shares the TPR domain for Hsp90 and Hsp70 interaction (Hainzl et al, 2004), has a domain to which no defined function could be assigned to date. It is an essential co-chaperone in yeast (Dolinski et al, 1998). The low copy number and evidence that it genetically acts in similar way as Cpr7 hints to very specific substrates (Tesic et al, 2003).

In contrast to the modular use of the TPR interaction, some co-chaperones, such as TPR1, are composed of only a TPR domain (Lotz et al, 2008). Thus, the TPR interaction to Hsp90 might in addition exhibit certain activities that are not well defined to date but important for a complete understanding of the chaperone cycle.

1.5.2 Non-TPR co-chaperones

Figure 9: Crystal structure of the N-terminal domain of yeast Hsp90 (residues 1-208) in complex with the human Cdc37 Hsp90 interacting domain (residues 138-378). Hsp90 is depicted in red. Cdc37 in a colour gradient from yellow to green form N to C.

Cdc37 is considered to be specific for kinase maturation in concert with Hsp90 (Caplan et al, 2007; Kimura et al, 1997). For its essential in vivo function phosphorylation at Serin 13 is required (Miyata and Nishida, 2004; Bandhakavi et al, 2003; Shao et al, 2003). The EM structure of the Hsp90-Cdk4-Cdc37 complex represents a glimpse on the structural background that underlies kinase activation by the Hsp90 chaperone system (Vaughan et al, 2006). The N-terminal domain of Cdc37 seams to interact with kinases and the C-terminal domain interacts with the N-terminal domain of Hsp90, possibly acting as an adaptor for kinases loaded on Hsp90 (Silverstein et al, 1998; Stepanova et al, 1996). Cdc37 is an inhibitor of Hsp90 ATPase activity but binds only with low affinity (Siligardi et al, 2002). A crystal structure of the Hsp90 N-terminal domain in complex with Cdc37 (Roe et al, 2004) explains the inhibitory activity on the ATPase. The inspection of the structure suggested that Lid closure is abolished when Cdc37 is bound, an arginine residue is inserted in the active site to prevent catalysis and the bound Cdc37 covers the surface required for N-terminal dimerisation. Cdc37 directly interacts with kinases and has a holdase function in this complex. Nascent chains of kinases are bound as mentioned by Hsp70 and Hsp40 in eukaryotic cells (Caplan et al, 2007). As the catalytic kinase domain matures, it is transferred to Hsp90, a process assisted by Sti1 and Cdc37 in yeast (Lee et al, 2004; Abbas-Terki et al, 2002). Main interaction sites of Cdc37 and Hsp90 are located in

the N-lob of the kinase domain including the alpha C/beta4 loop (Zhao et al, 2004; Scroggins et al, 2003). Treating cells with an Hsp90 inhibitor, like GA, leads to a rapid degradation of certain kinases (Neckers, 2000; Whitesell et al, 1994). Thus, it seems that not only folding of kinases requires Hsp90 and Cdc37, but the kinase cycle itself requires assistance, depending on the stability of the N-lob region.

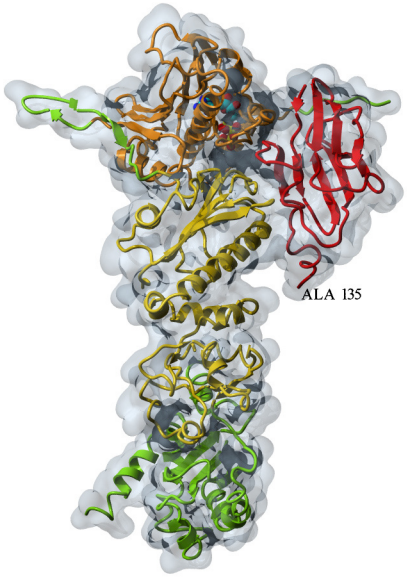

Figure 10: Crystal structure of p23 in complex with one protomer of Hsp90. N-terminal domain is shown in red, middle domain is depicted in yellow, the c-terminal domain in green. p23 is coloured in red.

p23 is a small acidic protein which consists of a beta-only domain (Weaver et al, 2000) required for Hsp90 interaction and a flexible C-terminal tail which seems to be natively unfolded (Weikl et al, 1999). In vivo, p23 is found in mature and hormone-binding competent SHR-Hsp90 complexes (see above) (Hutchison et al, 1995; Johnson et al, 1994). In yeast, the p23 knock out elicits growth defects at low temperatures when Sti1 is absent (Fang et al, 1998) and induces increased ansamycin sensitivity (Forafonov et al, 2008; Bohen, 1998). In mice the p23 knock out apparently develops normally as embryo. But upon birth these mice choke on retarded lung development (Grad et al, 2006). p23 inhibits the Hsp90 ATPase activity by 50% and competes with Sti1 for Hsp90 interaction (Richter et al, 2004; Prodromou et al, 2000). It interacts with a specific conformation of Hsp90 which requires N-terminal dimerisation (Ali et al, 2006; Richter et al, 2002; Johnson and Toft, 1995a). Thus to interact with p23, Hsp90 is required in its ATP bound conformation. The interaction domain of p23 contains the most conserved part of the protein, including a loop rich in aromatic amino acids (Weaver et al, 2000; Weikl et al, 1999). This loop connects the beta sandwich domain with the natively unfolded and very flexible C-terminal tail. The unstructured C-terminal part of p23 consists of

80 amino acids for the yeast version of the protein. A repetitive GGM region directly follows the connecting loop. Then a QL rich region of approximately 16 amino acids follows in front of the very acidic C-terminal tail that marks the end of the sequence (Oxelmark et al, 2003). The C-terminal tail shows random coil structure in CD, and in the crystal structure analysis of the human p23 it was not resolved due to high flexibility (Weaver et al, 2000; Weikl et al, 1999). Also, in the crystal structure of the N-terminally dimerised Hsp90 in complex with p23, the C-tail could not be resolved (Ali et al, 2006). Thus it was suggested to be completely devoid of structure. It has been shown that the tail exhibits the chaperone function of p23 in vivo and in vitro for the human and the yeast variant of the protein (Oxelmark et al, 2003; Weikl et al, 1999). The C-terminal tail is very variable in length especially GGM repeats and QL repeats might vary very strongly among organisms (**Figure 43**).

Figure 11: Crystal structure of the Hsp90 Aha1 complex. The N-terminal domain (residues 1-156) of Aha1 is depicted in green. The middle domain of Hsp90 (residues 273-530) is shown in a colour gradient form red to yellow from N- to C- respectively.

Aha1 and Hch1 are a more recently identified co-chaperones of the Hsp90 system (Panaretou et al, 2002). In vivo, Aha1 was shown to modulate Hsp90 pathways and it seems to play a role in the decision whether to fold or to degrade the substrate protein. An interesting example in this respect is the role of Aha1 in the CFTR folding (Wang et al, 2006). Folding of the CFTR protein depends on ER chaperones and on cytosolic Hsp70 and Hsp90 (Turnbull et al, 2007; Amaral, 2004; Loo et al, 1998). Knock down of Aha1 in this genetic background can rescue mutant phenotypes of the

CFTR pathway (Wang et al, 2006). In knock downs of Aha1 client protein activation is sensitised for Hsp90 targeting drugs (Holmes et al, 2008). Aha1 was identified as a strong activator of the Hsp90 ATPase (Lotz et al, 2003). The Hsp90 interacting domain has been crystallized in complex with Hsp90 **(Figure 10Figure 11**: Crystal structure of the Hsp90 Aha1 complex. The N-terminal domain (residues 1-156) of Aha1 is depicted in green. The middle domain of Hsp90 (residues 273-530) is shown in a colour gradient form red to yellow from N- to C- respectively.**)** (Meyer et al, 2004). It turned out that loop 370-390 of Hsp90, important to form the complete ATPase, becomes rearranged upon Aha1 binding to Hsp90 (Meyer et al, 2004). Thus this was suggested to be the major activating factor on the Hsp90 ATPase activity. The affinity of Aha1 to Hsp90 was measured with a K_D of 670 nM (Meyer et al, 2004). However the crystallized components bind with a weakened affinity of 3-4 µM (Meyer et al, 2004). Hch1 is highly homologous to the crystallized N-terminal domain of Aha1 and shows also a lower binding affinity compared to Aha1. Both the N-terminal domain of Aha1 and Hch1 stimulate the ATPase to the same extend. However, full length Aha1 has an increased stimulating potential indicating that the underling mechanism is not fully clear (Meyer et al, 2004).

1.6 Intent of this work

The Hsp90 ATPase activity has been analysed to in some detail (Weikl et al, 2000). It was known that conformational changes, at least in the N-terminal domain, play a key role for the turnover rate. Homology to the GHKL ATPases suggested a mechanism that involves N-terminal dimerisation (Dutta and Inouye, 2000; Prodromou et al, 2000). However, this was disputed until recently, when the crystal structure of yeast Hsp90 was solved in its closed conformation. For the crystallisation in this conformation massive manipulations and the use of the closed state stabilizing co-chaperone p23 were required (Ali et al, 2006). Loop regions in the C-terminal and the M-domain of Hsp90 remain undefined. Only recently, data accumulated that suggested a general conserved mechanism for the human Hsp90

and for the paralogs in the ER (Grp94) (Richter et al, 2008; Frey et al, 2007) and mitochondria (Trap1) (Leskovar et al, 2008).

Co-chaperones modulating the ATPase activity of Hsp90 have been analysed on the structural level with isolated domains of Hsp90. Thus primary binding sites are largely defined for p23, Cdc37, Aha1 and for the TPR co-chaperones, although secondary binding sites are likely involved in the regulation of the ATPase. The idea is supported by generally lesser binding affinity to isolated domains of Hsp90. For TPR co-chaperones it remained quite unclear how the regulation is achieved.

The focuses of this PhD thesis are the conformational changes of Hsp90. The high number of co-chaperones in the Hsp90 chaperone system raises the question of their functional meaning and the exact timing when they would bind to Hsp90. Data from steroid hormone receptor maturation suggested specific steps in the cycle, including an exchange of co-chaperones. Indicative for a complex conformational regulation is that p23 and Sti1 were shown to bind mutually exclusive to the chaperone (Richter et al, 2004). The idea of a conformational selectivity was suggested for this mechanism, as overlapping binding sites seem not to exist: p23 binds to the N-terminal domain and Sti1 via its TPR domain to the C-terminal end of Hsp90. Aha1 an activator of the Hsp90 ATPase was suggested to induce a movement in a loop involved in the catalytic mechanism of ATP hydrolysis (Meyer et al, 2003). However, the isolated N-terminal domain of Aha1 which exhibits loop motion in Hsp90 only partially supported activation and binds weaker to Hsp90 compared to the full length protein, suggesting a more complex underling mechanism (Meyer et al, 2004; Lotz et al, 2003).

To analyse the conformational cycle of Hsp90 and its modulation by co-chaperones, a FRET system should be developed which allows monitoring changes in the relative orientations of the domains in the dimer in response to nucleotide kinetically, with the view to reconstitute the entire conformational changes.

2 Material und Methods

2.1 Material

2.1.1 Strains

Strains	Geno- / Phenotype	Source / Reference
E. coli XL1 Blue	*rec*A1 *end*A1 *gyr*A96 *thi*-1 *hsd*R17 *sup*E44 *rel*A1 *lac* [F'proAB *lac*IqZDM15 Tn10 (*Tet*R)]	Stratagene, La Jolla, USA
E. coli XL1 DH10B	F- *mcr*A Δ(*mrr-hsd*RMS-*mcr*BC) Φ80*lacZ*ΔM15 Δ *lac*X74 *rec*A1 *end*A1 *ara*D139 Δ(*ara, leu*)7697 *gal*U *gal*K λ- *rps*L *nup*G *ton*A	
E. coli BL21 (DE3)	F– *omp*T hsdS(rB– mB–) *dcm*+ *Tet*r *gal* l (DE3) *end*A *Hte* [*arg*U *ile*Y *leu*W *Cam*R]	Stratagene, La Jolla, USA
S. cerevisiae BY4741	MATa; *his*3D1; *leu*2D0; *met*15D0; *ura*3D0	Euroscarf
S. cerevisiae BY4742	MAT□ ; *his*3D1; *leu*2D0; *met*15D0; *ura*3D0	Euroscarf
S. cerevisiae BY4741 ΔSBA1	BY4741 Mata; his3D1; leu2D0; met15D0; ura3D0; YKL117w::kanMX4	Euroscarf
S. cerevisiae BY4742 ΔSBA1	BY4742; Mat□; his3D1; leu2D0; lys2D0; ura3D0; YKL117w::kanMX4	Euroscarf

Vector / Plasmid	Discribtion / Origin	Cloning site
pET28b+	Merck Biosciences GmbH (Schwalbach, Germany)	
p2HGal	S. Lindquist, (Boston, USA)	
pMal	Expression of MBP fusion proteins	
pET28-Sba1	Sba1 expression/ Dr. Klaus Richter	Nde1 / BamH1
pET28-Sba1Δ17C	Sba1Δ17 expression/ This work	Nde1 / BamH1
pET28-Sba1Δ40C	Sba1Δ40C expression/ This work	Nde1 / BamH1
pET28-Sba1Δ69C	Sba1Δ69C expression/ Dr. Tina Weikl	Nde1 / BamH1
p2HGal-Sba1	Sba1 expression in *S. cerevisiae/* This work	Spe1 / Not1
p2HGal-Sba1Δ17C	Sba1Δ17C expression in *S. cerevisiae/* This work	Spe1 / Not1
p2HGal-Sba1Δ40C	Sba1Δ40C expression in *S. cerevisiae/* This work	Spe1 / Not1
p2HGal-Sba1Δ69C	Sba1Δ69C expression in *S. cerevisiae/* This work	Spe1 / Not1
pET28-Sba1I117V	Sba1I117V expression/ This work	Nde1 / BamH1
pET28-Sba1I117A	Sba1I117A expression/ This work	Nde1 / BamH1
pMal-Ctail	Fusion of MBP with Sba1 C-tail This work	BamH1 / EcoR1
pET28-Sba1GGM	Expression ofSba1GGM replacement mutant This work	Nde1 / BamH1

Vector / Plasmid	Discribtion / Origin	Cloning site
pET28-Sba1QL	Expression of Sba1QL replacement mutant This work	Nde1 / BamH1
pET28-Sba1Cys2	Expression of Sba1Cys2 variant Dr. Klaus Richter	Nde1 / BamH1
pET28-Hsp82	Hsp82 expression Dr. Klaus Richter	Nde1 / BamH1
pET28-Hsp82C61	Hsp82C61 expression This work	Nde1 / BamH1
pET28-Hsp82C159	Hsp82C159 expression This work	Nde1 / BamH1
pET28-Hsp82C333	Hsp82C333 expression This work	Nde1 / BamH1
pET28-Hsp82C385	Hsp82C385 expression This work	Nde1 / BamH1
pET28-Hsp82C411	Hsp82C411 expression This work	Nde1 / BamH1
pET28-Hsp82C433	Hsp82C433 expression This work	Nde1 / BamH1
pET28-Hsp82C462	Hsp82C462 expression This work	Nde1 / BamH1
pET28-Hsp82C478	Hsp82C478 expression This work	Nde1 / BamH1
p2HGal-Hsp82	Hsp82 expression in *S. cerevisiae/* Dr. Klaus Richter	Spe1 / Not1
p2HGal-Hsp82C61	Hsp82C61 expression in *S. cerevisiae/* This work	Spe1 / Not1
p2HGal-Hsp82C159	Hsp82C159 expression in *S. cerevisiae/* This work	Spe1 / Not1
p2HGal-Hsp82C333	Hsp82C333 expression in *S. cerevisiae/* This work	Spe1 / Not1

Vector / Plasmid	Discribtion / Origin	Cloning site
p2HGal-Hsp82C385	Hsp82C385 expression in *S. cerevisiae/* This work	Spe1 / Not1
p2HGal-Hsp82C411	Hsp82C411 expression in *S. cerevisiae/* This work	Spe1 / Not1
p2HGal-Hsp82C433	Hsp82C433 expression in *S. cerevisiae/* This work	Spe1 / Not1
p2HGal-Hsp82C462	Hsp82C462 expression in *S. cerevisiae/* This work	Spe1 / Not1
p2HGal-Hsp82C478	Hsp82C478 expression in *S. cerevisiae/* This work	Spe1 / Not1

2.1.2 Chemicals

Name	Origin
Acrylamide (38%, 2% Bisacrylamide)	Roth (Karlsruhe, Germany)
Agarose, ultra pure	Roth (Karlsruhe, Germany)
Ammoniumperoxodisulfate (APS)	Roche (Mannheim, Germany)
Ammoniumsulfate	Merck (Darmstadt, Germany)
Ampicillin	Roth (Karlsruhe, Germany)
Bacto Agar	Difco (Detroit, USA)
Bacto Tryptone	Difco (Detroit, USA)
Bacto Yeast Extract	Difco (Detroit, USA)
Benzamidin	Sigma-Aldirch (Hamburg, Germany)
Bromphenolblue S	Serva (Heidelberg, Germany)
Complete Protease Inhibitor Cocktail Tablets	Roche (Mannheim, Germany)
Coomassie Brilliant-Blue R-250	Serva (Heidelberg, Germany)
Coomassie Protein Assay Reagent	Pierce (Rockford, USA)
5,5' Dithio-bis-Nitrobenzoic acid (DTNB)	Sigma (St. Louis, USA)
1,4-Dithiothreitol (DTT)	Roth (Karlsruhe, Germany)
ECL-Westernblot Detection System	GE Healthcare (Munich, Germany)
Ethylendiamintetraacidic acid (EDTA)	Merck (Darmstadt, Germany)
Ethidiumbromide	Sigma (St. Louis, USA)
Formaldehyde, 37% p.A.	Roth (Karlsruhe, Germany)
Glutaraldehyd, 25% in water	Serva (Heidelberg, Germany)
Glycerol, 99 %	ICN, Costa Mesa, USA
Glycine	Roth (Karlsruhe, Germany)
N-(2-Hydroxyethyl)-piperazin-N´2-Ethansulfonic acid (HEPES)	ICN (Costa Mesa, USA)
Isopropanol	Roth (Karlsruhe, Germany)
Isopropyl-β-D-thiogalaktopyranosid (IPTG)	Roth (Karlsruhe, Germany)
Kanamycin	Roth (Karlsruhe, Germany)
β-Mercaptoethanol, pure	Merck (Darmstadt, Germany)
Sodiumdodecylsulfat (SDS)	Roth (Karlsruhe, Germany)
N,N,N´,N´-Tetramethylethylendiamin (TEMED)	Roth (Karlsruhe, Germany)
Polyoxyethylen-Sorbitan-monolaurat (Tween 20)	Merck (Darmstadt, Germany)
Ponceau S	Sigma-Aldrich (Hamburg, Germany)
Restriction enzymes	New England Biolabs (Beverly, USA)
T4-Ligase	Promega (Madison, USA)
Tris-(Hydroxymethyl)-aminomethan (Tris)	ICN, Costa Mesa, USA

2.1.3 Fluorophors

Name	Ex_{max} (nm)	Em_{max} (nm)	ε (M^{-1} cm^{-1})	Origin
ATTO488-maleimid	501	523	90,000	ATTO-TEC (Siegen, Germany)
ATTO550-maleimid	554	576	120,000	ATTO-TEC (Siegen, Germany)
5-iodoacetamido-flurescein	492	515	78,000	Invitrogen, (Karlsruhe, Germany)
5-idoacetamido Tetramethyl-rhodamine	543	576	87,000	Invitrogen, (Karlsruhe, Germany)

* Ex_{max}: Spectral excitation maximum, Em_{max}: Spectral emission maximum, ε: Molar extension coefficient

2.1.4 Size and molecular mass standard kits

Name	Origin
Low-Range Molecular Weight Standard	BioRad Laboratories (Munich, Germany)
Rainbow marker	GE Healthcare (Freiburg, Germany)
DNA-BstEII Molecular Weight Standard	New England Biolabs (Beverly, USA).
1 kb DNA Ladder Molecular Weight Standard	New England Biolabs (Beverly, USA).
QIAquick, Gel Extraction Kit	Qiagen GmbH (Hilden, Germany)
QIAprep Spin Miniprep Kit	Qiagen GmbH (Hilden, Germany)
QIAprep Spin PCR Purification Kit	Qiagen GmbH (Hilden, Germany)
Protein Standard for HPLC	GE Healthcare, (Freiburg Germany)

2.1.5 Proteins

Name	Origin
Citrate Synthase from pig heart	Roche (Mannheim, Germany)
Glutamate dehydrogenase from Bovine	Roche (Mannheim, Germany)
Lactat Dehydrogenase	Roche (Mannheim, Germany)
Pyruvat Kinase	Roche (Mannheim, Germany)
Bovine Serum Albumin	Sigma-Aldrich (Hamburg, Germany)
Purin-Nucleosid-phosphorylase	Invitrogen (Karlsruhe, Germany)
Chymotrypsin	Sigma-Aldrich (Hamburg, Germany)

2.1.6 Antibodies

Name	Origin
Polyclonal serum against Sba1 (Rabbit)	Pineda Antikörper Service (Berlin, Germany)
Polyclonal serum against Hsp82 (Rabbit)	Pineda Antikörper Service (Berlin, Germany)
Monoclonaler IgG-Peroxidase Conjugate against Rabbit-IgG (Goat)	Sigma (St. Louis, USA)

2.1.7 Chromatography

Name	Origin

Name	Origin
Amylose-Resin (15 ml)	New England BioLabs, (Hitchin, UK)
Ni-NTA (30 ml)	GE Healthcare, (Freiburg Germany)
Q-Sepharose (150 ml)	GE Healthcare, (Freiburg Germany)
Hydroxyapatide (50 ml)	BioRAD, (Hercules USA)
Resource-Q (6 ml)	GE Healthcare, (Freiburg Germany)
S Sepharose (10 ml)	GE Healthcare, (Freiburg Germany)
Resource-S (6 ml)	GE Healthcare, (Freiburg Germany)
Superdex 75 Prep Grade (320 ml)	GE Healthcare, (Freiburg Germany)
Superdex 200 Prep Grade (320 ml)	GE Healthcare, (Freiburg Germany)

2.1.8 Additional materials

Device	Origin
Amicon-Ultrafiltration Membrane YM10/30/100	Millipore (Bedford, USA)
Centricon 10/30/100- microconcentrators	Millipore (Bedford, USA)
Dialysis tubes Spectra/Por (6-8 kDa)	Spectrum (Houston, USA)
Cuvettes 1.5 ml	Zefa (Munich, Germany)
Cuvettes	Starna GmbH (Pfungstadt, Germany)
Filterpaper	Whatman (Maidstone, England)
Immobilon-P(PVDF)-Membrane	Millipore (Bedford, USA)
pH-Indicator paper	Roth (Karlsruhe, Germany)
Polyacrylamide gels (10-20 % Tricine)	Novex (Frankfurt, Germany)
Scientia EM-Film 23D56 (6,5x9 cm)	Agfa Gevaert (Belgien)
Sterile filter 0.2µm	Zefa (Munich, Germany)

2.1.9 Media and antibiotics

Name	Compounds	Quantities
LB_0:		
	Bacto Trypton	10 g
	Yeast extract	5 g
	NaCl	5 g
	H_2O	ad 1 l
	Use NaOH to adjust pH to 7.2	
	For plates: 12 g Bacto Agar	

Name	Quantities
Ampicillin for selection on p2µGPD	100 µg/ml
Kanamycin for selection on pET28b+	25 or 35 µg/ml

2.1.10 Buffers for molecular biological methods

Name	Compounds	Quantities
TAE (50x):	2 M Tris/Acetate pH 8.0 50 mM EDTA	
BJ Buffer for DNA Analysis	50 % (v/v) Glycerol 10 mM EDTA (pH 8.0) 0.2 % (w/v) Bromphenolblue 0.2 % (w/v) Xylencyanol	
1 % Agarose-Solution:	Agarose 100 ml TAE (1x) Ethidiumbromide-Solution	1 g 1 µl
Solution A	3 M NaAc (pH 5.5) 1 M $CaCl_2$ 2.8 M $MnCl_2$ H_2O	13 ml 100 ml 25 ml 862 ml
Solution A + Glycerol	Glycerol (87%) Solution A	69 ml 331 ml

2.1.11 Buffers for protein chemical methods

Buffer	Compounds	Quantities
SDS-Running Buffer (10x):	0.25 M Tris 2 M Glycine 1 % SDS	
Laemmli Sample Buffer (5x):	10 % (w/v) SDS 50 % (w/v) Glycerol 300 mM Tris 0.05 % (w/v) Bromphenolblue 5 % (w/v) b-Mercaptoethanol	
Western Blotting Transfer Buffer:	Glycine Tris Methanol H_2O	36 g 7.6 g 500 ml ad 2.5 l

Buffer	Compounds	Quantities
PBS (-T):	NaCl	5.84 g
	Na_2HPO_4	11.5 g
	NaH_2PO_4	2.96 g
	H_2O	ad 1 l
	Tween-20	1 ml

2.1.12 Devices

2.1.12.1 Absorptions spectrophotometer

- Varian Cary 50 Bio UV-Vis-Spectrophotometer, (Varian, Palo Alto, USA)
- Varian Cary 100 Bio UV-Vis-Spectrophotometer, (Varian, Palo Alto, USA)

2.1.12.2 Circulardichroism spectropolarimeter

- Jasco J715 including PTC 343 Peltier temperature device, (Jasco, Groß-Umstadt, Germany)

2.1.12.3 Fluorescence Spectrophotometer

- Spectrofluorometer: Fluoromax I, II and III (with autopolarizers) with temperature adjustable cuvette holder (Spex: Edison, USA)

2.1.12.4 Analytical ultracentrifuge

- XL-I equipped with absorbance and interference detection systems (BeckmanCoulter, Krefeld, Germany
- XL-A equipped with absorbance and fluorescence detection systems (BeckmanCoulter, Krefeld, Germany and AVIV Biomedical, Lakewood, USA)

2.1.12.5 Chromatography devices

- ÄKTA FPLC, (GE Healthcare, Freiburg Germany)

2.1.12.6 HPLC devices

- HPLC-Device (Jasco, Großumstadt, Germany)
  Pump system: PU-1580
  Fluorescence detector: FP-920
  UV-detector: UV-1575

2.1.12.7 Gel electrophoresis und blotting devices

- RHU10X (Roth, Karlsruhe, Germany)
- Hoefer Mighty Small II (GE Healthcare, Freiburg, Germany)
- Fast Blot B44 Apparatus (Biometra, Göttingen, Germany)
- Peqlab Gel apparatus P8DS for Novex-Tricin-Gele (Novex, Frankfurt, Germany)

2.1.12.8 Power amplifier

- LKB-GPS 200/400 (Amersham Bioscience, Freiburg, Germany)
- Pharmacia EPS 3500, 301 and EPS 1001 (GE Healthcare, Freiburg, Germany)

2.1.12.9 Scales

- BP 121 S (Satorius, Göttingen, Germany)
- BL 310 (Satorius, Göttingen, Germany)

2.1.12.10 Centrifuges

- Rotina 46 R Centrifuge (Hettich, Tuttlingen, Germany)

- Eppendorf-Centrifuge 5415 C (Hamburg, Germany)
- Avanti J25, JA-10 and JA-25.50-Rotor (Beckmann, Vienna, Austria)

2.1.12.11 Additional devices

- Varioklav EPZ H+P (Oberschleißheim, Germany)
- Ice maker Ziegra (Isernhagen, Germany)
- Electron microscope JEOL 100 CX JEOL (Munich, Germany)
- Eppendorf-Thermomixer Eppendorf (Hamburg, Germany)
- Certomat S Braun (Melsungen, Germany)
- Magnet stirrer Heidolph MR2000 Heidolph (Kehlheim, Germany)
- Metal Thermostat TB 1 Biometra (Göttingen, Germany)
- pH-Meter WTW (Weilheim, Germany)
- Thermo cycler MWG (Ebersberg, Germany)
- Ultra filtration cell 8050 Amicon (Danvers, USA)
- Sonifier B-12 Branson Company (Danbury, USA)
- Incubator New Brunswick Scientific (Nürtingen, Germany)
- Water bath Haake F6-K Haake (Karlsruhe, Germany)
- Cell Disruption Apparatus Basic Z Constant Systems (Warwick, UK)

2.1.13 Computer programs

Name	Origin
Adobe Photoshop CS	Adobe Systems (San Jose, USA)
Adobe Illustrator CS	Adobe Systems (San Jose, USA)
Borwin	Jasco (Großumstadt, Germany)
Berkeley Madonna	Robert I. Macey & George F. Oster (www.berkeleymadonna.com)
Microsoft Office 2007	Microsoft (Unterschleißheim, Germany)
Origin 7.5	Originlab (Northhampton, USA)
UltraScan 9.3	Borries Demeler (www.ultrascan.uthscsa.edu)
ProtParam Tool	ExPasy (www.expasy.org)
Reference Manager 10	ISI ResearchSoft (Berkeley, USA)
Endnoteweb	ISI ResearchSoft (Berkeley, USA)

2.2 Methods

2.2.1 Molecular Biology

2.2.1.1 Storage and cultivation of *E. coli*

E. coli was cultivated in a thermostated incubator at 37°C either on LB plates or in LB liquid medium. Strain selection was performed by antibiotica resistance. Resistance genes were either coded on the plasmid or in the genome of the respective strain.

Liquid cultures were inoculated 1:100 from fresh overnight cultures or by transferring single colonies from plates. Bacterial division was monitored at 600 nm. Alternatively, if large amounts of medium were inoculated, the overnight culture was centrifuged at 4000 rpm and the sedimented cells were washed and resuspended in fresh LB medium before inoculation (1 OD_{600nm} corresponding to approx. $8x10^8$ cells/ml) (Sambrook et al, 1989).

For long-term storage, 300 µl 50 % glycerol was added to 700 µl of a fresh culure resulting in a 15% glycerol culture stock. The culture was frozen using liquid nitrogen and stored at -80°C.

2.2.1.2 Storage and cultivation of *S. cerevisiae*

S. cerevisiae was cultivated at 30°C either on YPD plates or in YPD liquid media. Strains were selected by the lack of amino acids or nucleotides in the media, hence selecting strains containing the corresponding genes encoding for the missing amino acid or nucleotide. The complementation gene for amino acid synthesis was encoded on the plasmid. Liquid cultures were inoculated 1:100 using an overnight culture or by transferring a single colony from plates. Culture growth was monitored at 595 nm (OD595 nm corresponding to approx. $2x10^7$ cells/ml) (Walker, 1998).

For long term-storage, 5 ml of a freshly inoculated culture were sedimented at 2,000 x g and resuspended in 1 ml medium. 300 µl 50 % glycerol were added to 700 µl of

2.2.1.3 Transformation competent *E. coli*

Through chemical treatment *E. coli* cells can be transformed with an efficiency of 0.5 % (Hanahan, 1983). 5 mL of a stationary *E. coli* culture were used to inoculate 100 mL LB_0 medium. Growth was followed up to an OD_{600} to 0.5. Then 2 mL of a steril 2 M $MgCl_2$ was added. The cells were then incubated at 37° for 10 min and afterwards cooled on ice for 60 min. After gently harvesting the cells by centrifugation (3000 g, 5 min, 4°C) the cells were resuspended in Buffer A (3 M NaAc, pH 5.5, 1 M $CaCl_2$, 2.8 M $MnCl_2$). After 60 min incubation on ice cells were harvested gently by centrifugation at 4 °C (2000g, 10 min, 4°C). Treaded cells were gently resuspended in 4 mL Buffer A and 1 mL steril Glycerin 87% (v/v). Aliquots of 200 µL were frozen in liquid nitrogen and stored at -80°C until use.

2.2.1.4 Lithiumacetat-Methode to transform *S. cerevisiae*

To transform *S. cerevisiae* 100 ml of a culture in exponential growth phase were harvested by centrifugation (1000g for 10 min). The cells were washed 3 times with 100mM LiAc TE buffer. Cells were incubated in the LiAc TE buffer for 1 hour. Transformation was perfomed by mixing 5 µL (250 ng/µL) DNA and 50 µL cells and 5 µL salmon sperm DNA (Sigma-Adrich, Hamburg, Germany) with 40% PEG4000 in 100 mM LiAc TE buffer. This mixture was incubated at 30°C for 30 min. After application of a 15 minutes heat shock at 42°C, 1 ml sterile water was added. After harvesting by centrifugation at 1000g the cells were suspended in medium and plated on respective CSM selection medium.

2.2.1.5 Amplification of DNA

DNA amplication was performed by PCR methods (Mullis and Faloona, 1987). p23/Sba1 was intially cloned form yeast genomic DNA using respective

Oligonucleotides listed in table 1 allowing specific amplification of the DNA. Fragments of the p23 protein were planed on the DNA level using oligonucleotides that align inside the p23 gene at the respective site introducing a stop codon to create a shortend version of the p23/Sba1 gene. For these reactions the PWO polymerase was used. The Hsp90 wt plasmid which was a kind gift of Sebastian Wandinger which was used as starting material for site directed mutagenesis.
Typically the reaction was performed in the supplied buffer (containing $MgCl_2$) using oligonucleotides, nucleoside-tri-phosphates and template in the following amounts.

Template:	> 1 ng
Primers:	10 µM
NTPs:	200 µM

Typically the thermostated cycle for the amplification was started after heating to 95°C by addition of 0.5 U of the PWO polymerase to the reaction mixture. Usually 16-35 cycles were run that were designed as follows:

95°C	Denaturation for 20-30 s
55-65°C	Anealing for 5-10 s
68 or 72°C	Chain Elongation 1 min/ kb of DNA fragment

Site directed mutagenesis was performed using the quick change method. For the Hsp90 point mutated variants the N-terminal part and the C-terminal part from the site of mutation were generated using a PCR reaction with the exchanged codon in the primer. Then, in a following fusion PCR reaction N-terminal segment and C-terminal segment were fused containing the mutated site.

.

Primer	Sequence	Comment	Restriction site
P23Nde1forw	ggaatcccatatgtccgatwaaagttattaaccctcg	Sba1 forward Primer	Nde1
Sba1 Ser2cys	ggatctcattatgtgtgataaagttattaaccctcaagttgc	Sba1 forward Introduces Cys at position 2 for serin	
Spe1_SBA_forw	gactagtatgtccgataaagttattaaccctcaa	Sba1 forward	Spe1
Sba1 fwd	gtggatccatgtccgataaagttattaaccctcaag	Sba1 forward	BamH1
P23Bamh1rev1	Gatcggatcctcagctgaaatccattccttgagc	Sba1 reverse	BamH1
Not1_Sba_rev	ataagaatgcggccgcttaagctttcacttccggctcta	Sba1 reverse	Not1
Delta69rev	nnnnnngcggccgcttagctgaaatccattccttga	Reverse for the Δ69 Variant	BamH1
DELTA40rev	nnnnnngcggccgcttaagaaccagcgccaccagc	Reverese for the Δ40 variant	BamH1
N148p23	cgcggatccttaagccatatctggagaaccag	Reverse for the Δ69 Variant	BamH1
N167p23	cgcggatccttatttgaaatctcccatgtccaaa	Reverese for the Δ40 variant	BamH1
Not1_SBA_MDFSREV	ataagaatgcggccgcttagctgaatccatgcctccagc	Reverse for D40	Not1
Delta17rev	nnnnnngcggccgcttatttgaaatctcccatgtcc	Reverse for the Δ17 Sba1 variant	BamH1
Mbp_23for	cggaattcagccaaatgatgggaggtgctg	Fusion of the Sba1 C-tail to MBP	BamH1
Mbp-p23rev	cgggatccttaagctttcacttccggctctatttc	Fusion of the Sba1 C-tail to MBP	EcoR1
MUT P105G C-term	Gaatctgaatactgggga cgtttgacaaaggaa	Mutagenesis Oligo for P105G	
MUT P105A C-term	Gaatctgaatactgggca	Mutagenesis Oligo for	

Primer	Sequence	Comment	Restriction site
	cgtttgacaaaggaa	P105G	
Mut_SBA_I117A_for	gtgaagtacccttacgccaaaactgatt tcgata	Mutagenesis Oligo for Sba1 I117A	
Mut_SBA_I117V_for	gtgaagtacccttacgtaaaaactgattt cgata	Mutagenesis Oligo for Sba1 I117V	
Mut_SBA_I117A_rev	tatcgaaatcagttttggcgtaagggta cttcac	Mutagenesis Oligo for Sba1 I117A	
Mut_SBA_I177V_rev	tatcgaaatcagtttttacgtaagggtac ttcac	Mutagenesis Oligo for Sba1 I117V	
D61C_n	attggaaacagaaccatgtctctttatta gaatca	Mutagenesis Oligo for Hsp90 D61C	
D61C_c	tgattctaataaagagacatggttctgttt ccaat	Mutagenesis Oligo for Hsp90 D61C	
T159c_a	Aacgctggtggttctttctgtgttactct agacgaa	Mutagenesis Oligo for Hsp90 D159C	
T159C_b	aacttcgtctagagtaacacagaaaga accaccagc	Mutagenesis Oligo for Hsp90 D159C	
E183C_a	ttgaaagatgaccaattgtgttacttgga agaaaag	Mutagenesis Oligo for Hsp90 D183C	
E183c_b	tctcttttcttccaagtaacacaattggtc atcttt	Mutagenesis Oligo for Hsp90 D183C	
E333c_a	ggaccattcgacttgttttgtagtaaaaa gaagaag	Mutagenesis Oligo for Hsp90 D333C	
E333c_b	attcttcttcttctttttactacaaaacaag tcgaatgg	Mutagenesis Oligo for Hsp90 D333C	
Q385C_C	aaccttcatgatcttattacattgtaacat ttctctgga	Mutagenesis Oligo for Hsp90 D385C	
Q385C_N	tccagagaaatgttacaatgtaataaga tcatgaaggtt	Mutagenesis Oligo for Hsp90 D385C	
S411c_a	aacgaaattgctgaagactgtgaacaa tttgaaaag	Mutagenesis Oligo for Hsp90 D411C	
T433c_b	Aaagcagccctgttttgacaatcttcat gtacaccc	Mutagenesis Oligo for Hsp90 D433C	
S478C_a	tactacatcactggtgaatgtctaaagg	Mutagenesis Oligo for	

Primer	ctgtcgaa Sequence	Hsp90 D478C Comment	Restriction site
S478c_b	Cttttcgacagcctttagacattcacca gtgatgta	Mutagenesis Oligo for Hsp90 D478C	
T462C_a	tccttaactgattacgtttgtagaatgcc agaacac	Mutagenesis Oligo for Hsp90 D462C	
T462c_b	ttggtgttctggcattctacasaacgtaa tcagttaa	Mutagenesis Oligo for Hsp90 D462C	

2.2.2.1 Purification and restriction of DNA

Amplified DNA was purified as described in the QiaQuick Spin Handbook (Qiagen, Germany). Purified fragments were digested using the restriction enzymes Spe1/Not1 for p2HGAL, and Nde1/BamH1 for pET28b+ cloning, respectively (insert DNA: approx. 10 µg, restriction reaction buffer: 5 µl, restriction enzymes each: 2 Units, H_2O: add 50 µl, incubate for 2h at 37°C). Restriction reaction was stopped performing another purification step in accordance to the QiaQuick Spin Handbook.

2.2.2.2 Amplification and modification of Vector DNA

Vector DNA was amplified using *E. coli* DH10B. p2HGAL and pET28b+ were isolated from transformed *E. coli* DH10B in accordance to the QiaQuick Spin Handbook. Purified vector DNA was enzymatically modified as described above to match insert DNA modification.

2.2.2.3 Ligation of PCR products with Vector DNA

Insert DNA was ligated into the corresponding vector DNA resulting in the constructs listed on page 31 (vector DNA: 2 µl, insert DNA: 10 µl, ligation buffer: 2 µl, T4-ligase: 4 Units, H_2O: add 20 µl, incubate for 8h at 16°C). *E. coli* DH10B was transformed and selected on selective media. Ligation constructs were isolated in accordance to the QiaQuick Spin Handbook. Isolated DNA was stored at -20°C.

2.2.3 Protein chemical methods

2.2.3.1 Polyacrylamid gel electrophoresis

SDS-PAGE was performed in accordance to the protocol of Laemmli et al, 1970. SDS-PAGE gels were poured and contained the following compounds:

Separation gel:	X ml 40% Acrylamide (40% w/v, Acrylamide/Bisacrylamide 38:2)
	2.5 ml 4 x SDS-Buffer (0.8% SDS, 1.5 M Tris/HCl, pH 8.8)
	7.5-X ml bidest. H_2O
Stacking gel:	0.625ml 40% Acrylamide (40% w/v, Acrylamide/Bisacrylamide 38:2)
	2.5 ml 2 x SDS-Buffer (0.4% SDS, 0.25 M Tris/HCl, pH 6.8)
	1.875 ml bidest. H_2O

While X was varied to adjust the percentage of the acrylamide in the gel. Alternatively, a gradient gel was poured to analyse large complexes formed by cross-linking. In this case, a gradient acrylamide throughout the gel was created using a gradient mixing device supplied with a solution of 20 % acrylamid in the first chamber in contact with a secund chamber containing a 4 % Acrylamid solution under steady stiring the gel was poured. Polymerization of the solution was induced by adding TEMED and APS. Typically electrophoresis was carried out 30 mA for 1h. Gels were stained with Coomassie in accordance to the protocol of Fairbanks et al, 1972. When required, gels were silver-stained in accordance to the protocol of Heukeshoven et al, 1988.

2.2.3.2 Western blotting

SDS gels were performed as described above. Proteins were then blotted onto a PVDF membrane using 1.5 mA/cm² in a semi dry blotting apparatus for 50 min. Membranes were incubated with 5 % milk powder for at least 45 min to block free binding sites. Diluted primary antibodies (1:5000) were added, and incubated for 30 min. The membrane was washed briefly (3x5 min), and incubated with the secondary antibody (1:5000) for 30 min. Detection was carried out as described in the protocol of the ECL detection system.

2.2.3.3 Expression and purification of Hsp90 and variants

Hsp90 was expressed using the BL21(DE3) cod^+ strain and the Hsp90 gene with a N-terminal 6xHis-tag coded on a $pET28b^+$ vector. Expression was run on a 10 L scale. After inoculation and growth to a OD of 0,8, cells were cooled to 30° C. Expression was induced by addition of 1 mM IPTG. Harvesting was performed by centrifugation at 6000 rpm after 5-8 hours of expression.
Cells were resuspended in buffer A) and lysed after addition of protease inhibitor mix (EDTA-free) by french press.
Lysate was centrifuged for 45 min at 25000 rpm in a JA 25.20 rotor in a Beckmann centrifuge. The supernatant was loaded on a Ni-NTA column.

Buffer A)	50 mM	Na-Phosphate
	300 mM	NaCl
	ph 7.8	
Buffer B)	50 mM	Na-Phosphate
	300 mM	NaCl
	300 mM	Imidazol
	pH7.8	

Before elution, the column was washed extensively (20-30 times the column volume) using a concentration of imidazole of 50 mM. Then step elution was performed to

obtain a concentrated eluate using 300 mM Imidazol. Dialysis was performed using Buffer C) .

Buffer C)	40 mM	Hepes / KOH
	20 mM	KCl
	1 mM	DTT
	pH 7.5	

The dialysed protein was applied on a Q-Sepharose equilibrated with buffer C). A buffer with the same chemical composition but with 1 M KCl (Buffer D) was used to resolve the protein. Hsp90 elutes at a salt concentration of 300 mM under these conditions. Thus, a gradient was applied using a steep ramp up to 150 mM KCl and then a ramp of 10 times the column volume to 500 mM KCl in which fractionation occurs. Fractions were analysed by SDS page. The fractions containing Hsp90 were pooled and concentrated. The concentrate was applied to size exclusion chromatography using a prepacked Superdex 200 column and buffer E).

40 mM	Hepes / KOH
300 mM	KCl
5 mM	DTT
pH 7.5	

Purity was judged by SDS-PAGE analysis and determination of the ATPase background activity using the Hsp90 inhibitor radicicol (Sigma-Aldrich, Hamburg). If purity was not sufficient at this stage, a hydroxy apatide column was used to resolve last contaminations using a gradient comparable to that for the Q-sepharose column but with the buffers F and G.

Buffer F)	50 mM	Sodium Phosphate
	1 mM	DTT
	pH 7.7	

Buffer G)	1 M	Sodium Phosphate
	1 mM	DTT
	pH 7.7	

After purification, Hsp90 variants were concentrated to 50 µM and dialysis was perfomed using Buffer C) which can be used to store the protein at -80°C after freezing in fluid nitrogen.

2.2.3.4 Expression and purification of p23 variants

p23 variants were purified using a similar strategy as for Hsp90 proteins using the pET28 b^+ coded N-terminal His-tag, a Q-Sepharose column and a Superdex 75 column. Expression was performed in BL21 (DE3) cells and expression time after induction with 1 mM IPTG can be extended to 12-14 hours. Purity was analysed by SDS PAGE. The correct size of the protein was determined by MALDI TOF Mass spectrometry.

2.2.3.5 Protein labelling

Hsp90 was labelled with fluorescent dyes to analyse kinetics of conformational changes that change the distance between the fluorophores. p23 was labelled with fluorescein iodoacetamide to perform in solution binding studies.

Labelling was performed in a 5-10 mg scale. The protein was reduced for 30 min at room temperature by addition of DTT to a concentration of 10 mM. DTT was removed from the protein using a G25 desalting column with a bead size volume of 15 mL. Directly after elution, the protein was gently mixed with a 5 fold molar excess of label. Depending on the reactive group of the label, the reaction was performed in 40 mM Hepes pH 7.2 for iod-acedamide reactions or in 40 mM Hepes pH 7.8 for the malimide reactive group (**Figure 12**).

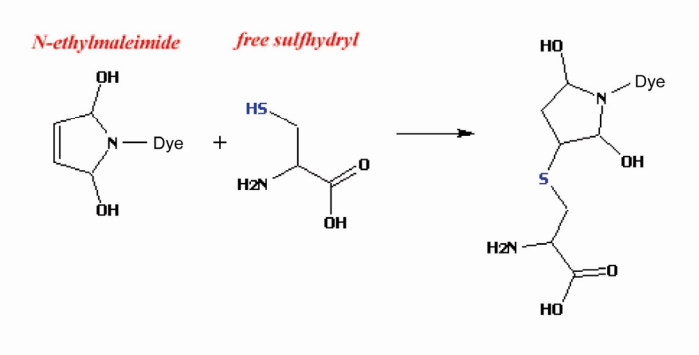

Figure 12: Reaction schema for the modification of sulfhydryl groups using maleimide chemistry. Using maleimide derivatives gives highest specificities for cysteines.

After 1 h labelling at room temperature, the educt of the label was modified and the reaction blocked by adding 10 mM DTT. The reaction mixture was again applied on a G25 desalting column to separate the free label form the protein-flurophore conjugate. Labelling efficiency was calculated form absorption spectra recorded from the modified protein as described by the manufactor´s protocol. Whether the protein-fluorophore conjugates are contaminated by free label was analysed by size exclusion chromatography.

2.2.4 Spectroscopy

2.2.4.1 Absorbance spectroscopy (UV-VIS)

Proteins and peptides contain two important functional groups that absorb UV light (Hesse, 1991; Galla, 1988). Amid groups like those forming the peptide bond absorb at 180 to 240 nm. At 250 to 300 nm the aromatic amino acids namely phenylalanine, tyrosine and tryptophan absorb.
Table 1 summarizes the absorbance properties of the aromatic amino acids and disulfide bonds.

Table 1 Summary of UV spectroscopic properties of the aromatic amino acids tryptophan, tyrosine, phenylalanine and disulfide bonds including the absorbance maxima and extinction coefficients (Schmid and Creighton, 1989).

Amino acid	λ_{max} (nm)	ε_{max} (M^{-1} cm^{-1})
Tryptophan	280	5700
Tyrosine	274	1400
Phenylalanine	257	200
Disulfide bond	250	300

* λ_{max}: Absorbance maximum, ε_{max}: Molar extension coefficient

UV spectroscopy was used to determine the concentration of a protein solution exclusively. The law of Lambert-Beer correlates the protein concentration with the measured absorbance.

$$A = \varepsilon \times c \times d$$

Equation 1 The law of Lambert-Beer, A: Absorbance, ε: molar extinction coefficient (M^{-1} x cm^{-1}), c: molar protein concentration (M), d: layer thickness (cm)

The extinction coefficient at 280 nm is in a first approximation the weighted (by using the table above) sum of the number of the aromatic residues in the protein sequence (Gill and von Hippel, 1989). However, in some cases, absorption can vary by solvent polarity. It is useful to measure the absorption in denaturant and under native conditions to determine the impact of solvent polarity on the particular protein of interest. The used extinction coefficients at 280 of all proteins were determined by protparam, a tool form www.expasy.org.

2.2.4.2 Fluorescence Spectroscopy

When chromophores absorb light, their electronic state transits form a ground state (s_0: $singlet_0$) to an exited state (s_1 :$singlet_1$). When the exited state relaxes back to the ground state, the energy difference between the exited and the ground state needs to be released. This energy can be transferred to vibration energy of the same or another molecule (solvent or quencher) or the energy is released by emission of a photon. The wavelength of the emitted light corresponds to the energy difference between the exited and ground state. This phenomenon is called fluorescence (Lakowicz, 1999). The wavelength of the emitted light is red shifted due to vibration energy and changing solvent interactions of the excited state. This vibration energy relaxes to the vibration ground state of the electronically exited state (s_1) from which the light is emitted and the system relaxes back to the electronic ground state (s_0). The life time of the exited state is on the ns timescale.

Different experiments can be performed using fluorescence. In proteins, tyrosine and tryptophan residues are the predominantly fluorescent amino acids. Especially tryptophan is a useful tool in protein biophysics. Its fluorescence is strongly depending on the polarity of the solvent. If unfolding occurs, the fluorescence is often shifted to longer wavelengths if the polarity surrounding the tryptophan increases (Schmid, 1998). Usually tryptophan is buried in the hydrophobic interior of folded proteins but in the unfolded state tryptophan becomes exposed to the solvent changing the fluorescence properties. In addition to the bathochrome shift in fluorescence spectra quenching is often observed in the unfolded state. Thus, the

folding equilibrium of a protein can be characterised by fluorescence spectroscopy (Eftink, 1998; Bolen and Santoro, 1988; Santoro and Bolen, 1988).
Binding of nucleotides to the N-terminal domain of Hsp90 can be measured using fluorescence. When nucleotides bind, the fluorescence is quenched significantly. This can be used in titration experiments with nucleotides (Leskovar et al, 2008). However care must be taken due to the overlap of absorption spectra for nucleotides and tryptophan causing a large reduction of light passing through the cuvette and thus affecting excitation of tryptophan. This effect is called the inner filter effect. For titrations with nucleotides, tryptophan can be exited at a wavelength above 295 nm to circumvent the problem.

2.2.4.3 Fluorescence anisotropy

If fluorophores are not fixed or if they are not in a very viscous environment, rotation and diffusion take place in timescales that are comparable to that of the exited state lifetime. When polarized light (oriented parallel to z-axis) is used to excite the molecule, depolarisation occurs due to the tumbling (and other processes) which depends on the size of the molecule. If the molecule is recruited into a larger complex then depolarisation is less pronounced. Here, the anisotropy (r) is used to plot the measured data (Lakowicz, 1999).

$$r = \frac{\mathrm{I_{parallel}} - \mathrm{I_{perpendicular}}}{\text{total Fluorescence}}$$

Equation 2: Fluorescence anisotropy is r: $I_{parallel}$ defines the fluorescence intensity in the polarization oriantation parallel to the z-axis; $I_{perpendicular}$ is the fluorescence intensity in the polarization direction perpendicular to the z axis. The difference is divided by the total fluorescence intensity.

p23 was modified at an engineered site (Cys2) with idoacetamido-fluorescein to follow binding reactions with Hsp90. Fluorescein was excited at 490 nm and the emission was measured at 520 nm. Slits were 2 nm band pass for the excitation monochromator and 5 for the emission monochromator. Measurements were performed in 40 mM Hepes, 150 mM Kl and 5 mM $MgCl_2$ pH 7.5 buffer.

Titrations were done in a competitive way. In the beginning p23-fluoresein (300 nM) was incubated with 1 µM Hsp90 and 2 mM AMP-PNP to form a complex (+/- substrates). Then unlabelled p23 were titrated, displacing the specifically bound p23-fluorescein from the binding site on Hsp90. The change in anisotropy can be correlated to the binding.
If kinetics were measured, Hsp90 and p23-fluorescein were preincubated in the described buffer at the desired temperature. Then the kinetic was started by adding 2 mM of the respective nucleotide.

2.2.4.4 Fluorescence resonance energy transfer

In FRET experiments a part of the exited donor flurophore transfers the excited state energy to an acceptor flurophore. This process is radiation-free and depends on three factors. First, it is necessary that the emission spectrum of the donor flurophore overlaps the absorption spectrum of the acceptor flurophore. Second, the transition dipolmoment of donor and acceptor have to be oriented parallel to each other to guarantee transfer. And third, the distance between donor and acceptor flurophore have to be below a certain upper limit. Interestingly, this dependence of the distance renders FRET useful to analyse conformational changes in proteins. The Förster radius is the distance between the flurophores at which 50% of the energy is transferred. The Förster radius can be determined form the quantum yield of the donor and the overlap integral form the donor emission and acceptor absorption spectrum. Making further assumptions about the orientation of the labels to each other, the distance between the flurophores can be calculated from the transfer efficiency.

$$E_T = \frac{R_0^6}{R_0^6 + r^6} = 1 - \frac{F_{DA}}{F_D}$$

Equation 3 The FRET efficiency (E_T), depends on the sixth power of the distance (r) between the donor and the acceptor chromophor given by the Förster radius R_0. R_0 is defined at the distance (r) between both chromophors that leads to 50% elimination of the donor fluorescence in the presence of the acceptor (F_{DA}) compared to the fluorescence in the absence of the acceptor (F_D).

FRET experiments were performed for the kinetic analysis of conformational changes in Hsp90 and in p23 binding experiments. For these experiments the distance was not calculated between the flurophores (Lakowicz, 1999).
In all experiments a buffer of 40 mM Hepes, 150 mM KCl and 5 mM $MgCl_2$ pH 7.5 was used. The concentrations of donor- and acceptor-labelled Hsp90 proteins were 200 nM. In experiments in which the double-labelled Hsp90 variant was used, the concentration of the labelled protein was 200 nM that of the unlabeled subunit was 3-5 µM.
p23 binding was monitored using the p23-fluorescein labelled variant in combination with the Hsp90C385-ATTO550 variant. In these experiments, 500 nM Hsp90C385-ATTO550 was used and 200 nM p23-fluorescein in the presence and absence of CS using AMP-PNP to follow complex formation.

2.2.4.5 CD Spectroscopy

Circula dicroism is a feature of obtical acitve substances that absorb light, when a Cotton effect is found in polarimitry. This effect is due to an different absorbtion of left and right circular polarised light. Proteins consist of optical active amino acids, hence displaying optical activity and show absorbtion (Fasman, 1996). Two regions can be distinguished: The near UV (350–250 nm) at which the aromatic residues absorb and far UV (260-170 nm) regions in which the peptide bond contributes predominantly to the signal. Near UV-CD spectroscopy delivers information about asymmetrically arranged aromatic rings, displaying a specific spectrum for each

protein (protein finger-print). The signal depends on the tertiary environment of the aromatic residues.

In far UV CD the conformation of the polypeptide displays characteristic signals, due to the differential absorption of the polypeptide backbone, placed in an asymmetric environment. α-helices e.g. shows two characteristic minima at 222 and 208 nm. β-sheet structure shows a less intense signal with a single minimum at 218 nm. Far CD spectroscopy can be used for secondary structure investigations. The mean residue elipticity can be obtained form the measured data using equation 4.

$$\Theta_{MRW} = \frac{\Theta \times 100 \times M}{d \times c \times N_{aa}}$$

Equation 4 Θ_{MRW} = mean residue ellipticity, Θ = obtained elipticity, M = molecular mass (g/mol), d = layer thickness (cm), c = concentration (mg/ml), N_{aa} = number of amino acids

For secondary structure analysis, p23 was dialysed against 10 mM sodium phosphate, pH 7.5, at 4°C over night. Afterwards the protein concentration was determined by UV-spectroscopy. CD spectra were acquired using a final concentration of 0.1 mg/ml in a 1 mm cuvette. Parameters for acquirements were set to a wavelength range of 250-185 nm, 20 nm/sec, 6 accumulations. Data were buffer-corrected and converted into mean residue elipticity using Equation 4. To exclude the posibilty that the positive signal at 230 is due to cystein oxidation, the protein was reduced before the experiment.

2.2.5 Temperature unfolding of p23 measured by CD spectroscopy

Thermal stability of p23 was analysed using CD-Spectroscopy. Protein concentration was adjusted to a final concentration of 0.1 mg/ml in 10 mM sodium phosphate, pH 7.5 using a 1 mm cuvette. Thermal transitions were monitored at a constant wavelength corresüonding to the maximum in signal change (230 nm). The transition was monitored over a temperature range from 10-95°C. Acquiring parameters were

set to a thermal gradient of 10°C/h. Acquired data were converted into mean residue elipticity (Equation) and plotted and analysed with Equation (Fersht, 1997).

$$y(T) = \frac{y_N - (y_N - y_U)}{1 + \exp^{\frac{-\Delta G(T)}{RT}}}$$

$$y_N = y_N^0 + m_N \times T$$

$$y_U = y_U^0 + m_U \times T$$

$$\Delta G(T) = \Delta H(1 - \frac{T}{T_M}) - \Delta C_P(T_M - T + T \ln \frac{T}{T_M})$$

Equation 5 Equation for non-linear thermal transition regression; y(T): regression as the function of the temperature; y_N: signal for the natively folded protein, y_U: signal for the unfolded protein; y^0_N and y^0_U represent the regressed values of y_N and y_U, to T = 0 K; m determines the corresponding slopes; T_M: midpoint of thermal transition; ΔH: van't Hoff-enthalpy in T_M; ΔC_p: change in temperature capacity correlated to the unfolding process.

2.2.6 Temperature unfolding of p23 measured by Differential scanning calorimitry (DSC)

DSC measures the heat absorbed by a protein while heating a sample in reference to a buffer cell. The change in heat absorption between the reference and the sample cell is analysed. Protein folding is a highly endothermic process. As the protein structure begins to melt at its Tm, the sample cell absorbs more heat than the reverence cell. The heat energy flux is ΔH_{Cal}. By subtraction of the baseline and integration of the measured heat capacity ΔH is directly accessible (Equation 6) (Fersht, 1997). The Tm is the maximum of the heat capacity in the transition region.

$$\Delta H_{cal} = \int \Delta C_{p,cal}(T) dT$$

Equation 6: ΔH_{cal} is the measured enthalpy of the unfolding process, $\Delta C_{p,cal}$ is the measured heat capacity change in the transition region.
The temperature unfolding of p23 is irreversible. Thus the van´t Hoff enthalpy cannot be derived from temperature unfolding experiments with p23. p23 variants have been characterized in the same buffer as the CD data were generated for a good comparison at concentrations between 10 and 50 µM.

2.2.7 Surface Plasmon Resonance Spectroscopy

Surface plasmon resonance spectroscopy is a useful tool to characterise interaction reactions in biochemistry. Irradiation occurs at an incident angle that gives total reflection on a glass plate. This glass plate is coated with a thin layer of gold introducing a conducting material. In such a system the polarised component of light in the direction of the interface can interact and excite the electrons in the conducting band of the gold material. This leads to a loss of reflection intensity at the exact resonance conditions for the excitation of the electrons in the conducting material (plasmons) producing an evanescent field. Resonance conditions depend on i) the angle of incidence, ii) the wavelength and iii) interestingly, on the refractive index of the medium in a certain distance from the gold that is not illuminated. The distance that plays a role to influence the refractive index is defined by the range of the evanescent field that attenuates within the length of one wavelength and though reaches only 600 nm into the medium. Macromolecules near the gold coating thus influence the refractive index and changes in resonance conditions can be used to measure the concentration of a macromolecule in the evanescent field. The signal measured is resonance units (RU) is directly correlated to the amount of protein bound (typically 1,000 RU = 1 ng bound protein mm^{-2}).

Here p23 was immobilized on the gold surface on which carboxymethylated dextran is coupled. This was performed using a method to acitvate the carboxyl groups on the surface using 50 mM N-hydroxy-succimid and 200 mM 1-Ethyl-3-(dimethylaminopropyl)-cardodiimid-HCl (EDC) then p23 was incubated on the activated surface at pH 4.0. A maximum of 1,000 RU were coupled to the surface, then the surface was inactivated using Ethanolamine.

For the measurements the buffer 40 mM Hepes, 150 mM KCl, 5 mM $MgCl_2$ pH 7.5 was used. Various concentrations of Hsp90 were injected after the samples were incubated with 2 mM AMP-PNP for at least 20 min. In addition competitive measurements were performed at which constant amounts of Hsp90 pre-incubated with AMP-PNP were injected with varying concentrations of p23 variants to determine the K_d values of the p23Δ69C variant.

2.3 Analytical ultracentrifugation

Analytical ultracentrifugation (AUC) consists of the application of centrifugal force with the simultaneous real-time observation of the sedimentation of macromolecules in the centrifugal field. Since proteins are studied in solution, AUC allows their hydrodynamic and thermodynamic characterization in solution, without interaction with any matrix or surface. There are two basic types of ultracentrifugation experiments for the characterization of proteins: sedimentation velocity (SV) and sedimentation equilibrium (SE) methods, which are described in the following sections (Rowe J.A., 2005).

In a sedimentation velocity experiment, application of a sufficiently large centrifugal force field leads to the movement of molecules toward the bottom of the centrifuge cell. The sedimentation process is determined by three factors – the gravitational force, the buoyancy and the hydrodynamic friction. Since the gravitational force is proportional to the square of the rotor speed, adjusting the rotor speed allows the study of a wide range of particle sizes, ranging from kDa to GDa molecular weights. From the balance of these three forces, one can derive the Svedberg equation (Equation 6).

$$s = \frac{v}{\omega^2 r} = \frac{MD(1-\overline{V}\rho)}{RT}$$

Equation 6 Svedberg equation. s = sedimentation coefficient (s), v = observed radial velocity (m/s), ω = angular velocity of the rotor (m/s^2), $\omega^2 r$ = centrifugal field, M = molar mass (g/mol), $\overline{V}$ = partial specific volume (cm^3/g), ρ = density of the solvent (g/cm^3), D = diffusion coefficient (m^2/s), R = gas constant (8.314472 J/K mol), T = absolute temperature (K).

The sedimentation coefficient represents the sedimentation velocity v in relation to the centrifugal field $\omega^2 r$. The s-values are commonly reported in Svedberg (S) units, which correspond to 10^{-13} s.

When the centrifugal force is sufficiently small, the process of diffusion significantly opposes the process of sedimentation, and an equilibrium concentration distribution

of macromolecules is obtained throughout the cell. For an ideal non-interacting single component system, the equilibrium distribution is an exponential function of the buoyant mass of the molecule, $M(1-\overline{V}\rho)$, as described by Equation 7.

$$c(r) = c_0 \cdot e^{\frac{M(1-\overline{V}\rho)\cdot\omega^2(r^2-r_0^2)}{2RT}}$$

Equation 7 $c(r)$ = sample concentration at radial position r, c_0 = sample concentration at reference radial distance r_0, $\overline{V}$ = partial specific volume, ω = angular velocity of the rotor, R = gas constant, T = absolute temperature

Sedimentation equilibrium experiments provide an accurate way to determine the molecular weight (M) and consequently the oligomeric state of macromolecules. In contrast to other techniques, such as analytical gel filtration, SE experiments are not subject to assumptions of globular shape or limitations by matrix interactions. For p23 this kind of analysis was performed by Klaus Richter. p23 was found to be a monomer.

Sedimentation Velocity Experiments

Sedimentation velocity (SV) experiments were carried out with a Beckman XL-I analytical ultracentrifuge equipped with an AN-60Ti four hole rotor and cells with two-channel 12-mm path length centrepieces. Sample volumes of 375 µl were centrifuged at 42,000 rpm.

SV data were analysed using the software package UltraScan (http://www.ultrascan.uthscsa.edu). The c(s) distribution, which is a distribution of sedimenting species taking into account their diffusion, was used to calculate hydrodynamic parameters.

2.4 Functional assays

2.4.1 Regenerative ATPase Assay

The ATPase activity of Hsp90 was characterized using an assay that is coupled to NADH consumption. The formed ADP is directly converted back to ATP by the pyruvate kinase reaction that uses ADP and phosphoenoylpyruvate to create ATP and pyruvate (Ali et al, 1993). This reaction is close to irreversibility as the reaction clearly favours formation of ATP and pyruvate. The lactate dehydrogenase reaction is used to couple the reaction to NADH consumption. Absorption at 340 nm is used to follow the consumption of NADH and though indirectly the consumption of ATP. The buffer was 40 mM Hepes, 150 mM KCl, 5 mM $MgCl_2$ pH 7.5 containing 2.5 mM posphoenolpyruvate, 200 µM NADH, a 1 to 750 dilution of the pyruvate kinase suspension (Roche, Manheim, Germany) and a 1 to 200 dilution of the lactate dehydrogenase suspension. In general, the following premix was used for the reactions:

8500 µl	buffer
240 µl	100 mM phosphoenolpyruvate
35 µl	50 mM NADH
12 µl	pyruvatkinase-suspension
44 µl	lactate dehydrogenase-suspension

The reaction was usually performed at 30°C. Premix and desired ATP concentration were mixed in in a 120 µL reaction mixture. In general, the reaction was started by adding Hsp90 to the cuvette.

It is useful for the comparism of modified proteins to the wild type protein to use the specific enzymatic activity. The specific enzymatic activity was calculated using the exstinction coefficient of NADH of 6200 $M^{-1}cm^{-1}$ and the respective Hsp90 concentration used in the reaction.

For the analysis of co-chaperone effects on the ATPase acitivy of Hsp90, a constant amount of Hsp90 was incubated with varying amount of co-chaperone.
For determination of the K_M value of Hsp90, different ATP concentrations were used concentration dependency of the activity was defined. The formula to fit these data was:

$$v_{spez} = k_{cat} \cdot \frac{c}{c + K_M}$$

Equation 8: v_{spez} is the specific maximal enzymatic activity. k_{cat} is the catalytic turnover number of Hsp90, c is the ATP concentration and K_M is the K_M value (half maximal activity).

2.4.2 Posphorylase based ATPase assay

To analyse the impact of the presence of ADP on the Hsp90 ATPase activity another assay is required, as ADP would immediately be converted to ATP by the regenerative system. The influence of ADP is a very important issue still under discussion in literature (Southworth and Agard, 2008; Shiau et al, 2006). Therefore the EnzChek (Molecular Probes, Leiden, Netherlands) was used. Basically, the assay relies on a single enzyme, the purin-nucleosid-phosphorylase which cleaves a chromogenic substrate (2-amino-6-mercapto-7-methylpurinriboside, MESG) using phosphate that originates from the cleaved ATP. The reaction shifts the absorption maximum from 330 nm to 360 nm. This wavelength was used to follow the reaction.
The substrate is consumed during the reaction. Thus the initial slope is used to correlate the enzymatic activity with the initial ATP concentration.
To analyse the impact of ADP increasing concentration of ADP were added to Hsp90. Permutations were assayed varying both ADP and ATP. The activity decreases with increasing ADP concentrations. The inhibition constants were determined by fitting to the equation.

$$v = v_{app}\left(1 - \frac{[\mathrm{ADP}]}{[ADP\}+K_{i,app}}\right)$$

Equation 9: v is the velocity of the reaction at the respective ADP concentration [ADP], v_{app} is the maximal activity at the respective ATP concentration, $K_{i,\,app}$ is the the apparent binding constant of ADP which leads to inhibition of Hsp90.

Then the apparent K_i values were plotted in a secondary plot versus the respective ATP concentration used and fitted to a linear equation. The intercept of the y-axis gives the K_D value of ADP.

2.4.3 Citric acid synthase activity assay

Citric acid synthase (CS) catalyses the condensation of oxalacetate and acetyl-CoA consuming the high energy thio-ester bond. The products of the enzyme reaction are citrate and free CoA. CS has a molecular mass of 49 kDa and forms homodimeres. Unfolding takes place at temperatures above 43°C leading to a loss of activity and later on to the aggregation of CS (Buchner et al, 1998).
The reaction of the CS can be followed by using DTNB (5,5´-dithio-bis-2-nitrobenzoic acid) to follow the increase in free sulfhydryl groups from the formed free CoA.

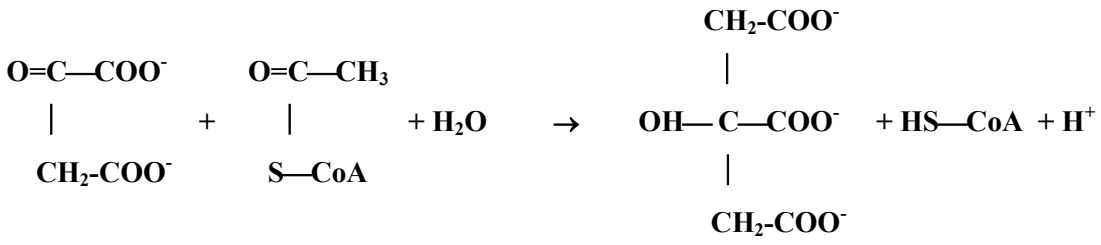

Oxalacetat + Acetyl-CoA → Citrate + CoenzymA

At 412 nm the formed thiobenzols can be detected. The initial slop is proportional to the activity of the enzyme. When CS is incubated at a temperature of 43°C, the activity will decrease over time. The rate of the activity decrease is the temperature inactivation rate which is correlated to the unfolding of the protein.
This activity assay was used to analyse the impact of p23 on the temperature-induced unfolding behaviour. A test solution was prepared using a CS concentration of 150 nM, p23 variants were included like indicated. Reaction mixtures were incubated at 25°C in the cuvettes. The typical reaction mixture was:

0,93 ml 50 mM TE-buffer pH 8,0
0,01 ml 10 mM DTNB (in TE-buffer pH 8,0)
0,01 ml 10 mM Oxalacetat (in 50 mM Tris/Base)
0,03 ml 5 mM Acetyl-CoA (in TE-buffer pH 8,0)

After varying times, aliquots from the CS test mixture incubating at 43°C were mixed with the preincubated reaction mixture to assay the activity. The activity without incubation at 43°C was set to 100% native protein. The specific activity of CS can be calculated using the extinction coefficient of the reacted DTNB of 13,600 $M^{-1}cm^{-1}$.

2.4.4 Inactivation of the p53 DNA binding domain

The DNA binding domain of p53; that was refolded and purified form inclusion bodies using the protocol of Christian Klein, was used as a substrate of the Hsp90 system. At elevated temperatures of 38°C in buffer containing 40 mM Hepes, 150 mM KCl at pH 7.5, the DNA binding domain looses its DNA interacting activity over time (Butler and Loh, 2006). The p53 DNA binding domain is bound by p23 or Hsp90 and can be partially rescued from rapid thermal unfolding. The binding activity was assayed using Cy5-labelled p53 DNA with the consensus sequence of the response element. In addition unlabelled unspecific single stranded DNA (poly dI-dC competitor DNA) was added to prevent unspecific sticking of the p53 protein. The mixture was loaded on a 4 % native acrylamide gel that had been prepared was poured by the following schema.

40 mM Hepes, 100 mM KCl pH 7.5
exces of poly dI-dC competitor DNA
500 nM labeled con DNA
Aliquot from inactivating p53 mixture

2.4.5 Protein aggregation

Thermal aggregation of proteins was used to analyse the chaperone function of Hsp90 and p23. At elevated temperatures, proteins unfold and tend to aggregate. Binding of chaperones to unfolded chains or unfolding intermediates leads to a prevention of aggregation and enhances the stability of the respective protein (Buchner et al, 1998).

The aggregation process can be analysed qualitatively by determining the amount of light scattered at a wavelength of 340 nm. However, aggregate composition and homogeneity cannot be addressed by this approach.

The scattered light can be measured directly using a fluorescence spectrometer or using turbidimitry in a UV-Vis spectrometer. Usually, the buffer used was 40 mM Hepes pH 7.5. The proteins CS, p53 DNA binding domain and glutamate dehydrogenase (GDH) were used in such assays. The temperatures used to were 43°C, 40°C, and 45°C for 500 nM CS, 500 nM p53 DNA binding domain and 1 µM GDH, respectively.

2.4.6 Modified ELISA to detect Hsp90 binding

Sti1, BSA and the p53 DNA binding domain were incubated at a concentration of 5 µM in a 96 well plate pre-treated for protein immobilisation at 4° C over night. After washing 3 times with PBS buffer Hsp90 labelled with fluorescein or tetramethylrhodamine were incubated in wells in 40 mM Hepes 50 mM KCl 5 mM $MgCl_2$ at pH p7.5. After additional washing steps, the fluorescence intensity was measured in each well with a Typhoon fluorescence scanner (GE, Munich, Germany). The amount of bound Hsp90 molecules correlates with to the binding affinity for the coated protein. Sti1, a known TPR co-chaperone of Hsp90, was used as a positive control in that assay. The K_D value is in the nM range (Richter et al, 2003; Prodromou et al, 1999) and can be reproduced by this assay. Thus proteins seem to retain a functional conformation on the surface of the elisa plates.

2.4.7 Protease-Coupled PPIase Assay

FKBP PPIase activities were measured as described previously (Pirkl and Buchner, 2001; Fischer et al, 1984). The synthetic peptide substrates were N-succinyl-Ala-Ile-Pro-Phe-p-nitroanilide and N-succinyl-Ala-Leu-Pro-Phe-p-nitroanilide. Assay mixtures contained purified recombinant FKBP (10–150 nM final concentration), substrate peptide (50 μM), and chymotrypsin (1 mg/ml) in 40mM HEPES (pH 7.5) at 10 C. Because chymotrypsin cleaves only the peptide amide bond preceding the proline moiety in its trans conformation, cis-trans proline isomerization becomes rate limiting for cis peptide cleavage. The generation of the free chromophore p-nitroanilide, which absorbs at 390 nm was monitored in a UV-Vis Spectrometer. Kinetic traces were fitted to a single exponential equation with floating end point with origin 7.5. The experimentally observed rate (k_{obs}) values were plotted against FKBP52 concentration and fitted by a linear regression to determine the specificity constants using origin 7.5.

2.5 Data analysis

Interaction data

Binding isotherms recorded by SPR spectroscopy and fluorescence anisotropy were plotted using the Origin 7.5 software. To fit the data, two equations were used. For low affinity interaction with a K_D above the protein concentration used, an equation can be used that neglects ligand depletion by the binding reaction.

$$S = \frac{S_{max} \times [\text{Ligand}]}{[\text{Ligand}] \times K_D}$$

Equation 10: S is the signal as a function of the ligand concentration ([Ligand]), S_{max} is the signal at saturation with the ligand, K_D is the dissociation constant of the protein ligand complex.

For high affinity interactions depletion of the ligand and protein need to be considered. Although the Hsp90 concentration is known, in some cases the value of

the protein concentration was included as a fitting parameter as conformation specificity of the co-chaperones can affect the stoichiometries.

$$S = S_{protein} + \left(S_{complex} - S_{protein}\right) \cdot \frac{M_t + L_t + K_D - \sqrt{\left(M_t + L_t + K_D\right)^2 - 4 \cdot M_t \cdot L_t}}{2 \cdot M_t}$$

Equation 11: S is the signal as a function of protein and ligand concentration M_t and L_t, respectively. K_D is the dissociation constant.

Kinetics

The kinetic analysis of p23 binding and Hsp90 conformational changes as well as subunit exchange data were analysed by fitting to single or double exponential decay functions. FRET kinetics however cannot in full be explained by these functions but seem to describe the dataset well for the slow phases in the progress curves. Thus temperature depend measurements could be performed.

$$S(t) = S_A - S_B \times e^{-k_B \times t}$$

Equation 12: Single exponential decay function: S(t) means the signal that changes with time (t). S_A is the initial signal S_B is the amplitude of the kinetic process that changes with the rate constant k_B

$$S(t) = S_A - S_B \times e^{-k_B \times t} - S_C \times e^{-k_C \times t}$$

Equation 13: Double exponential decay function: S(t) is the signal that changes with time (t). S_A is the initial signal intensity; S_B and S_C are the corresponding amplitudes of the kinetic processes occurring with rate constant k_B and k_C respectively.

The temperature dependence of kinetic data were analysed using the Eyring equation in a linear form. It is assumed that kinetic processes have an energy barrier that needs to be passed. A pseudo equilibrium is assumed between the educt state and the transition state at high energy. The state at high energy is very unstable and reacts with a certain frequency to the products or back to the educts. This frequency depends on the temperature, the Bolzmann constant and Planck´s constant. To describe the productivity of the reaction an additional factor for the likelyhood of a productive decomposition of the transition state to form the product state is included.

$$k_B = \frac{\vartheta \times \mathrm{k} \times \mathrm{T}}{\mathrm{h}} e^{\frac{\Delta \mathrm{G}^*}{\mathrm{RT}}}$$

Eqution 14: The Eyring equation describes the connection between the rate constant of a reaction and the activation enthalpy. kB is the rate constant, ϑ is the factor to describe likelihood of a productive reaction, k is the Bolzman constant, T the absolute temperature, h the Plank constant, ΔG^* is the enthalpy of activation and R is the gas constant.

The linear form of equation 14 is used to analyse the ploted data.

$$\lg \frac{k_B}{\mathrm{T}} = 10.573 + \frac{\Delta S^*}{19.12} - \frac{\Delta H^*}{19.12\mathrm{T}}$$

Equation 15: The linear form oft he Eyring equation. ΔH^* and ΔS^* are the activation enthalpy and entropy, respectively.

2.5.1 Global fitting using Berkeley Madonna

To establish a minimal reaction cycle for Hsp90, we used the program Berkeley Madonna 8.3.1 to perform a global fit of all experimental data sets [including the

fluorescence kinetic traces (N-N, N-M, M-M and intraprotomer N-M) and ATP/ATPγS hydrolysis] to one set of rate constants and conformation-specific signal contributions. A set of five species best represented the dataset. The program numerically solves the differential equations of the reaction path and calculates the concentrations of all species for every time point. Each state was assumed to give an individual contribution to the signal of the fluorescence traces measured. This allowed the progress curves of the fluorescence kinetics to be simulated. In the kinetic model, Hsp90 was assumed to be in the open nucleotide-free conformation before addition of ATPγS. An upper limit of 20 min^{-1} was set for the microscopic rate constant of the ATP hydrolysis reaction. For ATP□S, the hydrolysis rate was included as a fit parameter. The rate constants for conformational transitions were assumed to be independent of either ATP or ATP□S being used, supported by the comparison of the temperature dependencies of the ATPase activity and the ATPγS-induced conformational changes.

3 Results and Discussion

3.1 Characterization of the ATPase activity

3.1.1 Binding of ATP and ADP

To characterize the enzymatic activity of Hsp90, the dependency of the velocity on varying ATP concentrations was determined (**Figure 13**). This gives information about the K_M of Hsp90 and its maximal turnover (V_{Max}). yHsp90 has a K_M value of 300 µM and a V_{Max} of 1.4 at very high ATP concentrations of 5 mM and 37°C. Hsp90 is only active as a dimer but does not show cooperative properties upon ATP binding or any sigmoid behaviour (Weikl et al, 2000). Due to this it was discussed in the literature whether both subunits functionally interact like reported for other GHKL ATPases (McLaughlin et al, 2004). That the full ATPase activity requires the

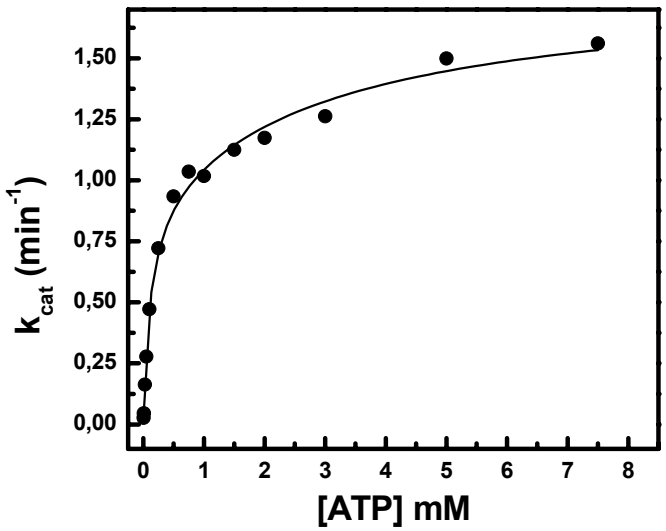

Figure 13: V/S Characteristic of yeast Hsp90 at 37°C. The buffer was 40 mM Hepes, 150 mM KCl and 5 mM $MgCl_2$. The assay used was the regenerative ATPase Assay (see Materials and Methods).

C-terminal dimerisation points to an interaction within the dimer (Wegele et al, 2003). A deletion of the C-terminal domain could be rescued in terms of ATPase activity by attaching both subunits via a disulfide bridge connecting the N-M constructs (residues 1-530) at the c-terminal end (Wegele et al, 2003). In addition, auto-inhibitory elements like the ATP-lid in the ATP binding domain of Hsp90 exist. Interestingly, with deleted ATP-lid Hsp90 is inactive but when recombined with wild type protein it is able to stimulate the opposing subunit by an order of magnitude, suggesting a communication of the N-terminal domains of both subunits (Richter et al, 2006).

An important issue in this context was whether ADP binding induces cooperative effects on the ATPase activity of Hsp90. The K_D value of ADP for the isolated N-terminal domain was determined to be in the lower µM range at 20°C under low salt conditions (Prodromou et al, 1997a). In contrast, ATP has a K_M value of 300 µM. To follow up on this, a phosphorylase-coupled assay was used which allows using mixtures of ATP and ADP in ATPase assays. Series with varying ATP concentrations in ATPase Assays were performed in the presence of successively increasing ADP concentrations (**Figure 14**). The apparent inhibition constant (K_I) was determined by fitting the data to the Michaelis-Menten equation. Increasing the ATP level used in the respective ATPase series also increases the apparent K_I value for ADP. The plot of K_I values for ADP versus the ATP concentration used in the ATPase assay gives a linear dependency which indicates that both nucleotides bind in a competitive way to Hsp90. The extrapolated value to zero [ATP] gives the affinity with which ADP is bound. Interestingly, these data suggest that both ADP and ATP are bound with similar affinity. The slope of the linear dependency of the K_I values with varying ATP concentrations is 0.9 which suggests that ATP is only slightly preferred over ADP.

The K_I of ADP determined in this way is 300 µM. ATP is bound in an unusual conformation to GHKL ATPases in which the gamma phosphate points outward the primary binding site in an angulated conformation explaining the results of largely equal interaction of ADP and ATP (Prodromou et al, 1997a).

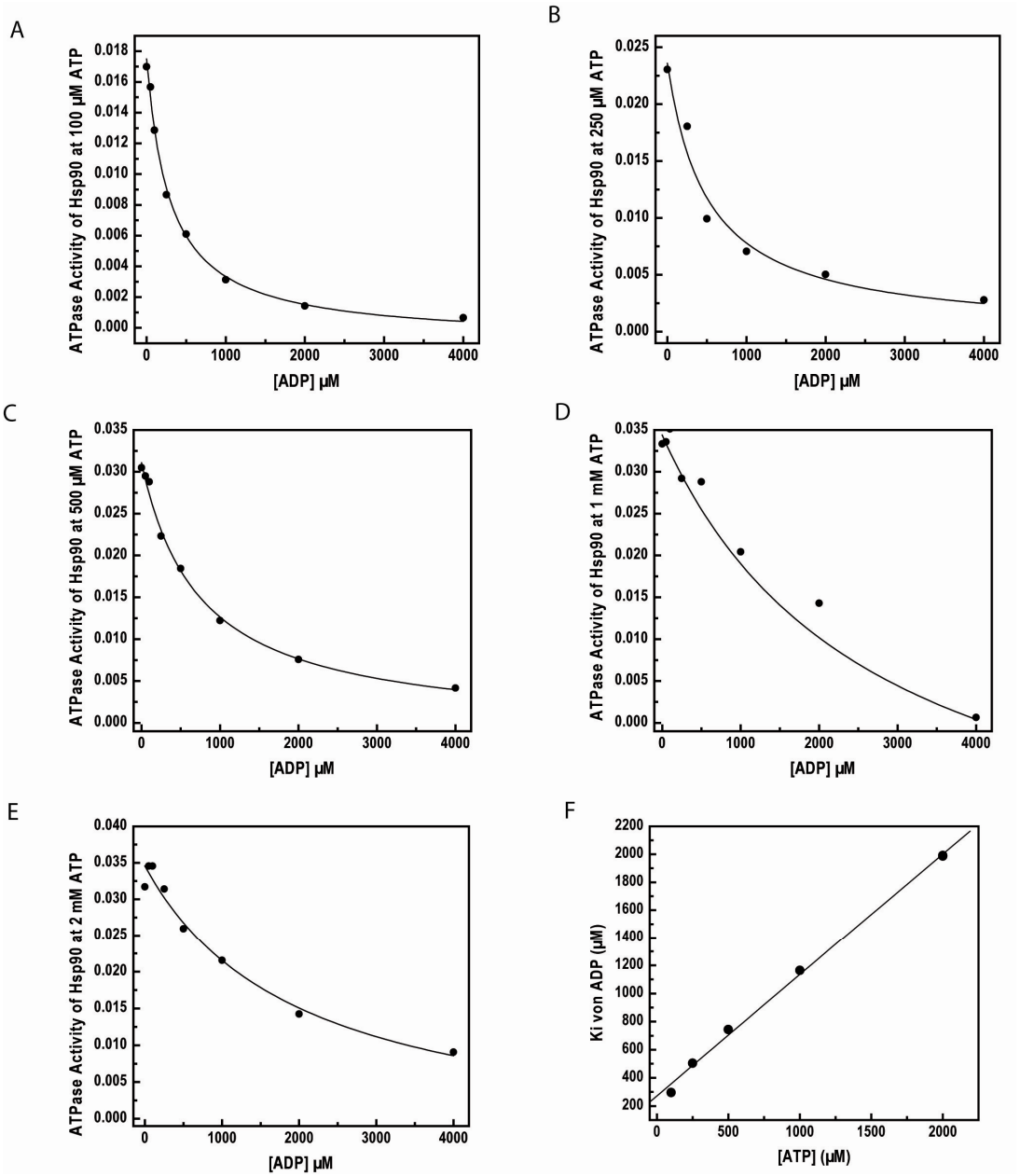

Figure 14: Analysis of the ADP inhibition of the Hsp90 ATPase. ATPase activity of Hsp90 in the presence 100 µM (A), 250µM (B), 500µM (C), 1 mM (D) and 2 mM ATP (E) inhibited by ADP. The efficiency of ADP inhibition increases with the ATP concentration used (F) in a linear way giving a slop of 0.9 and an y-axis intersection of app. 300 µM.

3.1.2 Temperature dependency of the catalytic cycle

Release reactions of ADP after the hydrolysis or initial ATP binding were ruled out as being rate-limiting for the Hsp90 cycle due to direct binding assays in stopped flow experiments using the fluorescence marked nucleotide MABA-ATP (Weikl et al, 2000). It was found that ATP binding and ADP release are much faster than the time required running through triggered catalysis for the yeast the mitochondrial and the ER paralog of Hsp90 (Leskovar et al, 2008; Frey et al, 2007; Weikl et al, 2000). Thus it is thought that conformational changes or the hydrolysis step of Hsp90 ATPase cycle determine the cycling number. To get further insight into the ATPase cycle, the temperature dependency of the ATPase was measured (**Figure 15**). Data were analysed according to equation 14 and 15 that relate the temperature dependence to thermodynamic parameters of the transition state. These data are

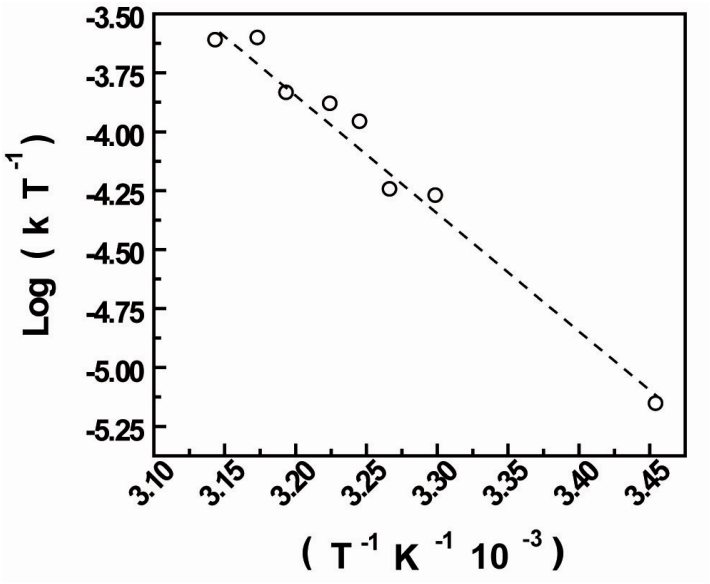

Figure 15: Temperature dependence of the ATPase activity of Hsp90. The ATPase was analysed by the regenerative assay coupled to NADH reduction. Hsp90 was incubated at varying temperatures before k_{cat} was determined. The data are depicted here in a Eyring plot that allows determination of the activation enthalpy and the activation entropy of the rate-limiting step in the ATPase cycle.

compared to Hsp90-related processes like co-chaperone binding and to rates for conformational changes (see below).

3.2 Direct measurement of conformational changes in the Hsp90 cycle

3.2.1 Cysteine variants

To analyse conformational changes in Hsp90 directly, a FRET system was established. Cysteines were introduced into Hsp90 by site directed mutagenesis to label the protein using cysteine-specific coupling chemistry with fluorescent dyes (page 57). This seemed straight forward, because yeast Hsp90 does not contain any cysteines in its sequence. Thus positions, predominately located in the N-terminal and M-domain of Hsp90, were chosen for mutagenesis. The exchanged residues were chosen to be positioned on the surface of the protein and point in the direction of the solvent.

Constructs were cloned in pET28b for expression in *E.coli* and in p2HGal for expression in yeast cells. The double knock out of HSP82 and HSC82 is lethal in yeast. The generated cysteine mutants were able to rescue the HSP82/HSC82 double knock out. This indicates that at least the cysteine mutants are functional in the environment of the cell (**Figure 16**).

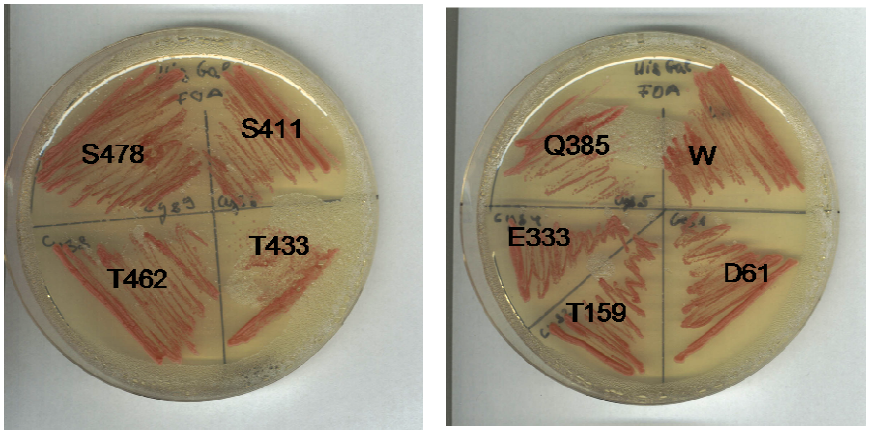

Figure 16 Complementation of the HSC82/HSP82 by wildtype Hsp90 (w) or cysteine mutants of Hsp90. All mutants rescue the lethal phenotype of the knock out.

3.2.2 Labelling of Cysteine mutants

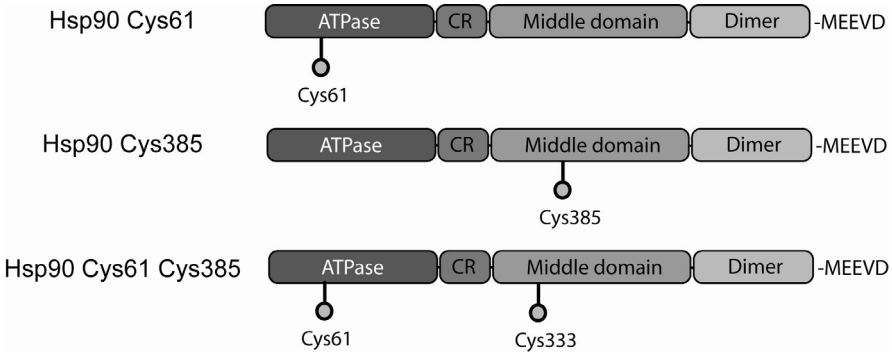

Figure 17: Chosen constructs labelled with donor and acceptor dye.

Hsp90 cysteine variants C61 and C385 were labelled with one dye attached per protein molecule (**Figure 17** & **Figure 19**). The efficiency was above 95%. This can be determined form absorption spectra recorded at the absorption maximum of the dye and at and at 280 nm for the protein absorption after correcting for the contribution of the absorption of the dye at 280. In addition, a variant with two cysteine residues was cloned in pET28b one in the N-terminal domain at position 61 and the other cytein in the middle domain at position 333 to label one subunit with both donor and acceptor dyes (**Figure 17** & **Figure 19**). Protein-dye conjugates were tested for free label retained in the sample by SEC HPLC and the ATPase activity was determined (**Figure 18**). The comparison with unmodified Hsp90 shows that the ATPase cycle is not influenced by the manipulation of the protein. The Hsp90 conjugates seem fully functional in this respect. Different labels were tested such as the combination of fluorescein tetramethylrodamin conjugates as FRET pairs or ATTO 550 and ATTO 650. High fluorescence quenching rates of the fluorescein moiety lead to complications in data analysis and reliability. Using the ATTO650 dye caused problems with the solubility of the respective Hsp90 conjugate. Using ATTO488 and ATTO550 gave good results. As specified by the manufacturer, these labels give a Förster Radius of 44 Å when used as a FRET pair.

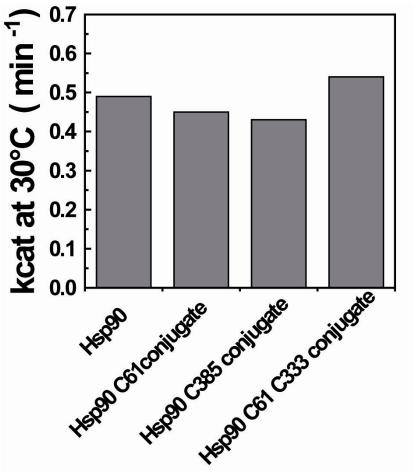

Figure 18: ATPase activities of the Hsp90 dye conjugates, measured using standard conditions.

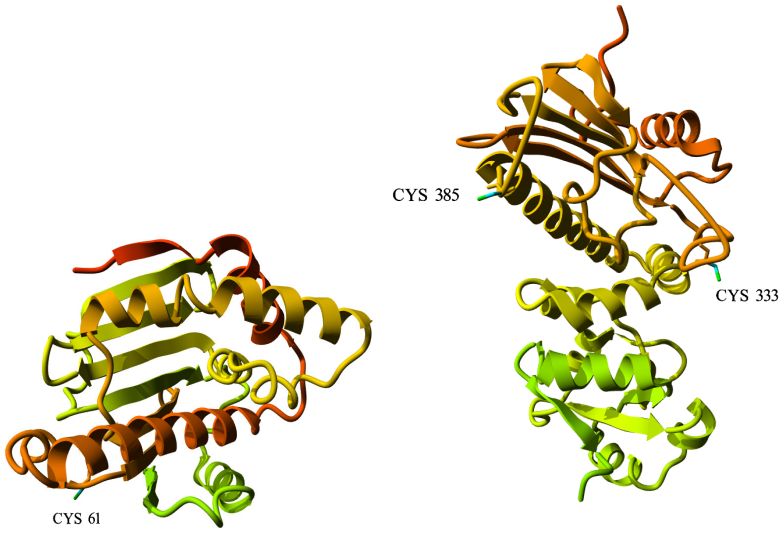

A) B)

Figure 19: Crystal structure of the N-terminal (A) and the M-domain (B) of Hsp90 that illustrate the position of cysteine moieties to which the fluorescent dyes were attached.

3.2.3 Subunit exchange of Hsp90

The monomer-dimer equilibrium of Hsp90 was studied by SEC-HPLC (Richter et al, 2001). The K_D was calculated to be in the range of 50 nM. It can also be followed by AUC experiments using a fluorescence-based detection system. The labelled protein conjugated with ATTO 488 can be detected down to nM concentrations where a certain amount of protein is monomeric (**Figure 20**). Evident for the dissociation is also the shift of the S value determined by the dC/dt analysis. The monomer has an S value of 5 S while the dimer in its open state shows a S value of 6.1 S.

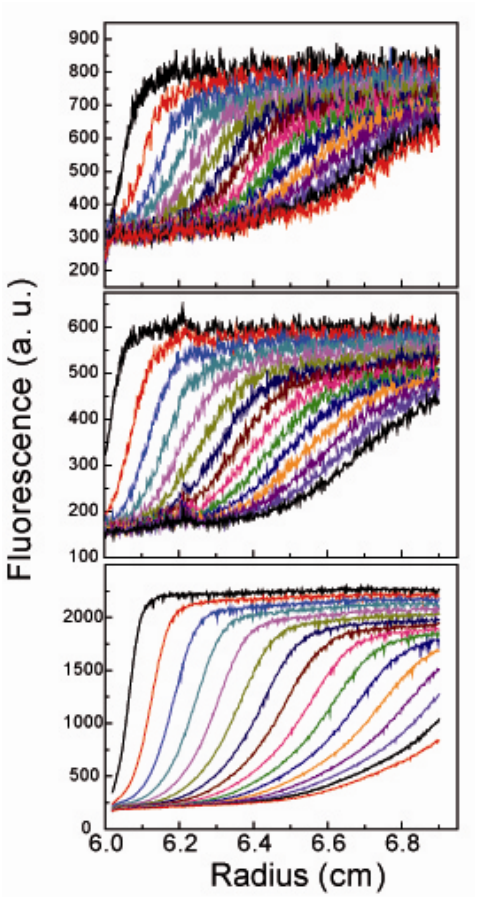

Figure 20: Sedimentation velocity experiments with increasing amounts of ATTO448 labelled Hsp90 (10 nM upper graph, 40 nM middle graph and 400 nM lower graph) with equal scan distance.

Mixing of equal amounts of donor- and acceptor-labelled Hsp90 leads to the formation of heterodimeres with single exponential kinetics and rate constants of 0.03 s^{-1} (**Figure 21A**).

Using the combination of the Hsp90 cysteine variants D61C and Q385C gave the most pronounced amplitudes in this kinetics. To further analyse the functionality of the Hsp90 fluorophore-conjugates, the K_D was determined by analysing the increase of relative amplitudes. The absolute Hsp90 concentration was increased but the 1 to 1 ratio of donor- and acceptor- labelled Hsp90 was kept constant. A statistical

mixture is assumed. By using equal amounts of donor- and acceptor-labelled Hsp90, 50% of Hsp90 is in a FRET competent heterocomplex (Richter et al, 2001). Thus relative amplitudes can be used to determine the K_D. This analysis suggests that the dimerisation is not influenced by the labelling procedure. The K_D value found in HPLC experiment could be confirmed (**Figure 21B**) (Richter et al, 2001).

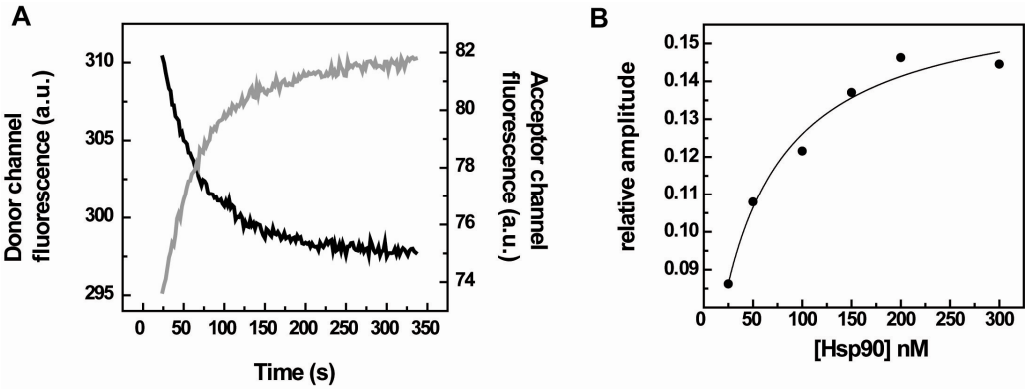

Figure 21: Subunit exchange of Hsp90. A) Subunit exchange kinetics after mixing donor- and acceptor-labelled Hsp90. Decrease in donor channel and increase in acceptor channel fluorescence indicate the emergence of FRET. B) Analysis of the relative amplitudes of the acceptor channel increase with varying final concentrations of fluorophore-labelled Hsp90 show a saturation curve with similar half maximum as expected form SEC analysis of the K_D value of the monomer dimer equilibrium

3.2.4 Influence of nucleotides on Hsp90

To analyse whether structural changes are induced upon addition of nucleotides, the heterocomplex of D61C acceptor-labelled Hsp90 and the Q385C donor-labelled Hsp90 was formed and co-incubated with nucleotides (**Figure 22**).

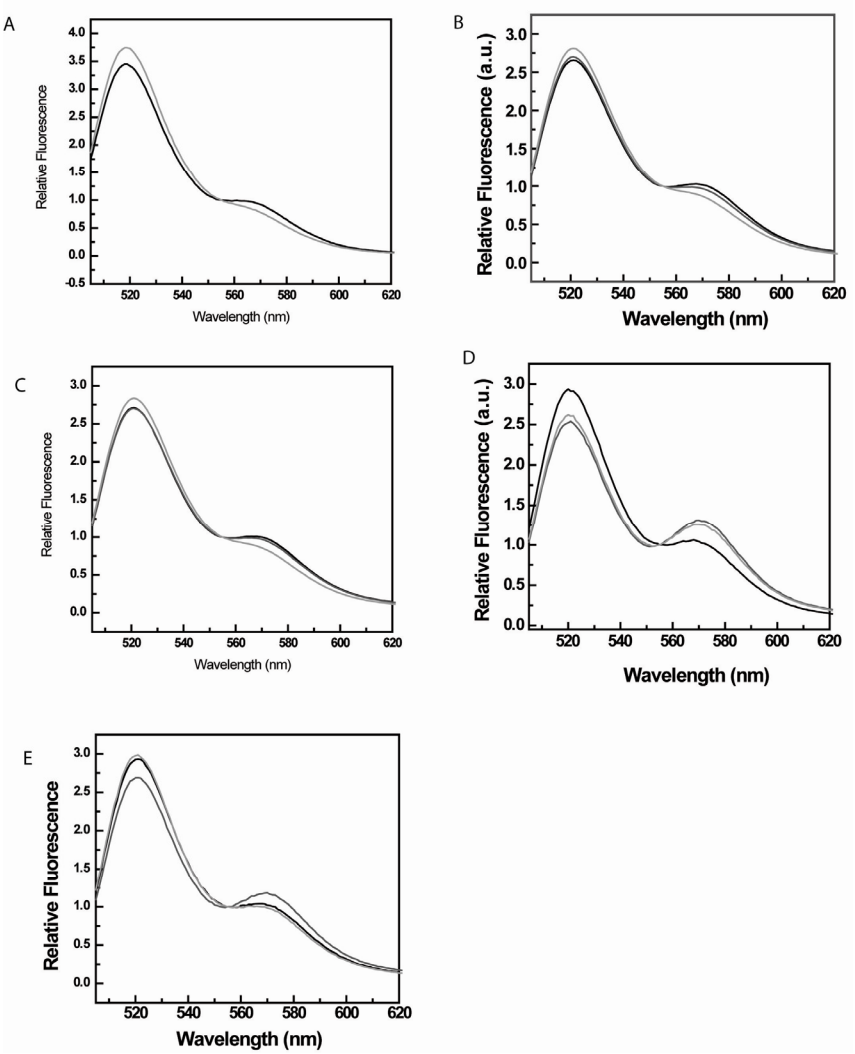

Figure 22: Fluorescence spectra of the N-domain M-domain labelled heterocomplex with different nucleotides and the addition of an excess of unlabelled Hsp90. In A) -E) the black trace shows the spectrum of the heterocomplex of N-terminal domain acceptor-labelled and M-domain donor-labelled Hsp90. The gray line shows the spectra with ADP in B), with ATP in C), with AMP-PNP in D) and with ATPγS in E). The light gray line shows the heterocomplex of labelled protein after preincubation with the respective nucleotide A) wo, B) ADP, C) ATP, D) AMP-PNP and E) ATPγS and after mixing with an excess of unlabelled Hsp90.

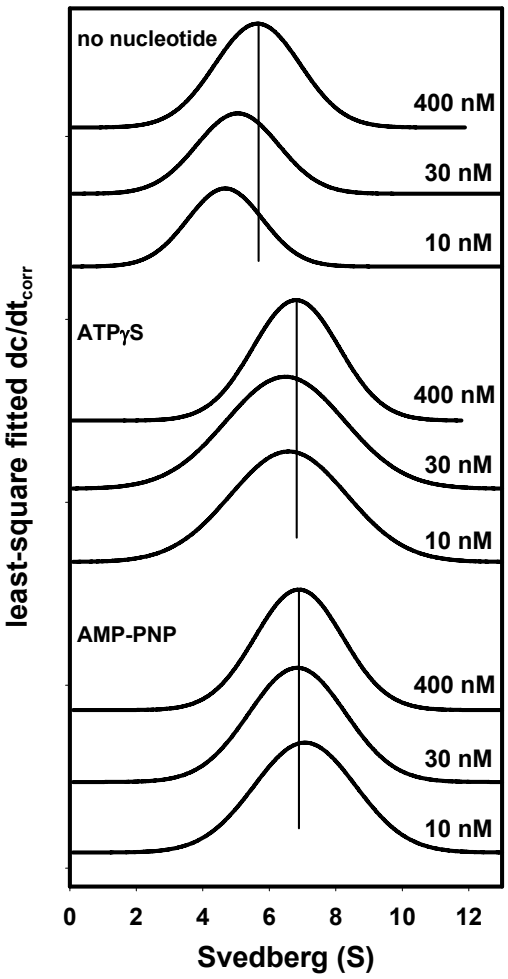

Figure 23: Analytical ultracentrifugation has been performed using ATTO488 labelled Hsp90 at concentrations of 400 nM, 30 nM and 10 nM in the presence of either no nucleotide or ATPgS, aMPPNP and ADP. Sedimentation analysis was performed at 45000 rpm and 24° C in a 40 mM HEPES/KOH, pH 7.5, 150 mM KCl buffer system. Raw sedimentation traces were converted to dcdt profiles according to the literature. Data were then fitted to obtain apparent sedimentation coefficients and to visualize the change in sedimentation coefficients with nucleotide binding and with concentration reduction. Reduction in sedimentation coefficients can be seen as dissociation of the dimeric protein into monomers.

ADP and ATP did not induce large FRET changes in this setup. Structural changes were reported to occur with ADP in a study using EM imaging of single particles. However for the yeast and the human Hsp90 homologs chemical corsslinking was performed to stabilise the ADP induced state (Southworth and Agard, 2008).

The ATP analogues ATPγS and AMP-PNP show changes in FRET which indicate structural rearrangements that can be detected with high sensitivity. In agreement with the crystal structural analysis the distance between the fluorescent dyes decreases (Shiau et al, 2006; Ali et al, 2006)(**Figure 22**).

The conformational changes induced by AMP-PNP and ATPγS could be confirmed using AUC experiments that indicate an increase of the sedimentation coefficient by 1 S for the Hsp90-AMP-PNP or –ATPγS complex (**Figure 23**). For ADP no change in the sedimentation behaviour could be detected.

In addition, the reversibility of the FRET complex formation was tested by adding unlabelled Hsp90 to an amount of 3 µM which represents a tenfold excess over the labelled protein. After incubation for 15 minutes, spectra of these mixtures were measured (**Figure 22**). For the ATP and the ADP samples, the formed FRET complex was dissociated which indicates that subunit exchange is still possible using these nucleotides. Using fluorescence AUC we could confirm that dissociation with ADP still takes place while ATPγS and AMPPNP showed no tendency to dissociate (**Figure 23**). In addition it can be deduced that both fluorescent dyes have to be located within one functional Hsp90 dimer for efficient energy transfer, demonstrating the specificity of the assay.

FRET complexes after incubation with ATPγS show decelerated subunit exchange. The AMP-PNP sample showed even more stable FRET complexes in which no detectable subunit exchange occurred (**Figure 22**).

To analyse this further, the disassembly of the FRET complexes was recorded kinetically. The FRET complex with ADP, ATP, ATPγS and AMP-PNP were formed. Donor channel fluorescence was recorded after addition of an excess of unlabelled Hsp90 (**Figure 24**). For ADP and ATP, the dissociation kinetics of the

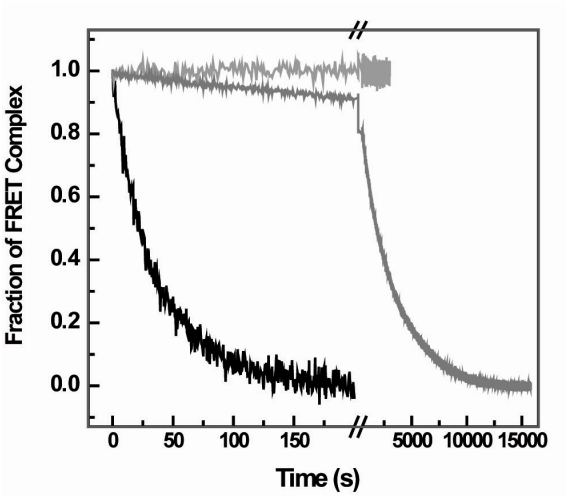

Figure 24: Disassembly of the Hsp90 FRET complex after incubation with different nucleotides. In black a representative trace for ADP, ATP and the disassembly without the addition of nucleotide. In gray the trace for ATPγS which suggested a massive stabilisation of the FRET complex. In light gray the trace for AMPPNP which did not dissociate on the time scale monitored after adding an excess of unlabelled Hsp90.

FRET complex were identical. The ATPγS sample showed a very slow disassembly with rates even far below that the k_{cat} value of the Hsp90 ATPase with a rate constant of 0.02 min^{-1}. The AMPPNP complex was stable for at least 60 minutes and no changes in donor channel fluorescence could be observed suggesting that subunit exchange was totally abolished under these conditions. Consistent with structural data, the dimerisation between the N-terminal domains in the "ATP state" of Hsp90 explains the stabilisation seen for the ATP analogues used.

The crux of this view is that no changes were observable for ATP. Therefore, a further analysis of the Hsp90 system was needed.

3.2.5 Kinetics of nucleotide induced conformational changes of Hsp90.

Next, the kinetics of conformational changes induced by ATPγS and AMP-PNP were analysed (**Figure 25A and B**). Heterocomplexes were formed with the D61C

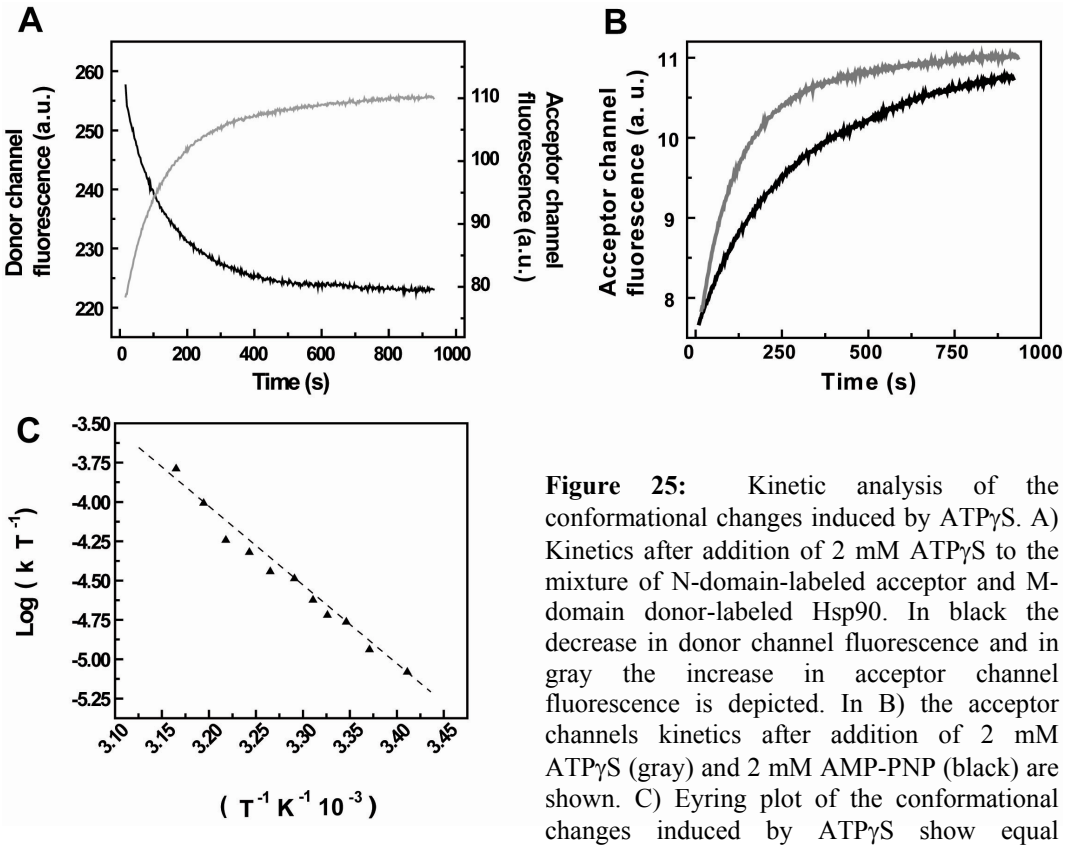

Figure 25: Kinetic analysis of the conformational changes induced by ATPγS. A) Kinetics after addition of 2 mM ATPγS to the mixture of N-domain-labeled acceptor and M-domain donor-labeled Hsp90. In black the decrease in donor channel fluorescence and in gray the increase in acceptor channel fluorescence is depicted. In B) the acceptor channels kinetics after addition of 2 mM ATPγS (gray) and 2 mM AMP-PNP (black) are shown. C) Eyring plot of the conformational changes induced by ATPγS show equal acitivation enthalpies and entropies as the k_{cat} value of the ATPase activity.

acceptor- labelled and the Q385C donor-labelled Hsp90 conjugate. In these experiments donor and acceptor channel fluorescence were recorded simultaneously. First trails were measured at 30°C. The traces were fitted to double exponential equations. A fast phase was found with a rate constant of 0.8 min^{-1}. The slow phase has a rate constant of 0.5 min^{-1}.

The kinetics of ATPγS induced differed significantly from the kinetic induced by AMP-PNP in that the conformational changes take place with a slower rate (see below).

The temperature dependence of the slow phase of the ATPγS-induced kinetics corresponds to that of the Hsp90 ATPase (Page 80). Kinetics were measured at varying temperatures and fitted to exponential equations to obtain the rate constant of the slow phase.

3.2.6 Conformational changes on the level of domain trajectories

The FRET kinetic induced by ATPγS does not display a single exponential behaviour. Thus intermediates on the pathway seem likely and to obtain more evidences we used our cysteine mutants to combine them to monitor movements from the N-domain to the N-domain by using donor- and acceptor- labelled D61C mutants. In addition, the M-domain to M-domain rearrangements were analysed by donor- and acceptor- labelled C385 mutants and compared to the kinetics of the N-domain mutant combined with the M-domain-labelled Hsp90.

The traces were recorded at 15° C to slow down the Hsp90 cycle which should enable the detection of fast phases. To resolve fast phases, the kinetics were recorded on stopped flow instrumentation.

N-domain to N-domain rearrangements are shown in Figure 26A. A burst phase lasting for app. 45 s is a characteristic feature in the trace. N-domain to N-domain contacts are therefore considered to be an early event in the conformational changes (**Figure 26**).

M-domain to M-domain motions do not show large changes in FRET. The kinetics show a negative overshoot implying that in the first phase a decreasing trace is followed by a slower increasing arm.

The N-domain to M-domain fluorescent changes show multiphase behaviour as discussed previously. All kinetic traces recorded indicate intermediates that are structurally distinct to from the starting conformation and the final closed conformation of Hsp90.

In addition, movements in one subunit were monitored using the D61C E333C double cysteine variant that was modified with both donor and acceptor dye. For that trace donor channel fluorescent change are depicted. The kinetic is characterized by a first decrease in fluorescence apparently followed by a lag phase after which fluorescence increases with a slower rate.

All measured combinations indicate time courses that are hardly explainable without assuming intermediates on the pathway. The kinetic phases observed show related time frames for each domain to domain movement, suggesting that all traces describe the same reaction but in different projections of the structural change.

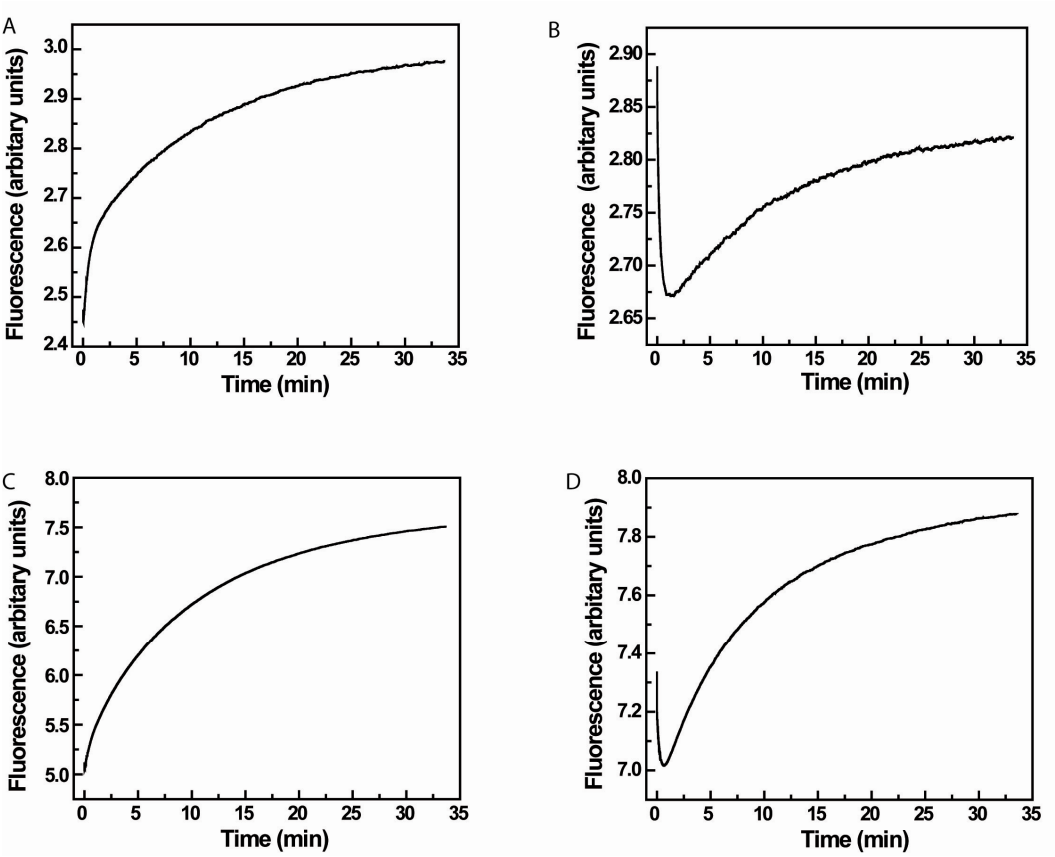

Figure 26: Kinetics of conformational changes induced by the addition of 2mM ATPγS at 15°C for different relative domain - domain movements. In A) the trace of acceptor channel fluorescence is shown for the N-domain donor-labeled and N-domain acceptor-labeled Hsp90 heterocomplex. Acceptor channel fluorescence of the heterocomplex with the middle domain labelled proteins is depicted in B). The trace for the N-domain M-domain heterocomplex which shows fluorescence kinetics with the highest amplitudes is shown in C). Donor channel fluorescence of the double labelled variant in the presence of an excess of unlabelled Hsp90 upon addition of ATPγS is shown in D).

3.2.7 Global fitting of conformational changes.

The time traces of fluorescence changes show comparable time scales of intermediate accumulation in each kinetic, but the signal changes differ because of alternative reaction trajectories for which the kinetics had been recorded. To analyse the kinetics in detail, a model using the software package Berkeley Madonna was built which includes ATP binding, hydrolysis and ADP release. ATP binding and ADP release were determined previously (Weikl et al, 2000). ATP binding and release were shown to be fast compared to the turnover number of the catalytic cycle using MABA-ATP, a fluorescent dye that binds to Hsp90 but cannot be hydrolysed (Weikl et al, 2000). Form the temperature dependence of the k_{cat} of ATP hydrolysis and that of the conformational changes we deduced that not the hydrolysis step of ATP but conformational changes are the rate-limiting process in the cycle. It also suggested that for ATP and ATPγS the same conformational changes take place, a fact that was very important to build the model and this view was also supported by the observation that the temperature dependency of ATP hydrolysis match the temperature dependency of the ATPγS induced conformational changes (compare **Figure 15**, **Figure 25**). It was thus considered that the rates of conformational changes are the same for ATP and ATPγS with ATPγS decelerating the hydrolysis step. In fact using ATPγS instead of ATP gives a 7 times decreased rate constant for hydrolysis, supporting this view (**Figure 30**). Since the kinetic traces show complex kinetics the conformational change does not take place in a single step. Therefore a

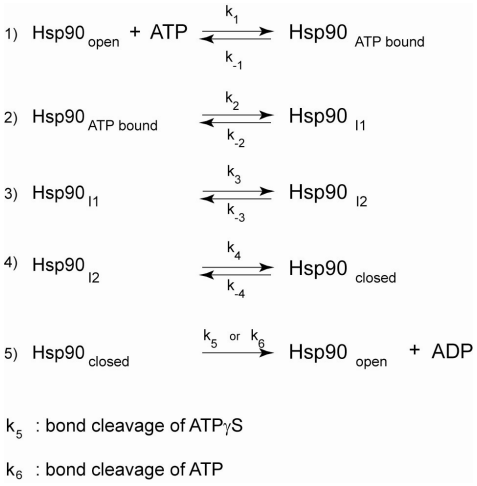

Figure 27: Chemical model for the global fit. Reaction 1 reflects the ATP to nucleotide-free Hsp90. Reaction 2 is a first conformational transition, reaction 3 is the second conformational transition and until with reaction 4 the final closed state is formed from which in reaction 5 free Hsp90 is regenerated in a single step.

minimum of four different states of Hsp90 is required to describe the ATP driven cycle. First, Hsp90 is in a nucleotide-free state which was crystallized for the *E.coli* homologue HtpG (Shiau et al, 2006). Upon mixing with nucleotide, a fast binding process follows which takes place on the second timescale. Because of the multiphase behaviour of all fluorescence kinetics, at least one intermediate on the pathway leading to the hydrolysis active final closed state was considered. However fitting to a four state model was not successful, but a five state model satisfied all fluorescent traces recorded in four different trajectories for the reaction (**Table 3.1**) (**Figure 27**; **Figure 29**, **Figure 30**). From the residuals, no systematic deviation of the fit from the experimental data could be observed. Importantly, also the hydrolysis rates for ATP and ATPγS could be included and fitted to the dataset (**Figure 30**). A sensitivity analysis of the rate constants was performed. Sensitivity is defined as:

Equation 16:
$$S(t) = \frac{V_2(t) - V_1(t)}{\Delta}$$

V_1 is the curve for the initially fitted rate constant. V_2 is the curve the same respective rate but varied for Δ, which was 1 % of the respective rate constant in this analysis. The procedure provides information about the definiteness of the respective rate constant (Berkeley Madonna software). This analysis for the rate constant indicated that the release rate of ATP/ATPγS and the reverse rate of the reaction 4) can only be estimated.

Thus the chemical model we suggest describes the data sufficiently but leaves the mentioned rate constants relatively undefined. The hydrolysis rate of ATP $k_{6,}$ was set to 20 min^{-1}. This has no major impact on the model, because the preceding reactions are rate-limiting. The hydrolysis step and the ADP or phosphate release are not important form the kinetic perspective. Also k_{-4} is not strictly defined because of its very slow rate constant which suggests that the reaction from I2 to the closed state is close to irreversibility.

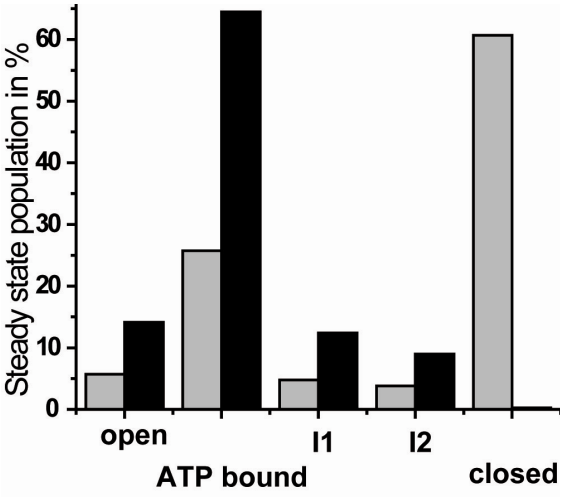

Figure 28: Population of the Hsp90 states using ATP (black) or ATPγS (gray) as a nucleotide. The states are the open nucleotide-free state, the ATP-bound state, the two newly identified intermediates I1 and I2 and the crystallized final closed state.

Now we were in the position to have an estimate of the cycle and the states involved in it. We could predict how much of each conformational state is populated under steady state conditions of Hsp90. As expected, the population of the respective conformational states using ATP and ATPγS deviate massively (**Figure 28**). ATPγS populates the final closed state to 60% while the amount of the closed state is below 1 % (**Figure 28**). This puts emphasis on the difference between the hydrolysis steps of ATP and ATPγS. Interestingly, with this view we could now explain our findings for the subunit exchange data in which we chased FRET complexes with different nucleotides with unlabelled Hsp90 (**Figure 24**). In the case of ATP, the FRET complex showed fast dissociation suggesting that the N-terminal dimerisation is not dominant. In contrast, Hsp90 ATPγS complexes showed a very slow exchange rate, which is due to the fact that the hydrolysis step is so slow and that the reverse rate for I2 to the closed state is even slower trapping Hsp90 in its N-terminal dimerised conformation and rendering the protein resistant to subunit dissociation. AMP-PNP is not hydrolysed at all and locks the protein in its N-terminal dimerised conformation and prevents dissociation of the subunits. The model also explains why the ATPγS-induced conformational changes are faster compared to AMP-PNP kinetics. When the hydrolysis is blocked completely, the equilibration of the system is not cyclic anymore and the reverse rates of all

processes become more pronounced in the kinetic behaviour. Thus the reverse rate form I2 to the closed state becomes more pronounced and slows the kinetic.

Table 3.1: Rate constants obtained from the global data analysis.

	Forward (min^{-1}) at 15°C		Reverse (min^{-1}) at 15°C	
Reaction 1	k_1	**40**	k_{-1}	**~ 7**
Reaction 2	k_2	**0.4**	k_{-2}	**1.5**
Reaction 3	k_3	**1.0**	k_{-3}	**0.8**
Reaction 4	k_4	**0.6**	k_{-4}	~ 0.003
Reaction 5	k_5	**0.03**		
	k_6	> **20**		

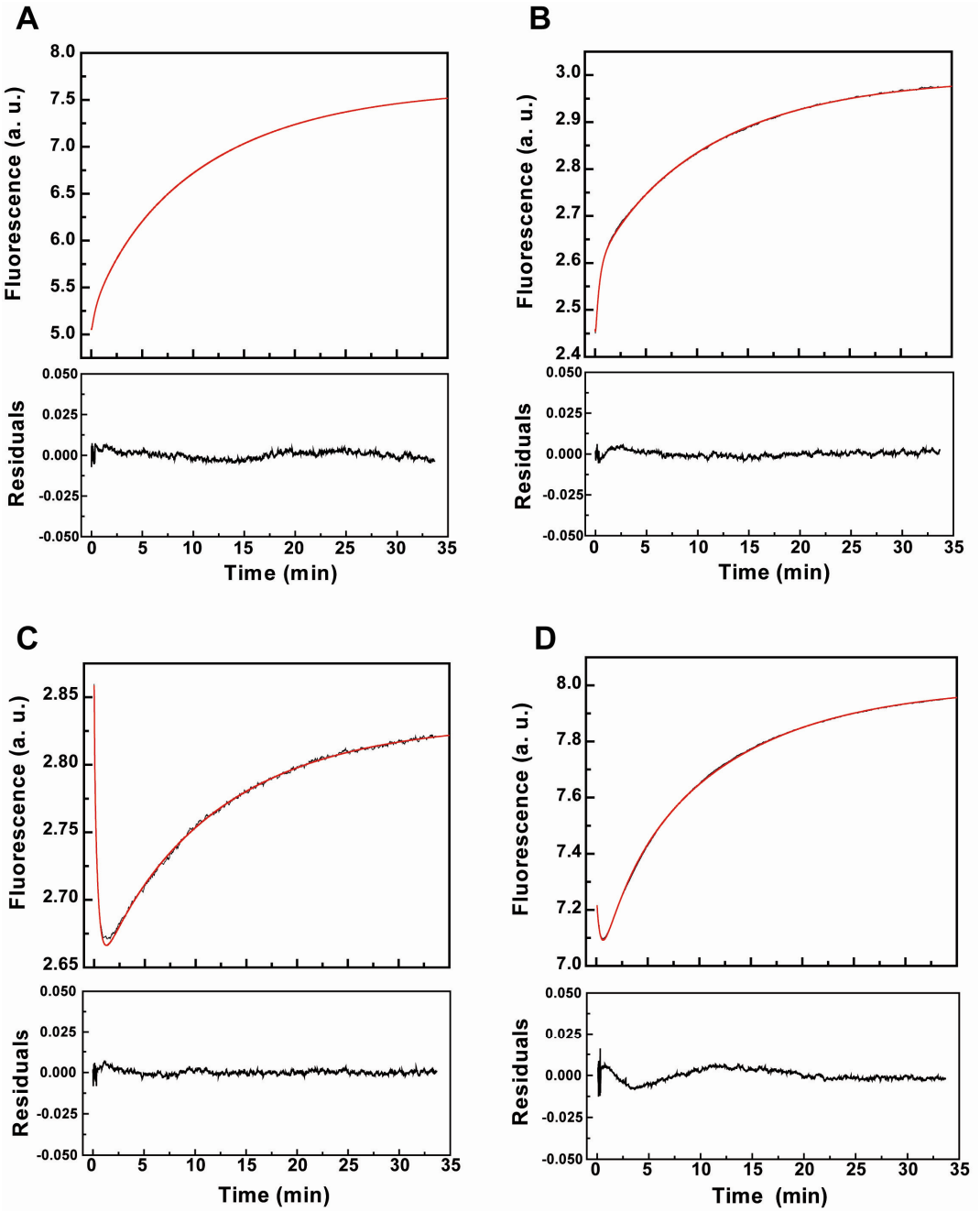

Figure 29: Data fitting to a 5 state model. Dataset recorded at 15°C. A) The N-M trajectory between the two subunits. B) The N-N trajectory. C) The M-M trajectory and in D) the N-M trajectory in one subunit. Below the kinetic traces the residuals using the global fit to each fluorescence trace is shown.

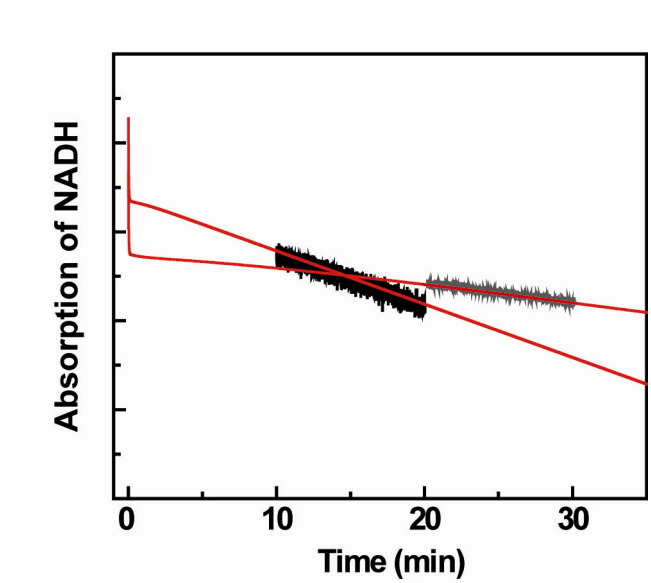

Figure 30: Implementation of the hydrolysis rates of ATP and ATPγS. Measured rates of ATPγS (gray) and ATP (black) hydrolysis also fit to the model. The traces derived from the global analysis is shown in red.

3.2.8 Order of events in the Hsp90 cycle

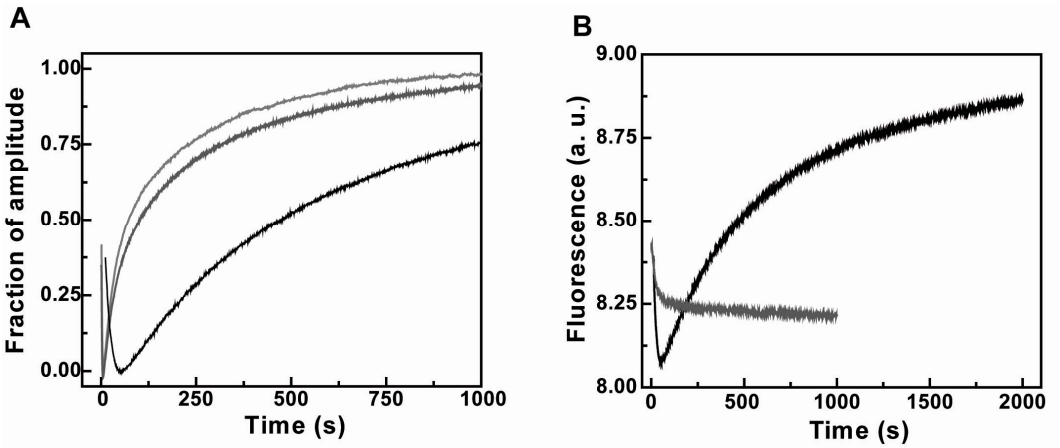

Figure 31: Heterocomplexes of double labelled Hsp90 with different mutants of Hsp90. A) Kinetics of ATPγS induced conformational changes of Heterocomplexes using the Lidless-Hsp90 (light gray) and the Δ8-Hsp90 (gray) were analysed and compared to the Heterocomplex with wild type Hsp90 (black). B) A heterocomplex using a subunit lacking the N-terminal domain (gray) does not undergo large conformational changes compared to the wildtype Hsp90 (black) upon addition of ATPγS. However a slight decrease in signal can be reproduced.

Two intermediates on the pathway were identified by the kinetic analysis. From the changes in the FRET efficiencies, it can be deduced that N-terminal contacts presumably form early on the pathway. To analyse this we used the double-labelled Hsp90 variant and added different unlabelled Hsp90 variants that either inhibit the Hsp90 ATPase or strongly stimulate it.

The lidless subunit of Hsp90 is inactive but forms stable dimers that show dissociation constant far below that of wild type Hsp90 (Richter et al, 2006). The lidless subunit does not seem to dissociate on SEC HPLC runs (Richter et al, 2006). Deletion of the ATP lid inactivates Hsp90 completely although ATP binding was detectable (Richter et al, 2006). Interestingly, when heterocomplexes are formed

using wild type Hsp90 with the lidless subunit a strong stimulation up to 10 times of the ATP hydrolysis was observed (Richter et al, 2006).

These findings led to the conclusion that the ATP lid region is required for the hydrolysis reaction in *cis* but acts in an inhibitory way on the subunit in *trans* (opposing subunit).

To gain insight into the effect of this variant on the conformational cycle we tested how conformational changes are affected in a heterocomplex with the lidless subunit (**Figure 31**A light gray line). Indeed we found that conformational changes are stimulated in the heterodimer. All kinetic phases seem affected and the characteristic overshoot in the kinetic trace is now shifted to the second times scale.

In contrast to the lidless Hsp90 subunit Δ8 Hsp90 is active and forms stronger N-terminally dimerized state (Richter et al, 2002). This view was supported by the modulation of the interaction of this Hsp90 variant with p23 and Sti1. P23 interacts more strongly while Sti1 binding was reduced compared to wt Hsp90. The ATPase activity is 50% higher than the activity of the wild type Hsp90. This N-terminally deleted variant also stimulates a wild type subunit in trans. Conformational changes were found to be stimulated in a similar way as for the lidless subunit (**Figure 31**A gray line). All phases are affected and the overshoot is shifted to the second timescale. Thus lid movement and displacement of the first beta sheet of the N-terminal domains are events early on the pathway that lead to N-terminal dimers.

The variant lacking the N-terminal domain, Hsp90 M-C has no ATPase activity and shows a dimerisation constant comparable to the wild type protein (Richter et al, 2001). Heterocomplexes using this variant (**Figure 31**B gray line) show only reduced conformational changes with an initial drop in the trace but a lack of following conformational changes. This indicates that after preparative events in each subunit, subsequent conformational changes become stabilized by the interaction with the N-terminal domain in the other subunit. This is important for the progress through the Hsp90 cycle.

3.2.9 The Hsp90 cycle

To summarize the analysis of the conformational changes of Hsp90, a new model is put forward that includes the new intermediates found by the kinetic analysis and the global fitting to the dataset (Table 3.1). The heterodimer experiments gave some clues about structural changes that govern the cycle and reveal that conformational changes are dependent on N-terminal dimerisation. The starting conformation was considered to be the open state. Then ATP binding takes place after which a disfavoured reaction, reaching I1 with a concominant stabilization by reaching I2, takes place. Presumably the first Intermediate I1 is still in an open conformation but is prepared for N-terminal contact formation. I2 and the fully closed conformation have dimerized N-terminal domains. The reaction from I2 to the fully closed state leads to ATP commitment for hydrolysis.

The characteristic of this last reaction is its slow reverse reaction that could be found experimentally with chase experiments using different nucleotide states of Hsp90 FRET complexes.

Chase experiments indicated that approximately 20% of the ATP is trapped during the cycle (Weikl et al, 2000). Thus intermediates might contribute to the trapping by kinetic partitioning in this complex kinetic pathway.

3.3 Regulation of Hsp90 by Co-chaperones

3.3.1 Sti1/Hop, the Hsp organising protein

Inhibition of the ATPase.

Sti1 is a heat stress protein in the cytosol of *Saccharomyces cerevisiae*. Its human homolog is Hop which was found to have profound function in the Hsp90 catalysed activation process of steroid hormone receptors (Morishima et al, 2000). It is thought to co-ordinate Hsp70 function with Hsp90 to provide a platform for substrate transfer between both chaperone machines.

Binding of Sti1 to Hsp90 leads to a nearly complete inhibition of the ATPase activity of the chaperone (**Figure 32**). However, it was shown that affinity for nucleotides remains unchanged in the complex (Richter et al, 2003). Thus Sti1 acts as a non-competitive inhibitor (Richter et al, 2004). Interestingly, Sba1´s binding to Hsp90 is inhibited by Sti1´s binding although primary binding sites do not overlay suggesting that conformations of Hsp90 are responsible for this exclusiveness of interaction (Richter et al, 2004).

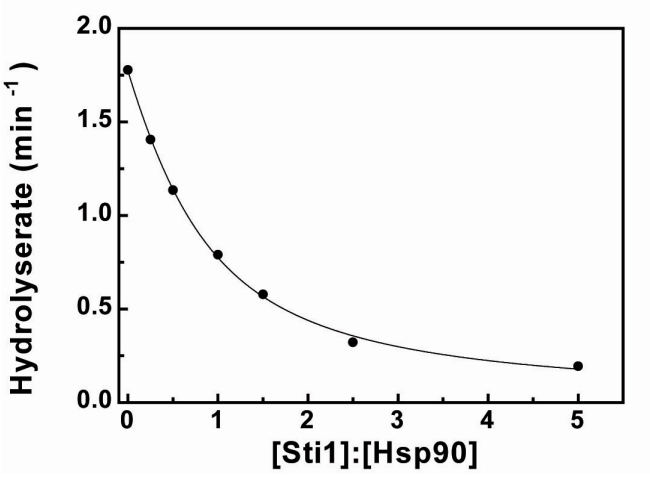

Figure 32: Inhibition of the Hsp90 ATPase by Sti1. ATPase kinetics were measured at 37°C.

The FRET experiments demonstrated that conformational changes govern the ATP hydrolysis cycle of Hsp90. Sti1 interacts primary on the C-terminus of Hsp90 which is far apart from the N-terminal domains that undergo large conformational changes. However Sti1 has an influence on N-terminal dimerisation as deduced form biochemical experiments using Δ8Hsp90 and p23 as probes (Richter et al, 2004). To test the influence of Sti1 on conformational changes directly we used FRET setup. These experiments indeed confirm the speculation about the influence of Sti1 on conformational changes. When an excess Sti1 was incubated with heterocomplexes containing donor- and acceptor-labelled Hsp90 no direct changes in FRET efficiency were observed. Addition of ATPγS did not indicate changes in conformation (**Figure**

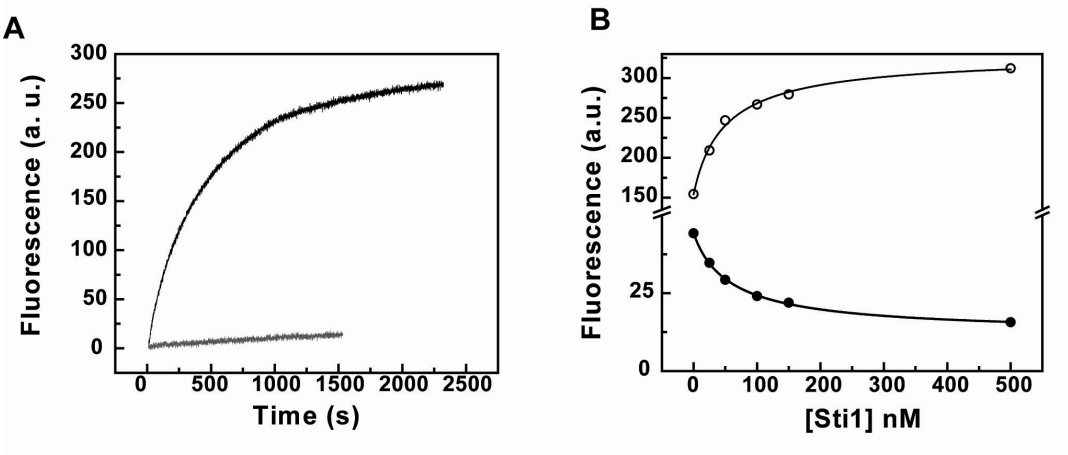

Figure 33: Influence of Sti1 on the ATPγS-induced conformational changes. A) Comparison of the kinetic trace of N-domain to M-domain conformational rearrangements upon ATPγS addition. In gray with 5 μM Sti1 in black the trace without Sti1. B) Development of donor channel amplitude (open circles) and acceptor channel amplitudes (closed circles) for the respective kinetics using increasing amounts of Sti1 in the N-domain to N-domain kinetic trace. Data suggest that the decrease in FRET efficiency is due to Sti1 binding as the saturation curve equals the binding curve for Sti1 to Hsp90.

33). Using sub-stoichiometric amounts of the co-chaperone gave much slower rates of conversion to the closed state along with a decrease in FRET amplitude for the donor and acceptor channel fluorescence (**Figure 33**), consistent with the view that Sti1 holds Hsp90 in an open conformation blocking N-terminal dimerisation and thus acts as an inhibitior of the ATPase function. This view also explains why p23 and

Sti1 bind in competition to the chaperone because the two co-chaperones bind to different conformational stages of Hsp90.

3.3.2 Sba1, the p23 homologue in yeast

Sba1 is a small acidic protein in the cytosol of yeast. Its human homolog p23 is found in mature hormone binding active SHR complexes. As mentioned, it associates with an N-terminal dimerized conformation of Hsp90 which requires a closed ATP lid (Ali et al, 2006). Sba1 is, as Sti1, an inhibitor of the ATPase activity but blocks the cycle only up to 50% as described (Richter et al, 2004; Sullivan et al, 2002)

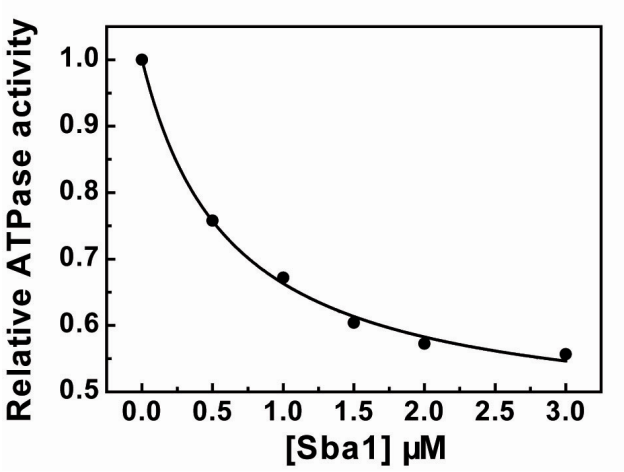

Figure 34: Inhibition of Hsp90 by Sba1. A maximum of 50% for the inhibition was found.

(**Figure 34**), Sba1´s inhibition is more complex than that of Sti1. It interacts with the N-terminally dimerised state of Hsp90 which is part of the conformational changes. Thus more complex kinetics was expected and observed by FRET. Although the reaction was inhibited also changes in amplitudes were observed. For the N- M-domain movement, the amplitude seems to be reduced and that of the N- to N-domain trace was increased (**Figure 35**). The change of N- to N-domain movement could be used to analyse Sba1 binding to the FRET complex which was found to be

of comparable affinity as to the wild type Hsp90 (**Figure 35**). The kinetic model suggested, that p23 binding inhibits the reaction from I_2 to the closed state under saturating conditions by a factor of 10, thus leading to a accumulation of I_2 even under saturation with ATP. Comparing the amplitudes of the acceptor channel fluorescence upon adding ATP instead of ATPγS confirms the prediction of the kinetic model of a 30 % accumulation of I_2 (**Figure 36**). The amplitudes with ATP increase by a factor of 3 using an excess of Sba1. A direct anisotropy and a FRET-based binding assay were established to monitor binding of Sba1 to Hsp90; certain conformational changes of Hsp90 are required to interact with the co-chaperone and the kinetic analysis of this binding reaction provided further evidence for the timing of the interaction (**Figure 36**). Lag-phases were observed in both assays which hint to a delay due to intermediates on the pathway that do not interact with p23. Therefore it was concluded that p23 binds to the first N-terminally dimerised Hsp90 form which is I_2.

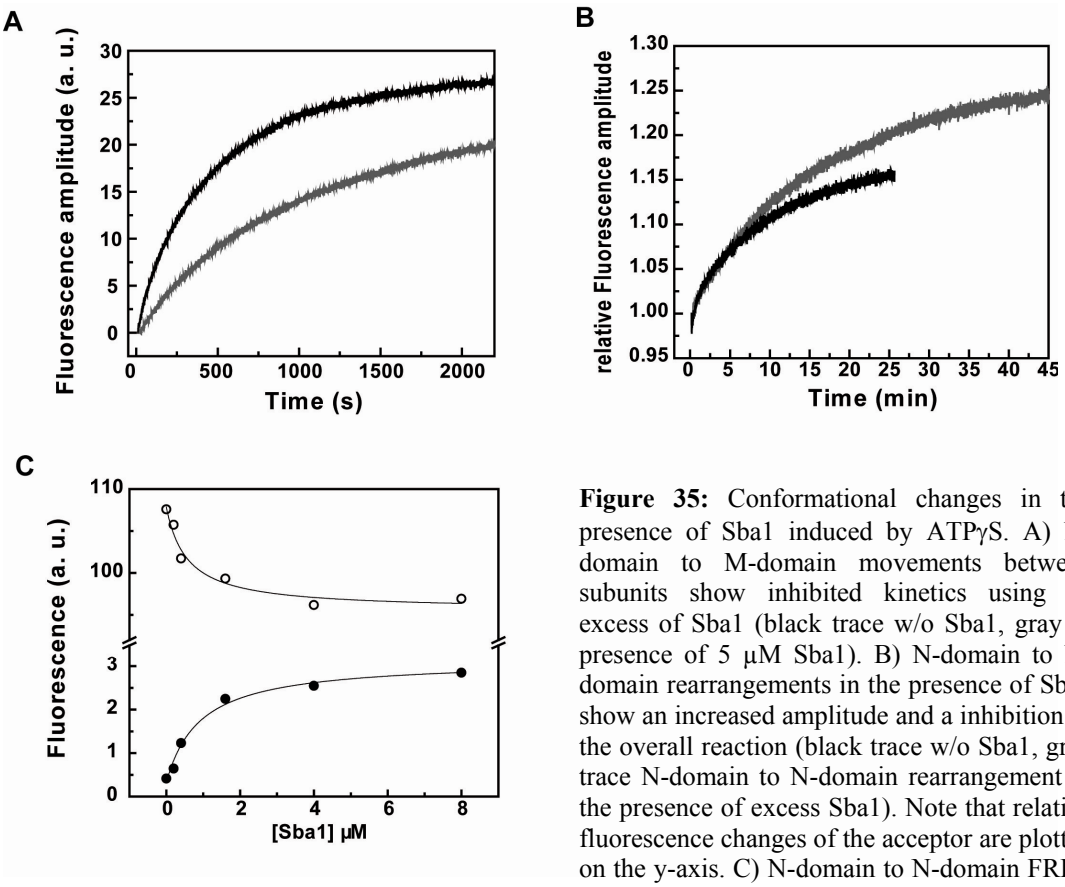

Figure 35: Conformational changes in the presence of Sba1 induced by ATPγS. A) N-domain to M-domain movements between subunits show inhibited kinetics using an excess of Sba1 (black trace w/o Sba1, gray in presence of 5 µM Sba1). B) N-domain to N-domain rearrangements in the presence of Sba1 show an increased amplitude and a inhibition of the overall reaction (black trace w/o Sba1, gray trace N-domain to N-domain rearrangement in the presence of excess Sba1). Note that relative fluorescence changes of the acceptor are plotted on the y-axis. C) N-domain to N-domain FRET setup was used to determine the increase in FRET amplitude with varying Sba1 concentration for the donor (open circles) and the acceptor channel (closed circles).

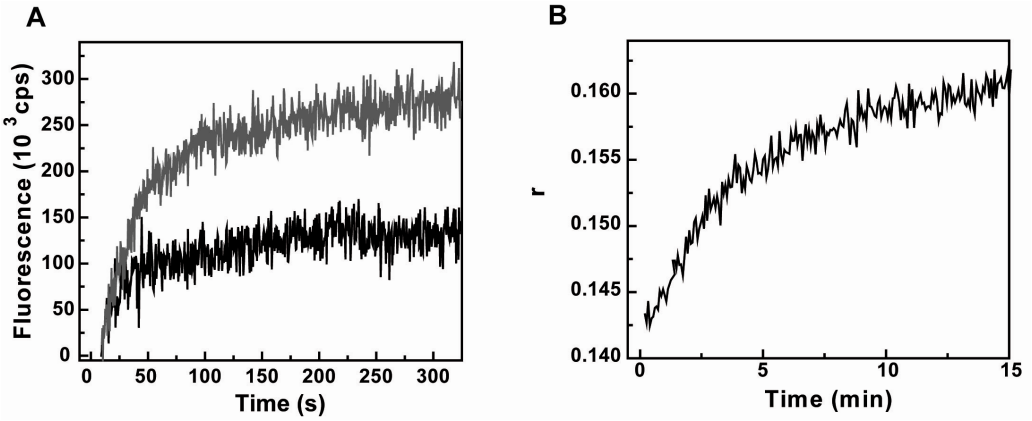

Figure 36: A) FRET kinetics using ATP for N-domain and M-domain labelled subunits without Sba1 (black) and with 5 µM Sba1. The amplitude is increased using an excess of Sba1. B) The anisotropy of Sba1 labelled with fluorescein. The assay was measured with 3 µM Hsp90 in the presence of 100 nM labelled Sba1. The reaction was started with 2 mM ATPγS. A lag phase becomes apparent which lasts for less than a minute which indicated that early intermediates of Hsp90 are not competent in binding Sba1.

3.3.3 Cpr6, a large PPIase

Cpr6 is a cyclophlin-type PPIase of 42 kDa that contains a TPR domain. The homologue Cyp40 in *homo sapiens* was shown to also be involved besides the PPIases FKBP51 and FKBP52 in SHR activation. Sti1 and Cpr6 compete for the C-terminal binding site on the chaperone. While Sti1 holds the molecular clamp in an open conformation, Cpr6 binds presumably to a closed form of Hsp90 in the cell, because it is detected along with p23 in Hsp90 complexes (Johnson et al, 2007). Cpr6 slightly stimulates the Hsp90 ATPase which suggests a direct influence on the conformation of Hsp90 (Prodromou et al, 1999).

Cpr6 supplemented in the FRET experiments observing ATPγS induced structural changes caused only slight modulation of certain phases in the kinetics and the FRET efficiency in the N- to M-domain setup increases (**Figure 37**).

An increase in fluorescence amplitude by a factor of 2 was found in the ATP-induced changes (**Figure 37**D). This hints to a higher accumulation of closed conformation in the Cpr6 complex thus explaining the activating effect in the ATPase experiments.
Cpr6 binds in concert with Sba1 to Hsp90 in vivo, thus both co-chaperones were tested for the effect on the conformational changes. Analysing the kinetics in the model predicts that Cpr6 catalyses the pathway to I_2, then Sba1 can bind and inhibit the reaction to the closed state leading to a high population of the I_2 intermediate. This explains that in the ATP-induced conformational changes, Cpr6 and p23 synergistically increase the amplitude (**Figure 37**). In our kinetic model this does not seem to be a cooperative effect between both co-chaperones but suggests that Hsp90 is shaped by Cpr6 for p23 binding.
This would suggest that p23 inhibiton in the presence of Cpr6 should be more efficiently with apparently increased p23 affinity. This experiment could confirm the view of the model.

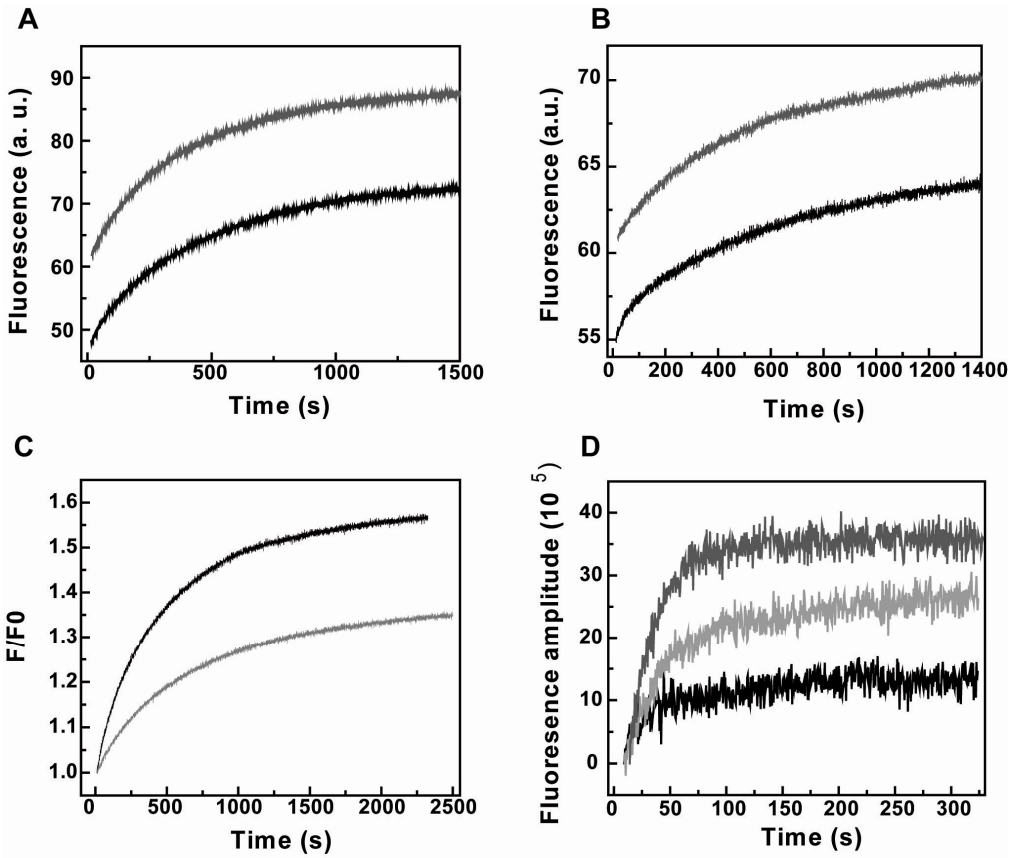

Figure 37: Effect of Cpr6 on ATPγS induced conformational changes. A) Acceptor channel traces in the N- to M- setup with Cpr6 (gray) or w/o Cpr6 (black). B) Acceptor channel traces in the N- to N- setup with Cpr6 (gray) or w/o Cpr6 (black). C) The Cpr6 traces produced reproducibly higher FRET efficiencies represented in the F/F0 plot in the N- to M- setup. D) ATP induced conformational changes without Cpr6 (black), in the presence of Cpr6 (light gray) and in presence of p23 and Cpr6 (gray).

3.3.4 Aha1, an activator of the Hsp90 ATPase

Aha1 is a strong activator of the Hsp90 ATPase (Panaretou et al, 2002). The analysis of the crystal structure of the N-terminal domain of Aha1 with the M-domain suggested that the loop including residues 370-390 is repositioned upon Aha1 binding (Meyer et al, 2004). By this the ATPase is activated, as a Lys-residue residue contacts the γ-phosphate of the bound ATP and is required for efficient catalysis (Southworth and Agard, 2008; Meyer et al, 2003).

In our FRET setup, Aha1 binding to Hsp90 led to a change in signal in the absence of nucleotide. This was detected for all cysteine variant combinations but was most pronounced in the N-N setup. The kinetics of the observed fluorescence changes had a rate constant of 0.02 s^{-1} and were independent of the Aha1 concentration used, suggesting a mechanism in which first Aha1 binds and then rearrangements in the Hsp90 dimer take place. Saturation of fluorescence change is observed in the concentration range expected by the Aha1 affinity to Hsp90 (**Figure 38**) (Panaretou et al, 2002). This was tested by plotting the amplitude of fluorescence changes vs. the

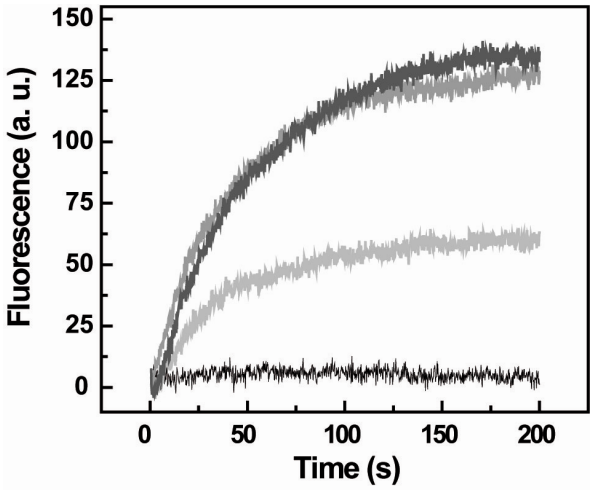

Figure 38: Aha1 induced structural changes of Hsp90. Using the N-N FRET setup the influence of Aha1 on structural changes was pronounced (acceptor channel is shown). In black a trace without addition of Aha1. The light gray trace indicates the rearrangements using 3 µM Aha1. 6µM and 10 µM did not differ in the amplitude of the acceptor channel (graduation of gray form light to dark represent the increasing Aha1 concentrations of 3 µM, 6 µM and 10 µM.)

Aha1 concentration used. Half saturation was observed at 3 µM Aha1 which nicely reflects the actual binding of Aha1 to Hsp90 under the conditions used.

Next, ATPγS induced conformational changes of the Hsp90-Aha1 complex were analysed. Using the N-N FRET setup, in which the induced fit after Aha1 binding was pronounced, a reduction of the overall fluorescence amplitude was observed (**Figure 39**). The reduction of the amplitude saturates again with the expected affinity for the Aha1 affinity to Hsp90. Thus, the conformational change in the Hsp90-Aha1 complex is on the reaction coordinate reducing the signal change induced by ATPγS. In addition, the burst phase disappears and the kinetic character reduces in complexity to a single exponential, indicating that intermediates are not pronounced for the ATPγS induced conformational changes in the Hsp90-Aha1 complex. Interpreting the data using the model predicts a fast transition of the first intermediate directly to a closed state.

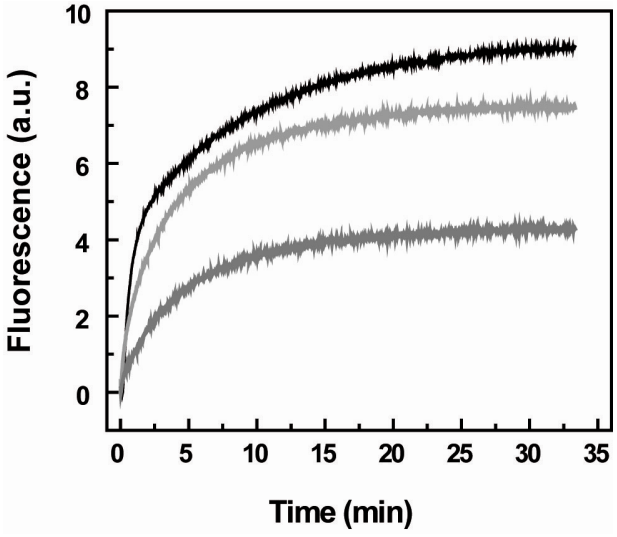

Figure 39: ATPγS-induced kinetics of the N-N FRET setup. In black, the trace without Aha1 is shown. The gray traces show the kinetics of the Hsp90-Aha1 complex with 3 µM Aha1 (light gray) and 6 µM Aha1 (dark gray).

Mixing of the formed Hsp90–Aha1 complex with ATPγS using the double labelled variant led to a strong acceleration of the conformational changes including the early phases of the kinetics (**Figure 40**). The Hsp90-Aha1 complex is preformed with respect to its N to N movements. Early conformational transitions are the most affected, confirming that N-N rearrangements take place early on the reaction coordinate. In addition, the Aha1-stimulated kinetic was similar to the kinetic observed with the lidless subunit (**Figure 31**) which was shown to form a stable N-terminal dimerised state (Richter et al, 2006).

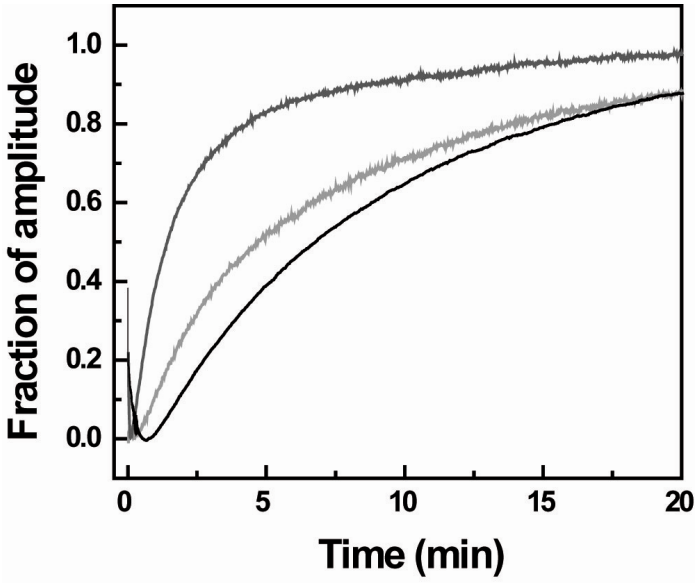

Figure 40: Acceleration of the ATPγS induced conformational changes using the double labelled variant setup. In black the trace without Aha1. In light gray the kinetic in presence of 3 µM Aha1 and in dark gray the trace using 6 µM Aha1.

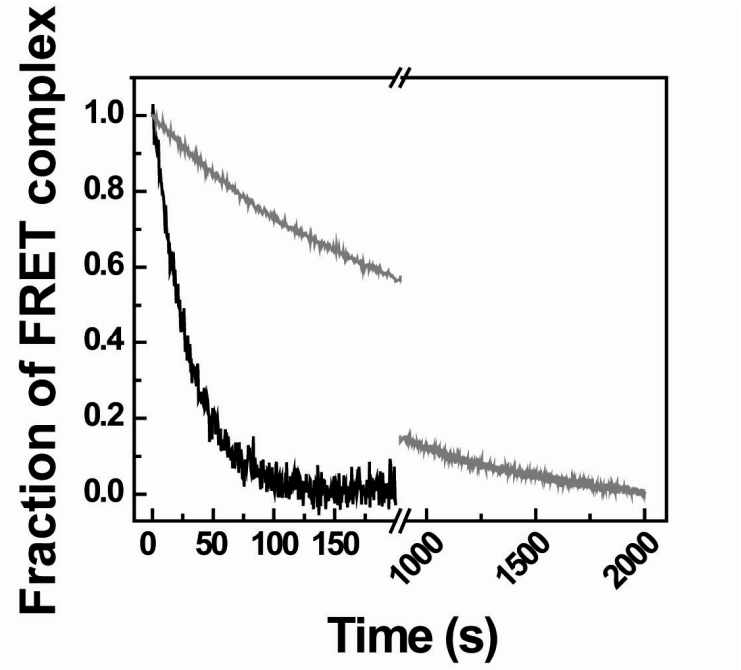

Figure 41: Subunit exchange of Hsp90. The trace of Hsp90 subunit exchange without Aha1 (black) is 10 times faster compared to the rate if Hsp90 is complexed with Aha1 (gray trace).

The Hsp90 Aha1 complex seems preformed for ATPγS-induced structural changes; we probed the stability of the Hsp90-Aha1 complex using subunit exchange rates as a tool. Indeed chasing an Aha1 Hsp90 complex with unlabelled Hsp90 indicated that the subunits interact by a factor of 10 more tightly than Hsp90 without the co-chaperone (**Figure 41**). The underling mechanism remains to be solved, Aha1 might stabilize the C-terminal interaction, the N-terminal interaction or might interact with two sites on the Hsp90 dimer one on each subunit their by connecting the subunits and stabilizing the dimer.

Aha1 leads to a strong acceleration of conformational changes which are the most potent target to regulate Hsp90 activity. When we compare the stimulation of Hsp90 ATP hydrolysis and ATPγS hydrolysis by Aha1, we find that factors of 17 for the stimulating effect are achieved for ATP while ATPγS hydrolysis can be stimulated 2.5 times. This suggests that ATPγS hydrolysis is not limited by conformational changes of Hsp90 but by the slow hydrolysis step.

3.3.5 Summary

The analysis of Hsp90 on its conformational level using the described FRET system led to the identification of intermediates that play a key role in co-chaperone regulation. The structural transitions determine the speed of the ATPase cycle and thus the ATPase activity. Hsp90 transits through four states that differ in conformations. The first intermediate is at higher energy as predicted by the rate constants (k_2 and k_{-2}). This reaction dominates the k_{cat} of the ATPase activity. We assume that the structural changes leading to I_1 are influenced by the surrounding of the nucleotide binding pocket. Structural changes that presumably are involved at this stage represent the closure of the ATP-lid or the initial displacement of the first β-sheet of the N-terminal domain which is swopped to the N-terminal domain of the second subunit (**Figure 31**). The contact surfaces set free in I_1 then lead to contact formation between the N-terminal domains leading to I_2, presumably trapping the bound ATP. Further rearrangements then lead to the hydrolysis active conformation (closed state) which disassembles fast using ATP because it gets hydrolysed quickly using ATP analogues instead like ATPγS or AMP-PNP renders the closed state very stable since the reverse rate (k_{-4}) is so small, indicating strict commitment of the ATP in this conformation. Afterwards the N-terminal domains dissociate and the next round of the cycle can start. Kinetically phosphate or ADP bound species do not populate during the reaction cycle.

Sti1 modulation of the conformational changes of Hsp90 seems to be comparable to a bracket that stalls the reaction completely. The open conformation is stabilised in the Hsp90-Sti1 complex preventing N-terminal dimerisation. Cpr6 favours closing indicated by modulating the ATPγS induced conformational changes. ATP-induced structural changes become detectable using Cpr6 (**Figure 37**). p23 in concert with Cpr6 stabilised the closed conformation by binding presumably to I_2 and decelerating the conformational change to the closed state. This view of the p23 action in the Hsp90 cycle stresses that inhibition of p23 is complex and does not saturate with its affinity.

The analysis of these co-chaperone induced modulations observed by the FRET system stressed the importance of the conformational level of Hsp90s regulation. Interestingly, through the knowledge of defined stages in the SHR maturation pathway it tempts to speculate how the conformation of Hsp90 might be at the respective maturity stage of the receptor.

In contrast to the modulation of Sti1, Cpr6 and p23 co-chaperones, Aha1 induced structural changes that accelerate the conformational cycle. Interestingly, the accelerating effect was very similar to the effects observed with the Hsp90-lidless and the Δ8 Hsp90 heterocomplexes (**Figure 31** and **Figure 40**) suggesting that early structural changes on the pathway are affected by Aha1. In addition, the heterocomplex with wt Hsp90 and lidless-Hsp90 cannot be stimulated by Aha1 indicating that matching steps of the cycle are affected (Richter et al, 2008).

3.4 p23/Sba1 in the Hsp90 cycle

The co-chaperone p23 interacts with Hsp90 in a defined state that requires ATP binding (Ali et al, 2006; Richter et al, 2004; Johnson and Toft, 1995b). Thus demanding conformational constrains are governing its interaction. For binding and inhibition of the ATPase, the N-terminal β-sandwich structure consisting of an 8-stranded β-sheet in the IgG topology is required (Weaver et al, 2000; Weikl et al, 1999). The loop formed by residues 97-114 connecting the last sheet is very interesting in this structure. It forms a hook-like protrusion which is important for interaction with Hsp90. In complex with Hsp90, this site is located below the closed ATP-lid of Hsp90. Its sequence is highly conserved in p23 proteins. Structural data for residues c-terminal of Alanin 135 are missing. However, the crystallized fragment is able to inhibit the Hsp90 ATPase function (Weikl et al, 1999). Interestingly, when GR is expressed in yeast cells it requires the C-tail of p23/Sba1 for its activation indicating that the inhibition of the ATPase is only part of the function of p23 (Oxelmark et al, 2003). Sba1 ko in yeast are more sensitive to Hsp90 inhibitors stressing the point that the ATP-bound state becomes stabilized by p23 interaction (Forafonov et al, 2008). For this activity, p23 does not require its C-tail. In vivo p23 mobility dictated by recruitment to Hsp90 complexes (Picard et al, 2006; Picard, 2006b). Yet, substrate related-pathways require both the

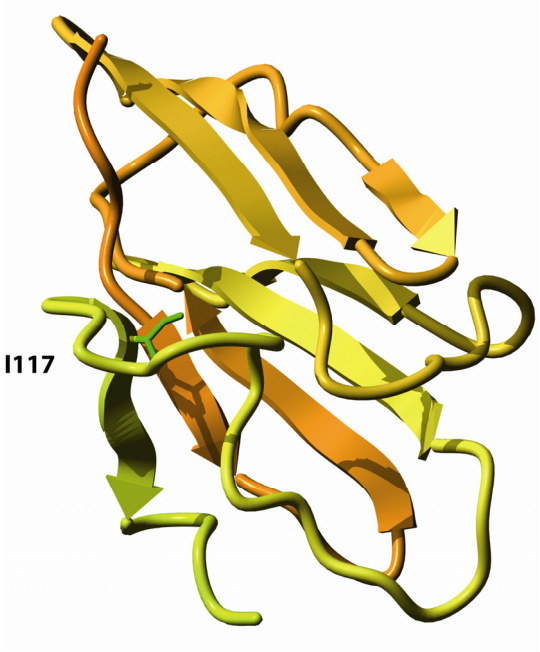

Figure 42: Crystal structure of the N-terminal domain of p23 (1ejf). The interacting surface is facing to the front in which the hook-like loop is coloured in green. I117 is important to stabilise the last β-strand anchoring the loop in its correct conformation. A high content of aromatic residues in the loop region are responsible for the characteristic positive CD signal at 230 nm.

N-terminal Hsp90 interacting domain and the C-terminal part of the protein (Toogun et al, 2007; Freeman and Yamamoto, 2002; Weikl et al, 1999; Bose et al, 1996; Freeman et al, 1996).

The C-terminal tail exhibits chaperone function to p23. In vivo data hint to a functional involvement of the C-tail in client protein activation (Oxelmark et al, 2003). Also the p23 C-tail becomes cleaved early by a caspase 3 / 7 in the apoptotic pathway upon which substrates proteins become released from Hsp90 (Mollerup and Berchtold, 2005; Gausdal et al, 2004). Yeast ΔSba1 cells are more sensitive to Hsp90 inhibitors but this is not depending on the C-tail of p23 (Forafonov et al, 2008).

The sequence of the C-tail of *S. cerevisiae* contains M/G-rich parts and also L/Q-rich motifs which we suspected to be involved in substrate binding, as M/G rich regions in Hsp60s were found to face in the interior of the folding chamber (Tang et al, 2008; Tang et al, 2006). Their role in substrate folding is disputed to date (Farr et al, 2007). But also substrate interaction has been assigned to this sequence inside the folding chamber of GroEL (Elad et al, 2007).

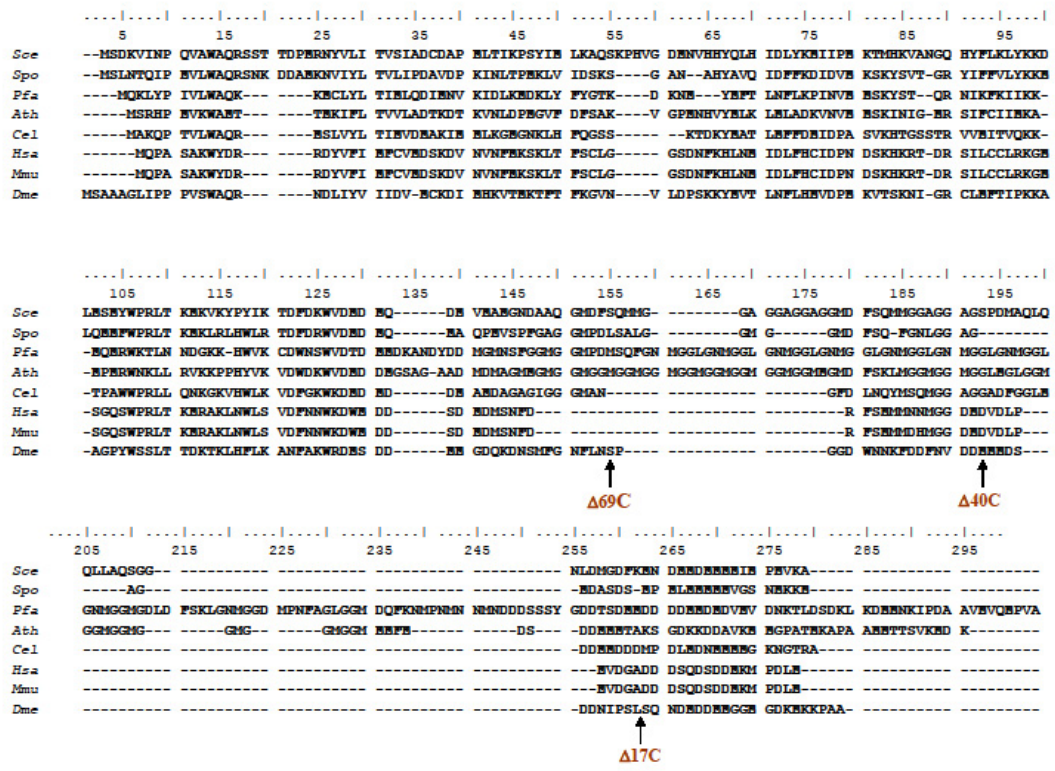

Figure 43: Alignment of p23 proteins from *Saccaromyces cerevisiae* (Sce), *Saccaromyces pombe* (Spo), *Plasmodium falciparum* (Pfa), *Arabidobsis thaliana* (Ath), *Caenorhabditis elegans* (Cel), *Homo sapiens* (Hse), *Mus musculus* (Mmu) and *Drosophila melanogaster* (Dme).

Also DnaJ-like proteins show sequences that are comparable to the M/G rich region found to different extents in p23 proteins. In the signal recognition particle which binds to the hydrophobic site of an amphiphatic helix of the export signal to stall translation, also methionine-residues are involved in the process (Driessen and Nouwen, 2008).

An alignment of a set of p23 proteins highlights that the N-terminal part and especially the interaction loop (residues 97-114 in *S. cerevisiae*) are highly homologous, leading to the conclusion that this part forms the major interaction site

with Hsp90 (**Figure 43**). In contrast, the C-terminal domain is of high sequence variability. The region varies in length of the repetitive sequence motifs. The p23 form *P. falciparum* and that of *A. thaliana* show a large number of repetitions of the M/G rich part, while for p23 form *H. Sapiens*, *M. musculus* and *D. melanogaster* the sequence region is very short. The Q/L rich regions do not seem to be conserved compared to the M/G rich stretch, but leucine glutamine and asparagine are found throughout in the C-tail of p23 genes. The very C-terminal tail is of negative charge in all variants depicted in the alignment.

3.4.1 Characterization of Sba1

To analyse the contribution of the C-tail on p23 functions deletion variants were analysed for their activity in vivo and in vitro. Deletion variants of the C-tail were generated that have the acidic tail deleted (Δ17C); the Q/L-rich region (Δ40C) and a fragment with a deletion of all three characteristic sequence regions, the acidic, the QL rich and the M/G rich region (Δ69C).

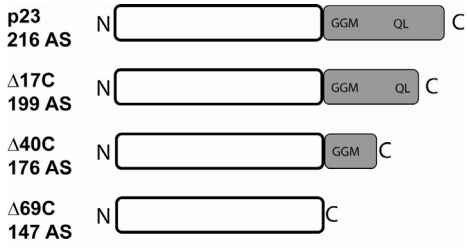

Figure 44: p23 constructs used to characterize the chaperone function. The C-tail is shown in gray with the M/G rich and Q/L rich regions marked in the illustration.

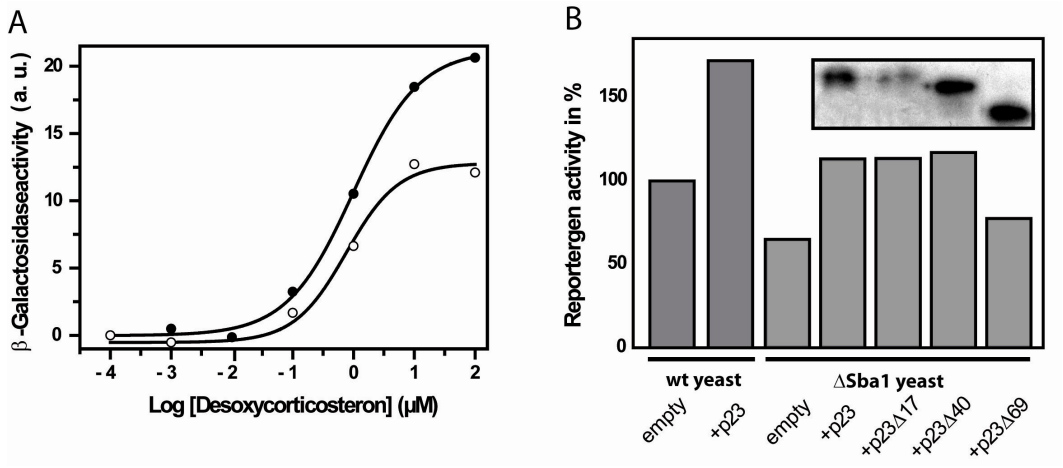

Figure 45: GR activity in vivo depends on the C-tail. A) Dose response curves of GR signaling in wild type (circles) or ΔSba1 yeast (open circles) cells. The IC 50 in both cases is 1 μM but the amplitude for the Sba1 ko cells is reduced up to 50 %. B) p23 expression in yeast p23 ko indicates that the GR signaling efficiency can be rescued by all C-terminal truncated fragments but the p23 Δ69C variant. Expression of p23 in the wild type yeast also increases the level of GR activation indicating that the amount of GR activation depends on the p23 concentration in the cell.

The dependence of GR activity on the Hsp90 system can be analysed by expressing the protein in yeast cells. β-Galactosidase is expressed by a promoter that is responsive to GR signalling. The dose response curves of Desoxycorticosterone show that in yeast, GR is activated less efficiently compared to mammalian cells with an IC50 of 1μM hormone.

Analysing the dose response in p23 ko cells (**Figure 45**) shows that the maximal activation is reduced upon p23 deletion indicating that p23 is involved in GR maturation (Oxelmark et al, 2003). Reconstitution of p23 in the p23 ko cells showed that this effect can be rescued by p23 wildtype, p23 Δ17C, p23 Δ40C but not by p23 Δ69C (**Figure 45**). Additional expression of p23 in the wildtype cells also increased the reporter gene activity suggesting that the data are also dependent on the expression level of p23.

3.4.2 CD spectroscopic analysis of p23.

For the in vitro analysis, p23 variants were expressed in *E. coli* and purified to homogeneity. These variants were structurally characterized using CD spectroscopy (**Figure 46**). The negative CD signal at 200 nm which is a characteristic feature of random coil structured polypeptide chains is decreased for the C-terminal truncated p23 proteins indicating that the C-terminal tail is devoid of secondary structure and largely adopts random coil structure.

CD spectra show an interesting maximum at 230 nm which presumably derives from high amounts of aromatic residues in the long loop between sheet 2 and sheet 8 that are anisotropically fixed in the structure. This signal is a characteristic of p23 proteins (**Figure 42**). Deletions from the C-terminal tail cause an increase in the positive CD signal at 230 nm which exceeds the expected increase due to the higher weight put on that spectral band by reducing the number of residues for the mean residue weight calculation. The deletion of 40 % from the C-tail leads to a change in increase in this spectral band of more than 200 % raising the possibility of a cross talk between random coil structured C-tail and the N-terminal β-sandwich domain.

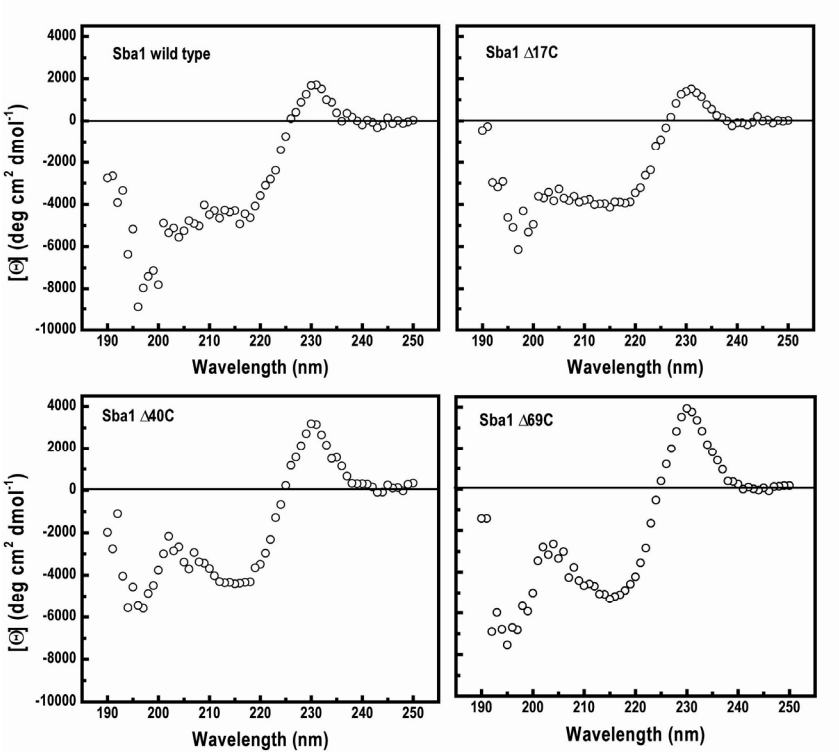

Figure 46: CD-Spectra of p23 proteins. The spectra indicate a reduction of negative CD signal at 200 nm which corresponds to random coil signal. The positive CD signal at 230 nm increases upon deletion of the C-terminal tail. The increase at 230 nm partially comes from the higher contribution of the N-terminal domain in [Θ] due to the deletion of the C-tail, but the fact that the increase in the positive CD-signal at 230 nm is 240 % for Sba1 Δ69C removing only 41% of residues hints to structural change upon deletion.

3.4.3 Analysis of the stability of p23

CD spectroscopy was used to follow the unfolding of p23 at the characteristic positive CD signal at 230 nm. All p23 deletions show a cooperative unfolding in the temperature transitions but with changing T_M values (**Figure 47**). Interestingly, the p23 wild type protein is not the most stable variant of the analysed p23 variants; instead the p23 Δ69C variant was the most stable, followed by p23 wt and p23 Δ40C. p23 Δ17C was lesser stable than the wild type protein or any other fragment. However, the analysed temperature-unfolding was not reversible, indicating that the thermal transitions cannot be fitted to determine the ΔG value of temperature unfolding. To compare such irreversible unfolding processes it was important to keep the heating rates constant. The stability data show that the C-tail has an influence on the N-terminal β-sandwich domain. To have a point of reference for the melting of the p23 structure, we performed differential scanning calorimetry (DSC) with p23 and its fragments (**Figure 47**). Cooling the denatured sample did not show cooperative changes in heat capacity suggesting that thermal unfolding was again irreversible. Thus heating rates as in the CD experiments were used to record the heat capacity changes for p23 unfolding. The peak maxima found matched the melting temperatures in CD transitions. The ΔH_{cal} values also report on varying stability of the proteins with the same tendencies found in the CD melting experiments. The structural characterisation indicated that the C-tail has an impact on structure of p23, suggested by the CD analysis.

The p23 chaperone function was known to be dependent on the C-tail of the protein. The structural impact of the C-tail on the N-terminal Hsp90 interacting domain was surprising. The mechanism and especially the functional importance needed further analysis.

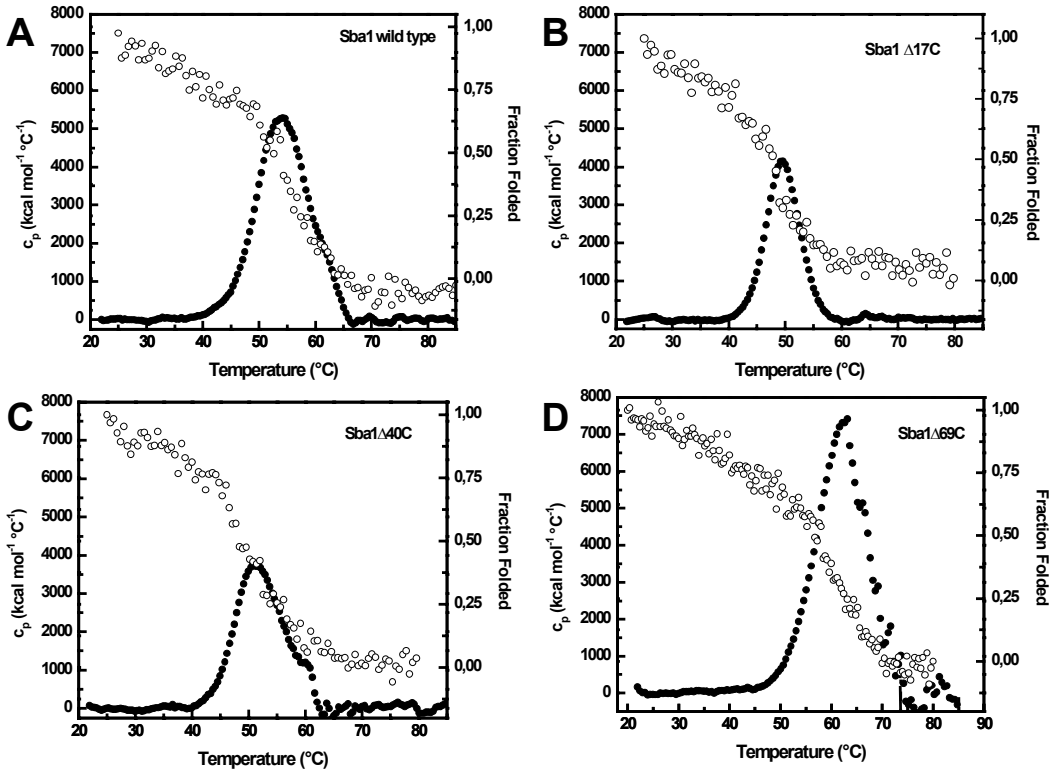

Figure 47: Thermal stability of p23 proteins. Temperature transitions of p23 wild type (A), p23 D17C (B), p23 D40C and p23 D69C measured by CD (open circles) or by DSC (closed circles) with the same heating rates.

3.4.4 Chaperone function of p23

The chaperone active site of p23 had been localized to the C-terminal tail which was considered to be random coil structured (Weikl et al, 1999). The large content of glycine residues in the C-terminal tail supports this view of stabilizing an unfolded state because of to large entropy accounted for by the high flexibility of the glycines (Braig et al, 1994b). The high flexibility is locally concentrated in the M/G rich regions with hydrophobic amino acids that presumably are important for contacting hydrophobic surfaces in aggregation-prone substrates. In some species, these M/G rich regions can be extended to more than 80 amino acids which might reflect an adaption that depends on the substrate set with which p23 operates in these organisms. Thus, we deal with a chaperone activity that transiently interacts with substrates because binding locally puts constraints on glycine flexibility. This loss of entropy then might be important for the release reaction and depends on the constraints put on the C-tail flexibility. This makes it difficult to predict interaction profiles. To analyse the chaperone function of p23 we used different substrates and p23 vvariants.

3.4.4.1 p23 inhibits CS unfolding.

The citric acid synthase (CS) is a dimeric enzyme which catalyses the aldol-condensation of oxal-acetate Acetyl-CoA. The energy for this is derived from the hydrolysis of the high energy thio-ester bond of the CoA moiety in the reaction. CS has been extensively characterized and used to analyse chaperone activities of different classes of Hsps (Buchner et al, 1998; Bose et al, 1996). The protein unfolds thermally via intermediates that are bound by chaperones. Due to the binding of intermediates, the unfolding reaction can be prevented and the bound CS is kept in a state that can refold upon substrate addition or relief of temperature stress. Thus the activity can be preserved for a longer time course in the presence of chaperone. In the presence of p23, the activity is preserved for 2 times longer compared to the sample where no p23 was present during the high temperature incubation. A 6-fold excess of p23 vs CS was used to compare full-length p23 with the C-terminal

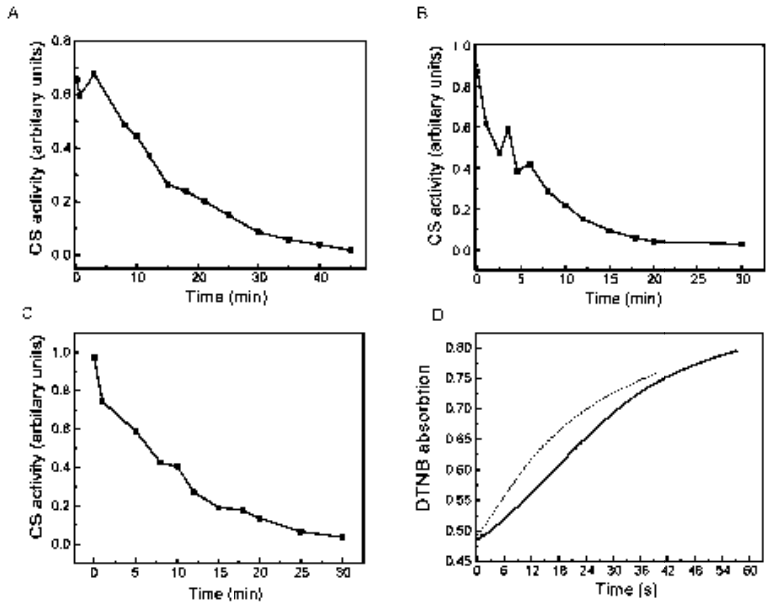

Figure 48: CS temperature unfolding experiments. CS was incubated 42°C for times as indicated on the X-axis in presence of 1µM p23 wt in A), 1 µM p23 Δ17C in B) or 1 µM p23 Δ40C in C). In D) progress curves of CS without incubation at 42°C (dashed line) and in presence of p23 wt after incubation at 42 for 10 min are shown to demonstrate the interesting lag phase in the first seconds in presence of p23 after heat incubation.

truncated variants (**Figure 48**). The chaperone activity of p23 was found to depend on the C-tail. Any deletion form the C-terminal tail rendered the protein inactive towards delay of the temperature induced unfolding and aggregation of CS. Already p23 Δ17C is inactive at the conditions used. The progress curves of CS activity without high temperature incubation show no significant pre-steady state phase (**Figure 48**D gray line). At high temperature incubation a lag phase becomes apparent in the presence of full length p23. This lag phase observed potentially corresponds to the refolding kinetics of the intermediate of CS to its active conformation (**Figure 48**D black line).

Thus, a near-native intermediate which refolds in the second time scale to the active conformation of the enzyme presumably interacts with p23 and then refolds upon adding substrates and returning to more stabilizing conditions. Thus p23 prevents unfolding by binding to early unfolding intermediates.

3.4.4.2 p23 prevents CS aggregation

Temperature-induced unfolding of CS leads to aggregation after 2 minutes at 42°C. This can be measured using turbidimetry or light scattering. The aggregation process is delayed by p23. As in the assay using the enzymatic activity the fragments of p23 do not show a significant chaperone function indicating that the C-terminus as a howl is important for substrate interaction in this case (**Figure 49**).

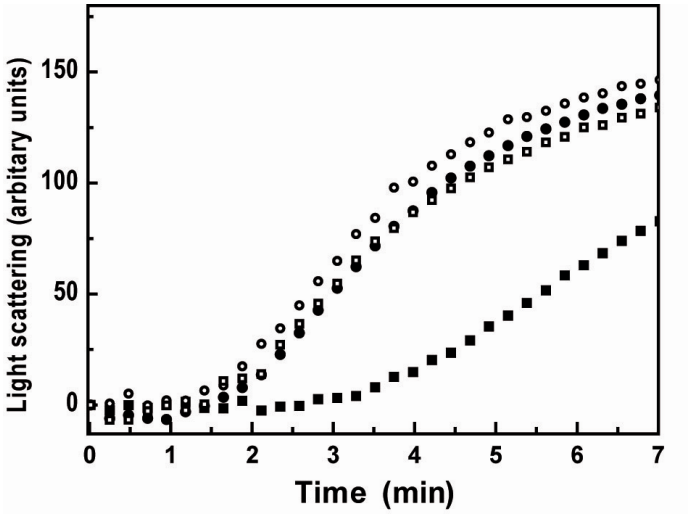

Figure 49: CS aggregation measured by light scattering. At elevated temperatures of 42°C CS unfolds and aggregates (closed circles). Addition of p23 Δ17 (open squares) or p23 Δ40C (open circles) do not prevent or delay the aggregation, in contrast to p23 wt (closed squares) which delays the aggregation process. p23 proteins were used in a 3-fold excess over CS.

3.4.4.3 p23 prevents GDH aggregation

Glutamat dehydrogenase (GDH) oxidatively deaminates glutamate to give alpha keto-glutarate and ammonia. The aggregation was observed using either light scattering or monitoring the turbodimitry of the respective sample. p23 has a chaperone activity for this substrate comparable to that observed for CS. P23 was active but C-terminal deletions were again inactive for chaperoning the GDH (**Figure 50**).

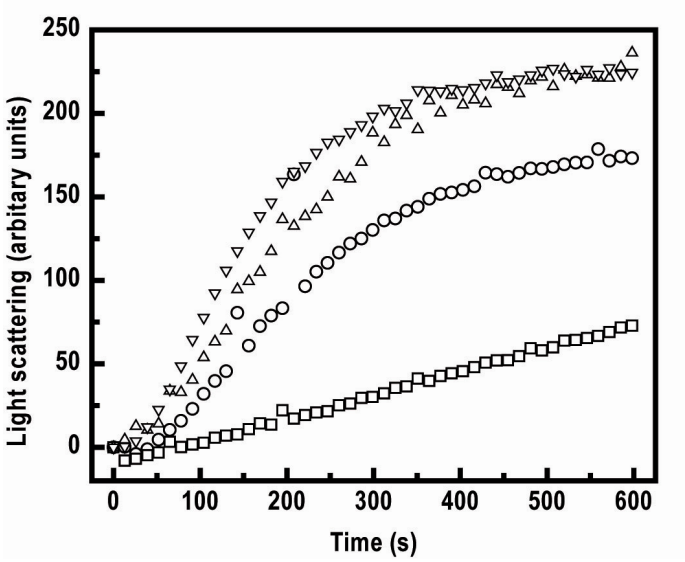

Figure 50: GDH aggregation measured by light scattering. At elevated temperatures of 45°C, GDH unfolds and aggregates (closed circles). Addition of p23 D17 (open up triangles) or p23 D40C (open down triangles) do not prevent or delay the aggregation, in contrast p23 wt (open squares) inhibits the aggregation process. p23 proteins were used in a 3-fold excess over GDH.

3.4.4.4 p23 inhibits p53 inactivation

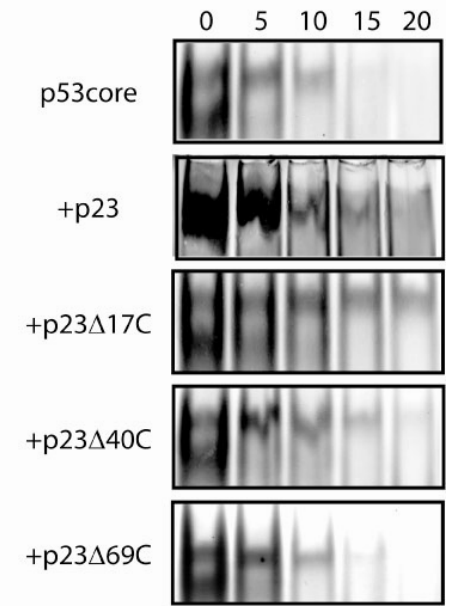

.
Figure 51: Inactivation of the p53 core domain at 38°C. In the upper row the decrease of p53 DNA binding activity with incubation times at 38°C for 0, 5, 10, 15 and 20 minutes is shown. Addition of p23 variants stabilizes the protein in dependence of the C-tail. p23 and p23 Δ17C show equal efficiency second and third row while p23 Δ40C (fourth row) and p23 Δ69 (fifth row) loose chaperoning activity.

The tumor suppressor p53 is an Hsp90 client that is sensitive to mild temperature stress. The p53 core domain which is the DNA interacting part of the protein, can be used as a model system for biochemical analysis (Dehner et al, 2005; Klein et al, 2001). In vitro, p53 looses DNA binding activity very quickly. At temperatures of 38°C it starts to unfold which leads to a reduction in DNA binding activity (Butler and Loh, 2006). Hsp90 was shown to partially rescue the temperature sensitivity (Muller et al, 2004). The middle domain of Hsp90 was identified as the primary binding site. To analyse whether p23 has an effect on p53 stabilisation we performed DNA band shift assays in the presence or absence of p23 variants and analysed the DNA binding activity (**Figure 51**).

p23 indeed stabilized the p53 DNA binding activity. Full length p23 and p23 Δ17C were the most active protein variants. p23 Δ40 retained a minimal level of stabilising activity while p23 Δ69 lost the stabilising activity on p53 DNA binding activity. For this substrate the p23 gradually looses chaperone activity in contrast to the results form CS and GDH temperature unfolding.

3.4.4.5 p23 influences p53 aggregation

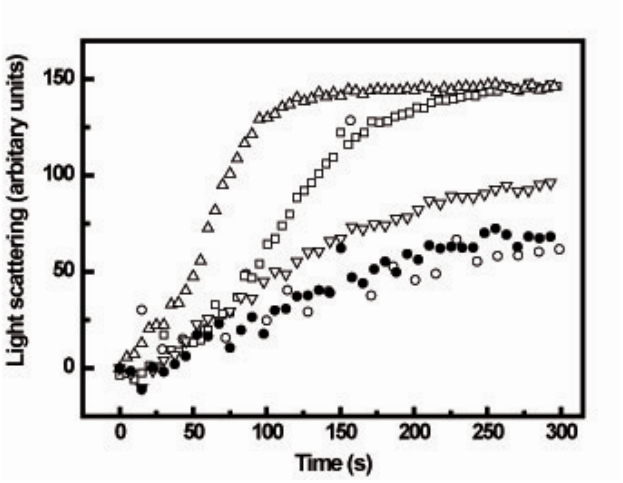

Figure 52: Aggregation of p53 DNA binding domain. The p53core domain aggregates at temperatures of 42 °C without a characteristic lag phase seen for CS or GDH proteins (closed circles). Addition of p23 proteins leads to co-aggregation not to a inhibition of the aggregation process. Co-aggregation depends on the C-tail of p23. P23 wt (open squares) and p23 D17C (up triangles) show co-aggregation. In the case of p23 D17C the aggregation process is accelerated. For p23 D40C (down triangles) and p23 D69C co-aggregation (open circles) is reduced or not detectable respectively.

Temperature-induced unfolding of p53 core leads to aggregation that can be monitored by light scattering (**Figure 52**). The aggregation process does not include significant lag phases suggesting that no soluble intermediate is on the unfolding pathway. Interestingly in this case, p23 seems to co-aggregate with p53 core domain instead of preventing the aggregation (**Figure 52**). Co-aggregation takes place for the p23 wt, p23 Δ17 and slightly also for p23 Δ40. p23 Δ69C does not show co-aggregation. These data seem to challenge p53 inactivation data. However, both assays indicate gradual loss of interaction with an intermediate structure on the unfolding pathway. This suggests that the respective intermediate is soluble at the buffer conditions and the lower p53 concentration used in the inactivation assay while this intermediate is insoluble under the experimental conditions used for p53 aggregation assays.

3.4.5 Biacore measurements to determine the binding affinity

A method to analyse protein-protein interactions is surface plasmon resonance (SPR) spectroscopy. p23 was immobilised on a gold surface coated with polysaccharides which provide the active groups for immobilisation of proteins via lysine residues under mild (see materials and methods). A beam of monochromatic light is deflected on the gold surface. The angle of deflection depends on the mass residing at the surface close to the gold layer. Thus, mass increase due to binding of another protein can be measured and analysed.

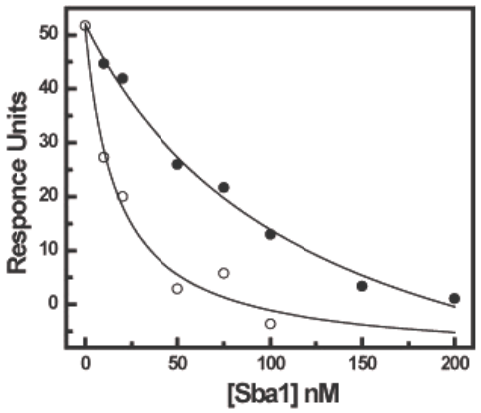

Figure 53: Interaction of p23 wt and p23 Δ69C with Hsp90. P23 wt (closed circles) shows a apparent K_D of 80 nM in this competition assay while p23 Δ69C has a apparent KD of 20 nM.

p23 binding to Hsp90 was measured in a competitive way at low concentration of Δ8Hsp90 for p23 wild type and p23 Δ69C.

In this experiment, it becomes evident that the C-tail truncated p23 shows improved binding to Δ8Hsp90 indicating that binding to Hsp90 is influenced by the C-tail (**Figure 53**). The stability changes of p23 full length and the C-tail truncated variant suggest that the C-tail indeed influences the N-terminal β-sheet structure of p23 (**Figure 47**). The stability gain becomes apparent in the binding reaction to Hsp90. The secondary structural analysis of p23 variants by CD spectroscopy indicated that truncation of the C-tail has some impact on the structure of the Hsp90 interacting domain. Especially the positive signal at 230 nm which indicates the anisotropic environment of aromatic residues surrounding the loop including residues 97-114 was affected (**Figure 46**). This interesting feature of

the C-terminal tail which was unexpected from previously observed data required a detailed analysis.

3.4.6 Fluorescence anisotropy assay for p23 binding

p23 S2C was used to label the protein with fluorescein-iodacetamid. The p23 fluorescein conjugate was analysed using fluorescence polarization in which the anisotropy was recorded. When Hsp90 wild type was added no change in anisotropy was observable. Adding AMP-PNP or ATPγS to this mixture leads to change in anisotropy with kinetics that give rates comparable to the conformational changes of Hsp90. The temperature dependence of ATPγS-induced binding corresponds to the k_{cat} of the ATPase activity and with the slow phase observed in the FRET experiments using N-domain-labelled and M-domain-labelled Hsp90. This shows that p23 binds to a state of Hsp90 after the rate limiting step and stabilizes the N-terminal dimerized state followed by a step that is inhibited by p23 and eventually becomes rate-limiting if p23 is present at higher concentrations. This assay can be used in solution and does not require immobilisation of p23.

A competitive binding assay was set up in which a complex of Hsp90-AMP-PNP and

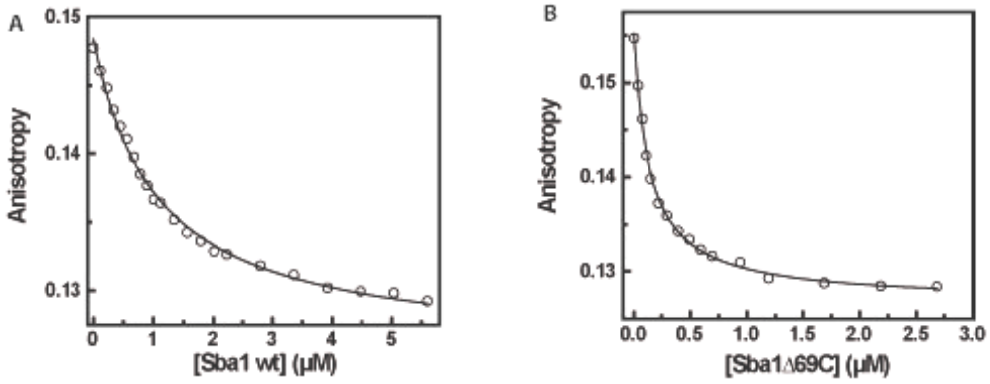

Figure 54: Anisotropy p23 binding assay. Complexes of fluoresceine-labelled p23 and Hsp90 were formed by addition of AMP-PNP. Then p23 wt (A) or p23 Δ69C (B) were added to compete for the binding of the labeled p23 which is then displaced form the large Hsp90 complex and a decreasing anisotropy is observed.

the labelled p23 was pre-formed. Then unlabelled p23 was added to compete for p23 binding. Comparing the binding of p23 wild type and p23 Δ69C to Hsp90 wild type revealed that indeed binding to Hsp90 is altered by deletion of the C-tail. Consistent with the previous experiments performed, the p23 Δ69C variant showed a 5-7 times increased binding affinity towards Hsp90 in complex with AMP-PNP.

3.4.7 Binding of p23 to Hsp90 p53 substrate complexes.

In vivo p23 is part of Hsp90 substrate complexes (Johnson et al, 1994). For some substrates it was shown that p23 stabilises the substrate interaction with Hsp90 (Johnson and Toft, 1994). For productive formation of the PR-Hsp90 complex, p23 seems essential (Oxelmark et al, 2003). Considering that, we analysed whether p23´s binding properties change upon the presence of a substrate protein. A physiological substrate available for biochemical analysis is p53 for which the main interaction site that is located in the M-domain of Hsp90 (Muller et al, 2004).
Complex formation of p53 core with Hsp90 was assayed using immobilized p53 coated in 96 well plates, a method described in the PhD thesis of Lin Römer (**Figure 55**). To monitor binding, fluorescently labelled Hsp90 was incubated in the p53-

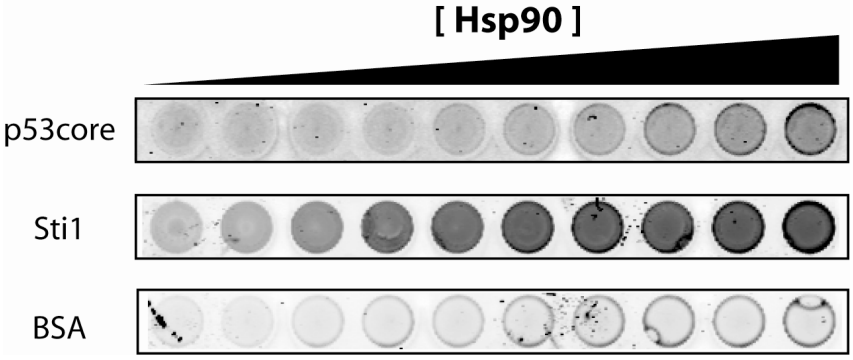

Figure 55: Coating assay developed to monitor Hsp90 substrate interactions. P53 (upper row) Sti1 (middle row) or BSA (last row) were coated on activated ELISA plates. Then increasing amount of fluorescently labeled Hsp90 was added and incubated over night at 4°C. After washing fluorescence signal was scanned.

coated wells. Washing steps were performed that remove both Hsp90 in the supernatant and unspecific bound protein. Then the amount of bound Hsp90 was assayed using a fluorescence scanner. In addition, Sti1 and BSA were coated on the same plate as controls. Binding signals for the BSA-coated wells represent unspecific binding to the wells. Sti1 serves as a positive control because its affinity for Hsp90 is very high. It turned out that the washing steps were effective in reducing the unspecific binding (**Figure 55**). The signals in the BSA wells do not significantly exceed the normal background signal. Sti1 shows a strong binding and saturates with a K_D-value comparable to the SPR measurements or ITC titrations (**Figure 56**).

p53 under these conditions binds only weakly to Hsp90 with a K_D value of 2-3 µM. Thus, a large amount of protein would be required to saturate all binding sites immobilized on the surface. The signal intensity is lower compared to the sample in which Sti1 has been immobilized. This can be explained if the binding is considered to be reversible. In the washing steps performed, labelled Hsp90 dissociates form the

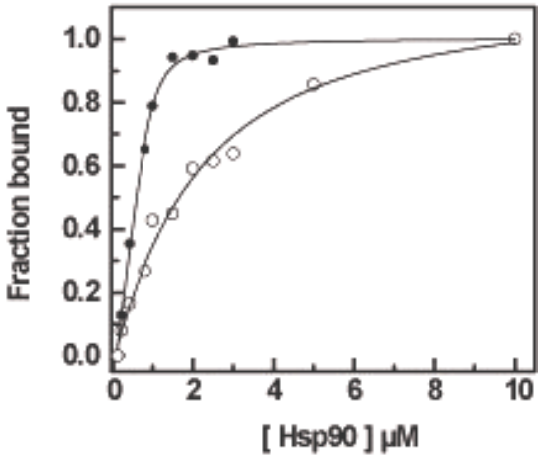

Figure 56: Densitometric analysis of the coating experiments using the ELISA assay. Interaction of fluorescently labelled Hsp90 with coated Sti1 (closed circles) and coated p53 (open circles). The experiments with Sti1 show a strong interaction with high signal intensity. The interaction of Hsp90 with the p53core domain is much weaker also indicated by the lower signal intensity in the ELISA plates.

immobilized p53 core in an amount which is determined by the chemical equilibrium. Thus, the loss of fluorescence with the washing steps is also correlated to the strength of the binding explaining why the signal strength is decreased compared to the Sti1 samples (**Figure 55**).

3.4.8 Stimulation of p23 binding to the Hsp90 substrate complex.

To test how the presence of substrate influences p23 binding to Hsp90, the p53 Hsp90 AMPPNP p23 complex with labelled p23 was formed. To this complex unlabelled p23 was titrated and the anisotropy was recorded. Interestingly, binding of p23 in the presence of p53 core was stimulated by a factor of 5-7 (**Figure 57**). To check whether this depends on the C-terminal tail of p23, we analysed binding of p23Δ69 to the p53 Hsp90 complex. Interestingly, the affinity for the Hsp90-p53core complex remained unchanged compared to the binding of p23 Δ69 to Hsp90 not loaded with substrate (**Figure 59**). Thus, the C-tail seems to influence p23 binding negatively if binding to unloaded Hsp90 is analysed. When binding of p23 is

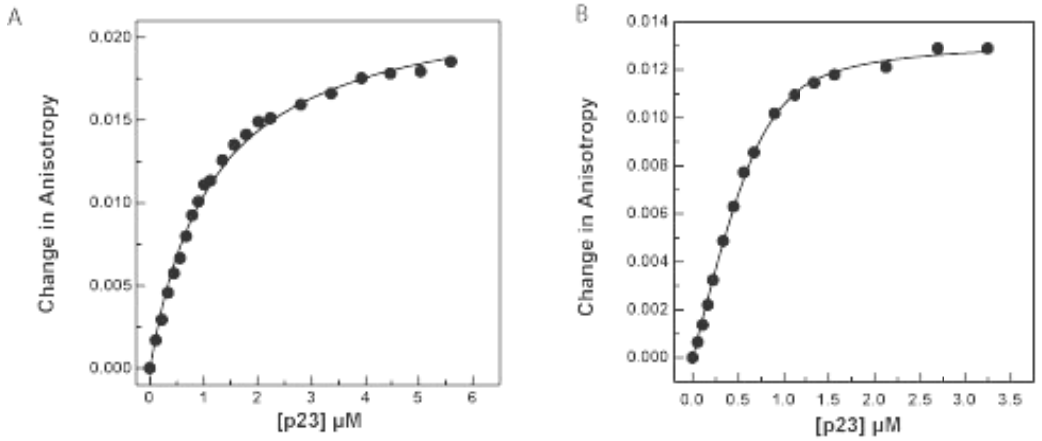

Figure 57: Competitive anisotropy assay to analyse binding of p23 to Hsp90. The apparent K_D values of p23 binding to Hsp90 is 1.2 µM (A) while the apparent KD value of p23 binding to substrate loaded Hsp90 is increased by a factor of 5-7 with a apparent K_D of 150 nM (B).

analysed in the presence of substrate, binding affinity reaches K_D values that are comparable to that of the p23Δ69 variant.

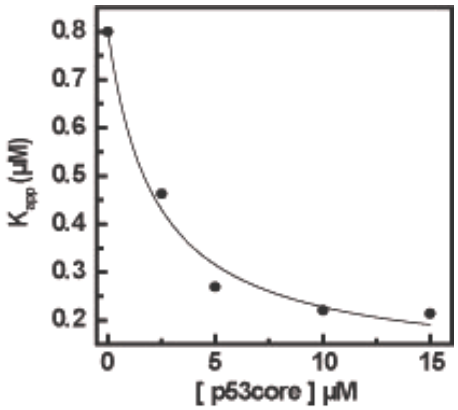

Figure 58: Determination of apparent KD values of p23 with different p53 concentrations using the competitive anisotropy approach. The apparent KD changes with concentration of the p53core domain used. Comparing these data to the binding data of p53 to Hsp90 suggest that binding to hsp90 by p53 is the decisive factor determining the association behavior of p23.

Next, titrations with varying concentrations of p53 core were performed to analyse whether the increase of p23 affinity to Hsp90 correlates with the formation of a putative triple complex containing Hsp90, p23 and p53. The apparent K_D values resulting from a titration experiment were plotted vs. the respective p53 concentration used (**Figure 58**). The affinity of p23 is half saturated at a p53 concentration between 2-3 µM which was also found for the binding of p53 to Hsp90, suggesting that indeed formation of the Hsp90 p53 core complex is the decisive factor for generating high affinity p23. It seems that p23 itself is rearranged because the binding of p23 Δ69 to Hsp90-p53 complexes was not stimulated, as the high affinity binding state of p23 is already formed. The stabilizing effect in the thermal unfolding experiments using p23 wild type and p23 Δ69 support this view. Careful analysis of the existing crystal structural data of free p23 and p23 in complex with Hsp90 lead to the suggestion that p23 adopts an alternate structure in the Hsp90 complex.

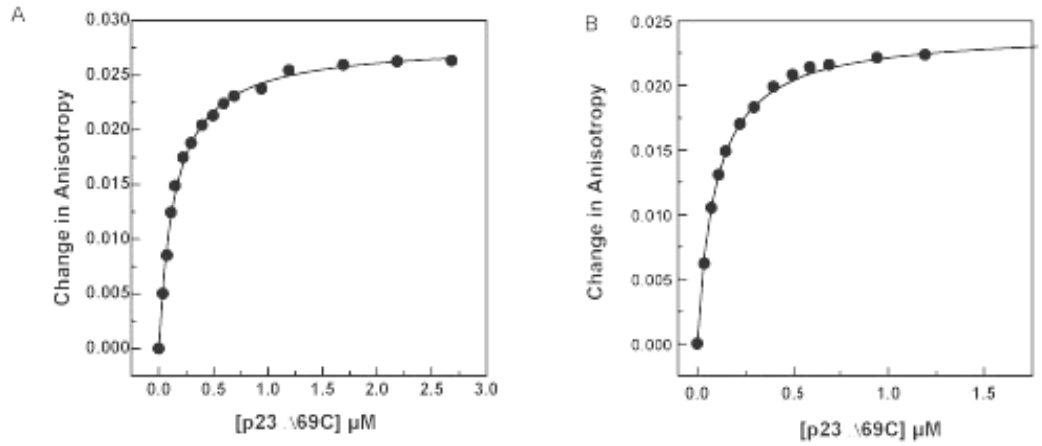

Figure 59: Binding of p23 Δ69C to Hsp90 (A) and to Hsp90 in complex with p53 (B). In contrast to the interaction profile of p23 wt, the p23 C-terminal truncated variant D69C does not show stimulation by the presence of substrate. This suggests that the high affinity state of p23 is influenced by the C-tail and seems to involve a structural change of p23 itself.

3.4.9 Involvement of G/M and Q/L rich regions in the C-tail.

The C-tail of p23 has G/M and Q/L rich regions. To check whether these sequence stretches are involved in sensing of substrates bound to Hsp90, the affinity of the fragments p23 Δ17C and p23 Δ40C was determined using the anisotropy assay and labelled p23 for competition (**Figure 60**). The p23 Δ17 protein is devoid of the acidic residue stretch terminating the protein sequence. p23 Δ40C, in addition to the acidic tail, has the Q/L-rich region deleted, while p23 Δ69C has the G/M-rich region deleted.

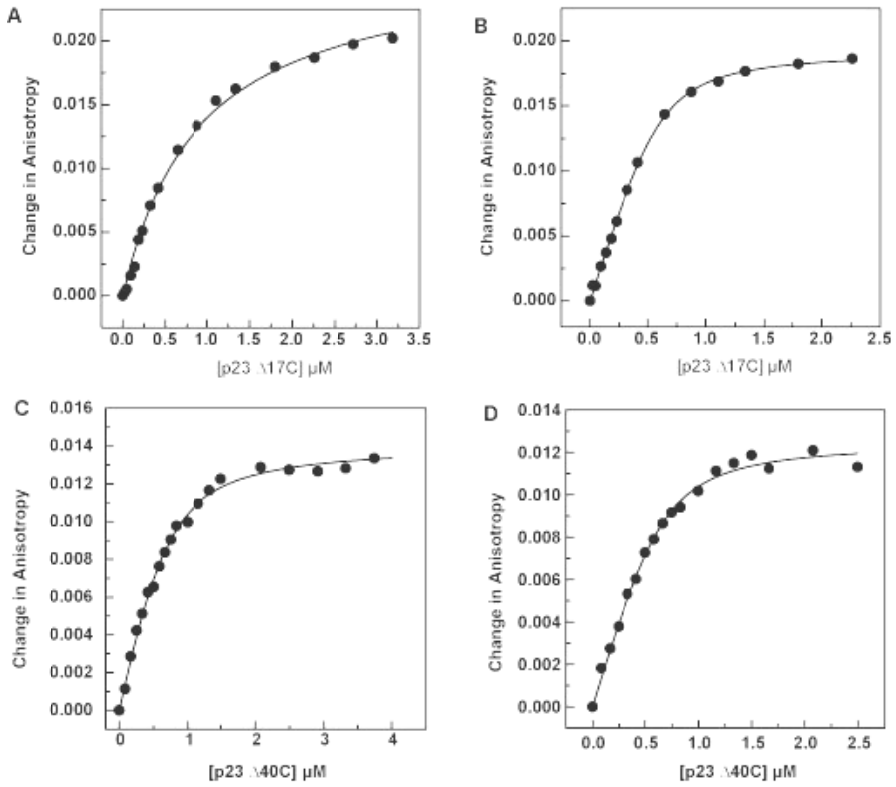

Figure 60: Binding of p23 Δ17C and p23 Δ40C to empty and substrate-loaded Hsp90. A) p23 Δ17C interacts with a apparent KD of 900 nM. In the presence of 10 µM p53 the affinity increases to 150 nM (B). p23 Δ40C binds with 300 nM to the empty Hsp90 (C) and about 150 nM in the presence of 10 µM p53.

The affinity of the p23 Δ17C variant was markedly unchanged compared to the wild type protein. In contrast, p23 Δ40C showed higher affinity than p23 Δ17C and p23 wild type proteins but lower affinity then the p23 Δ69C variant. The K_D values obtained from fitting the data to the respective binding isotherms (see Materials and Methods) show that the presence of the G/M- and Q/L-rich regions prevent high affinity binding of p23 to Hsp90.

Next, titrations in the presence of p53 core were performed. p23 Δ17C binding to Hsp90 is stimulated to the same extent as the wild type protein. p23 Δ40C is

stimulated such that it shows comparable binding as the wild type protein in the presence of p53. p23 Δ69C is not stimulated by the presence of p53 core, presumably because p23 in that variant is already in its high affinity state. Importantly, the p23 C-tail truncations show reduced stimulation of binding to Hsp90 in the presence of p53 suggesting that the C-tail is involved in recognizing the substrate that is bound by Hsp90. Both the Q/L-, and the G/M-rich region seem contribute to that activity.All p23 variants show the same high affinity binding for Hsp90 substrate complexes.

3.4.10 Replacements of the G/M and Q/L rich region

To further analyse the involvement of the G/M and Q/L rich regions stretches of 16 residues in both regions were substituted by 8 glycine alanine repeats. These mutants were tested in chaperone assays using the temperature inactivation of p53 (**Figure 61**). Temperature-induced unfolding of p53 is less delayed compared to p23 wt using both the p23 exchange mutant in the G/M-rich region and the exchange mutant in the Q/L- rich region. In a further set of experiments, the aggregation prevention activity was assayed using GDH as substrate (**Figure 62**). In these experiments, the p23 replacement mutants perform less efficient compared to the p23 wild type protein. The data suggest that both regions in the C-tail contribute to the chaperone function of p23. Both the G/M and the Q/L rich region show a reduction in chaperone activity to an equal extent. The G/M and the Q/L replacement mutants have an equally reduced number of potential substrate interacting residues, tempting to speculate that this is because the C-tail is flexible and can remodel its hydrophobic patch that can interact with a variety of substrates. This might explain the similar reduction in chaperone activity removing specific sequence stretches. In summary, the replacement variants retain chaperone activity although it seems to be reduced compared to the p23 wild type and the p23 Δ17C in the p53core assay.

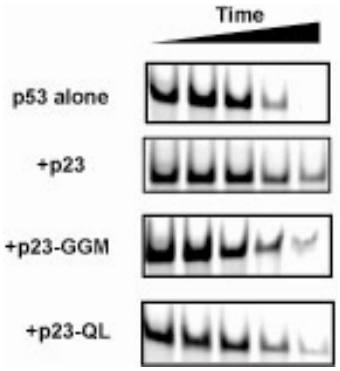

Figure 61: p53 inactivation experiment comparing p23 wild type and p23-GGM an p23-QL mutants in chaperoning p53.

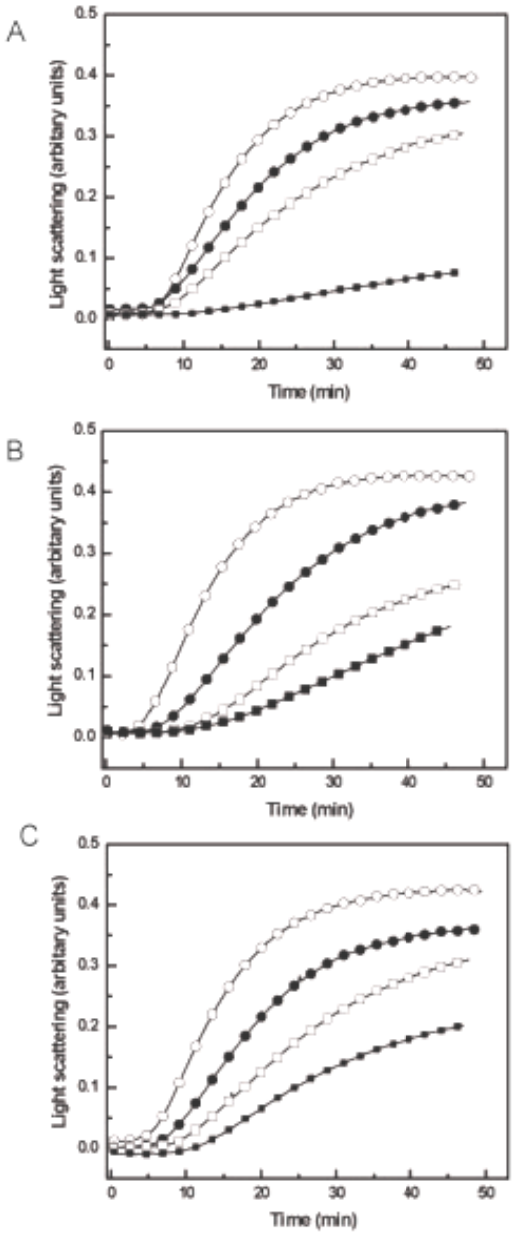

Figure 62: Chaperone activity of p23 and the replacement mutants in GDH aggregation assays. A) GDH aggregation assays using increasing concentrations of p23 wt B) p23-GGM or p23-QL C). Shown is (open circles) GDH aggregation wo p23, 1:1 ratio of p23 to GDH (closed circles), 1:3 (open squares) or 1:10 (closed squares).

3.4.11 Interaction of the p23 replacement variants with Hsp90.

The reduction in the chaperone activity by replacing the G/M-rich and the Q/L-rich region raised the question if, as observed for the truncated p23 variants, a correlation between chaperone function and the increase in affinity to Hsp90 exists. To test this, the anisotropy assay was used to characterize the affinities of the p23 G/M replacement and the Q/L replacement variant for Hsp90 and the Hsp90-p53 complex (**Figure 63**). The binding isotherms determined show that indeed a slight increase in affinity for both replacement variants for unloaded Hsp90. Increased affinity for the Hsp90-p53 complex indicated an upper limit affinity between 0.1-0.2 µM as found for all other p23 variants analysed so far.

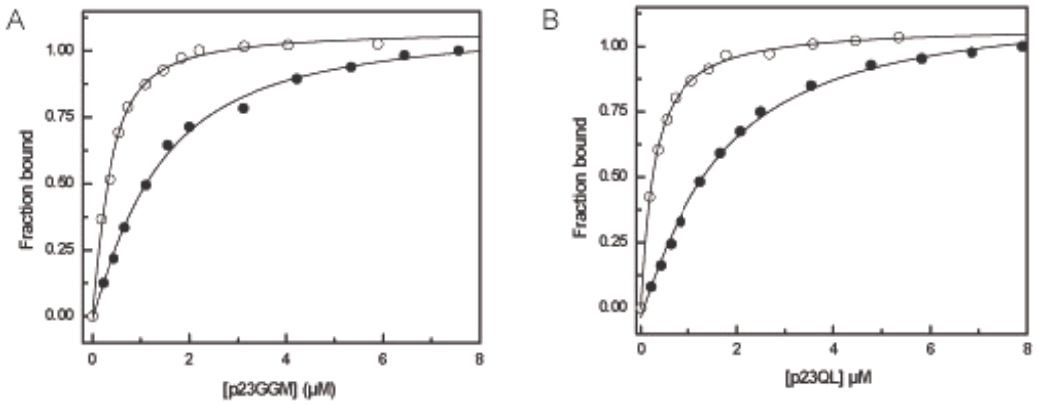

Figure 63: p23 replacement mutants interacting with empty and substrate loaded Hsp90. A) The titration of p23-GGM variant in the absence of p53 (closed circles) and in the presence of p53 (open circles) indicates stimulation. B) The same titration for the p23-QL replacement mutant with p53 (open circles) and without p53 (closed circles).

3.4.12 Analysis of p23s interaction loop

Next, I analysed the state that defines the high affinity form of p23. Looking at the structures available of the free form and that of the p23 Hsp90 complex suggest that the loop region of residues 97-114 is very important for this interaction. The loop is anchored by the short last β-strand at the C-terminal end of the domain suggesting that displacement of this strand would lead to disintegration of the loop structure required for Hsp90 interaction. This structural part of p23 seems to form a large surface for the interaction with Hsp90 which can be regulated by the C-tail. Isoleucin 117 supports β-sheet formation in the local surrounding. To test the effect of this residue the variants I117V and I117A, which destabilize the anchoring of the last β-sheet to the rest of the domain, were cloned (**Figure 42**). The chaperone function of these mutants is not influenced by the mutation indicated by the CS and GDH aggregation assays and the temperature inactivation assay of p53. Thus chaperone function is considered fully functional for the point mutant variants I117V and I117A.

3.4.13 Structural analysis of p23 I117V and I117A variants.

CD spectra of the I117V mutant overlay the spectrum of the wild type protein suggesting that the fold of this variant is not abrogated upon the deletion of a single methyl group. However the I117A variant shows clear deviations in the CD spectrum from the wild type protein, especially the maximum found at 230 nm, which is a characteristic of p23 proteins, is markedly reduced (**Figure 64**). The signal at 230 nm originates from aromatics found in the interaction loop region which is the most conserved part of p23 making the signal a characteristic feature.

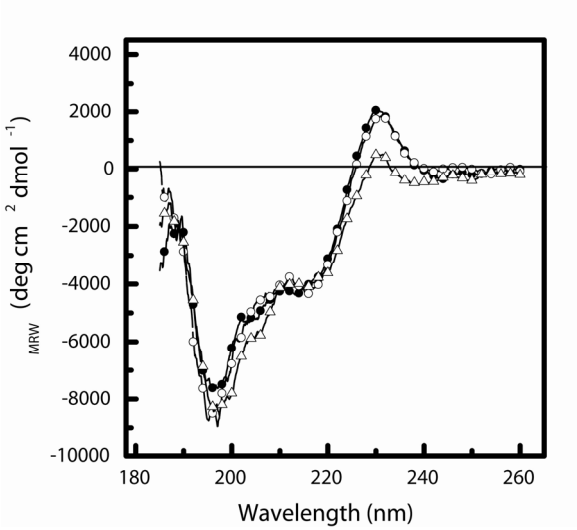

Figure 64: Overlay of CD-spectra of p23 wt and I117 mutated proteins. The CD-spectra indicate that p23 wt (closed circles) and p23 I117V (open circles) have the same structure. The CD-spectrum of p23 I117A (open triangles) deviates from the CD-spectrum of p23 wt.

These data suggested that the I117 residue has an effect of the stability on the p23 interaction loop region. Thus the question arose, whether loss of structural integrity is correlated with a change in the interaction with Hsp90. The anisotropy assay was used to analyse the binding of p23 I117V and p23 I117A to unloaded Hsp90 (**Figure 65**). p23 I117V showed equal binding affinity compared to p23 wild type indicating that the mutation behaves silent. p23 I117A shows a reduction in affinity by a factor of 1.5 to 1.8 indicating that the interaction site is affected.

Next, the interaction of the p23 I117V and p23 I117A variants to Hsp90-p53 complexes was analysed (**Figure 65**). p23 I117V can be stimulated but interacts with

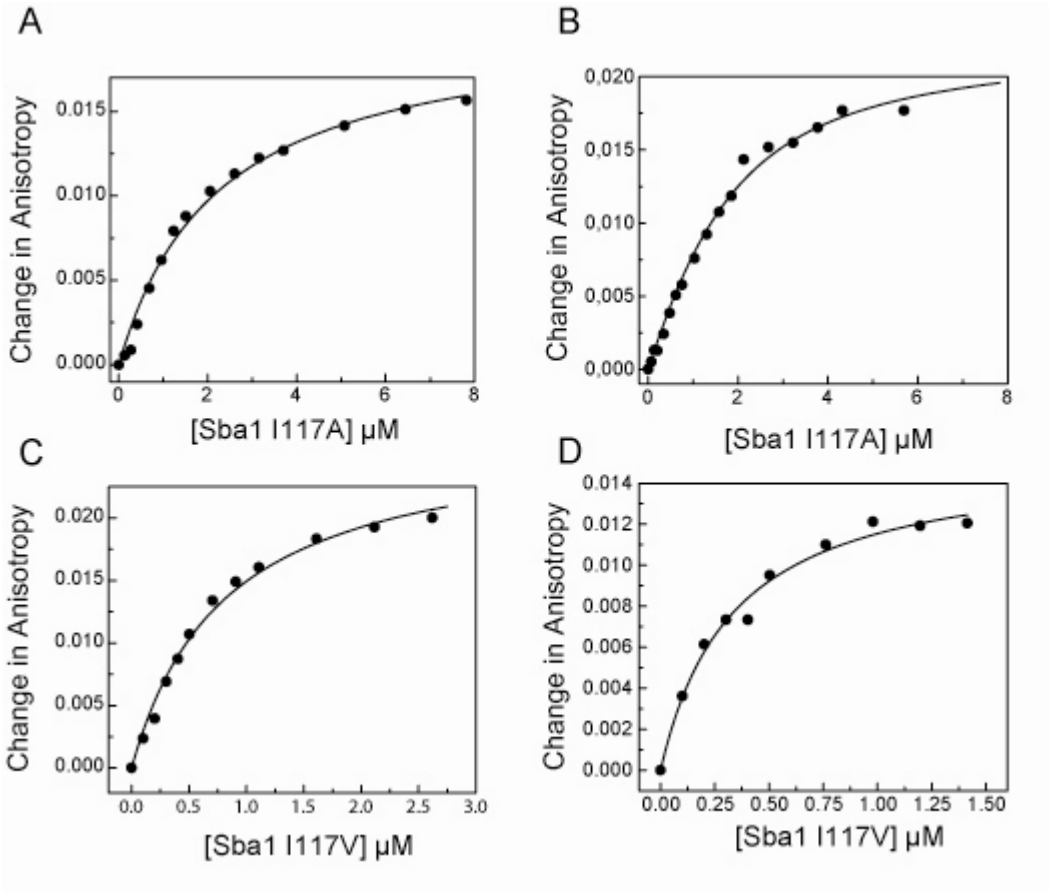

Figure 65: Binding of p23 I117A to empty and p53core loaded Hsp90 A) and B). The same experiments were performed using p23 I117V point mutated variant.

lower affinity compared to the interaction of p23 wt protein to Hsp90 p53 complexes. The p23 I117A variant is not stimulated in presence of p53 and binds with a K_D of 2 µM to the Hsp90-p53 complex indicating that the substrate recognition is lost. The proposed mechanism by which substrates are recognised requires a high affinity state of p23 that we perturbed with the I117V and I117A mutations. This suggests that the high affinity state is defined by the structural integrity of the interaction loop, a prerequisite for sensing of substrates bound to Hsp90.

3.4.14 Stimulation of p23 binding by other substrates.

Several model substrates were used to characterise the Hsp90 chaperone activity. To answer the question if p23 recognizes other substrates bound to Hsp90, we used CS and Luciferase instead of the p53core domain in anisotropy assays. The CS was added to a 5-fold excess over Hsp90, the Luciferase only to a 2.5-fold excess due to a strong aggregation tendency. The titrations indicate that in the presence of CS binding affinity of p23 to Hsp90 was increased to a K_D of 300 nM. The prescence of Luciferase was not recognized by p23 the K_D-value observed matches that of substrate unloaded Hsp90 (**Figure 66**).

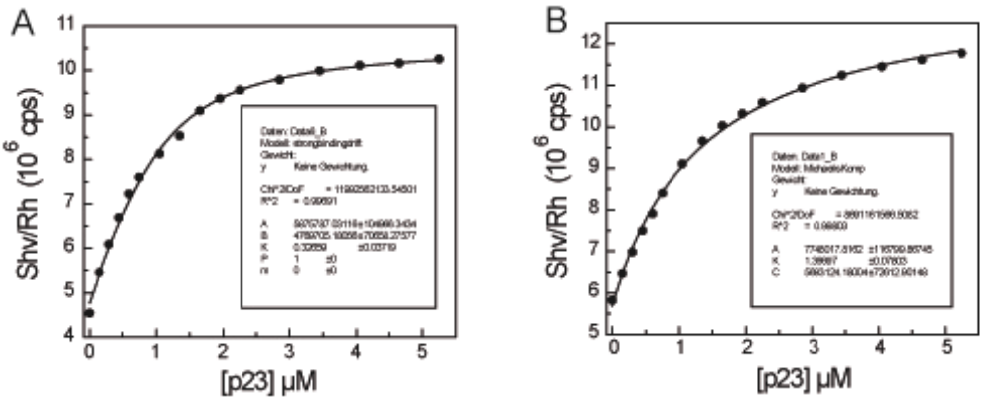

Figure 66: Titration of p23 to Hsp90 complexes in the presence of 5µM CS A) or 2.5 µM Luciferease. Apparent Kd values are 320 nM for the CS or 1,4 µM for Luciferase. In this experiments the polarized Shv channel was used a signal that is proportional to anisotropy changes.

3.4.15 FRET analysis of the CS Hsp90 p23 complex

Using Hsp90 conjugated at the N-terminal domain with the fluorescent dye ATTO550 and p23 conjugated at the Cys2 with fluorescein were used to measure p23 binding by FRET. Interaction of labelled p23 with fluorescently labelled Hsp90 reduces the distance between the fluorophores and increases the FRET signal. Mixing of labelled p23 and labelled Hsp90 did not change the FRET efficiency. The ATP bound state is required for this interaction. Indeed AMP-PNP is required to induce a conformational change in Hsp90 that is recognized by p23 and enables p23 binding which can be followed by a decrease in donor channel and an increase in acceptor channel fluorescence (**Figure 67**). Observed rates match those identified in FRET experiments that trace conformational changes in Hsp90. Interestingly, in the presence of CS also an increase in the FRET signal is seen, suggesting that p23 is more efficiently recruited to the complex or that a structural change takes place that reduces the distance between the flurophores. However, the anisotropy binding data propose the first explanation. The kinetics after the addition of CS were analysed by a double exponential. Further analysis is required to understand the reactions behind the observed kinetics.

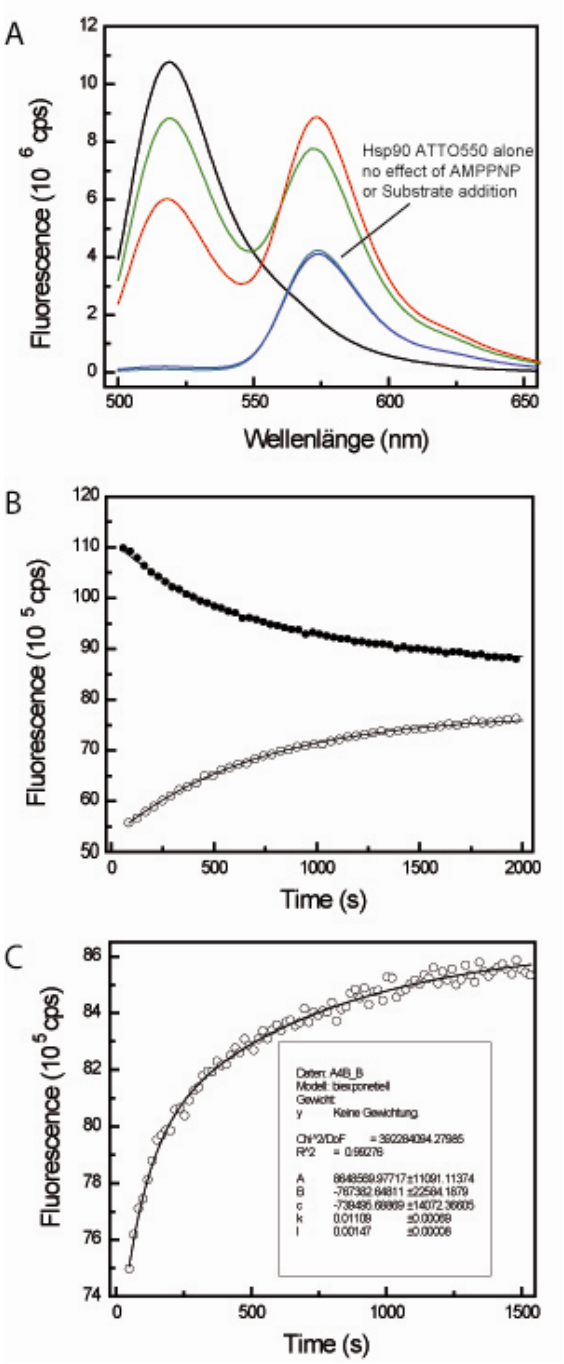

Figure 67: FRET assay for p23 interaction. A) Spectra of p23-labelled with fluorescein exited at 490 nm (black trace). Addition of Hsp90 in a 1 to 1 ratio and 2 mM AMP-PNP shows spectrum depicted in green. Addition of CS is represented by the red spectrum. B) Kinetics recorded by donor channel (black circles) and acceptor channel (white circles) fluorescence upon addition of AMP-PNP to a mixture of Hsp90-ATTO 550 and p23-fluorescein. C) Kinetics of CS addition to the preformed p23 Hsp90 complex (acceptor channel only).

3.4.16 Summary

The unstructured C-tail of p23 elicits its chaperone function in which the M/G- and Q/L-rich regions are involved. The flexible character of the C-tail presumably adapts the chaperone active site to the requirement of the substrate.

In addition, the C-terminal tail has an impact on the structure and destabilises the N-terminal domain of p23 leading to a lower binding affinity of wild type p23 compared to the C-terminal deleted variant.

The presence of p53 elicits high affinity binding of p23 wild type to the Hsp90-p53 complex indicating that the C-tail might in this case contact the Hsp90 bound p53. This allows remodelling the N-terminal domain of p23 to its high affinity form.

The observed affinities for the deletion or replacement variants indicate an increase of the affinity to unloaded Hsp90 while the high affinity binding to substrate loaded Hsp90 remains unchanged (**Figure 68**). The high affinity state can be perturbed by introducing destabilising mutations in the β-sheet that connects the Hsp90 interaction loop (residues 97-114) with the C-tail. The interplay between the unstructured C-terminal tail and the Hsp90 interacting domain might help to regulate the p23 recruitment to Hsp90 complexes. In vivo, the Hsp90 concentration exceeds that of p23. But p23 senses both the conformational state of Hsp90 and the substrate load suggesting that the co-chaperone connects the ATPase cycle and the substrate maturation.

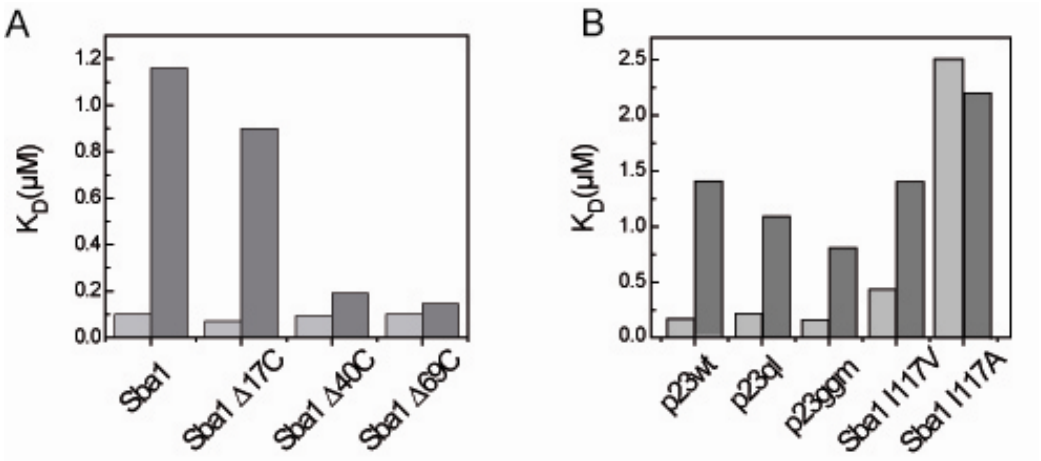

Figure 68: Binding affinities with (light gray) and without p53 (dark gray) of C-terminally truncated p23 proteins (A) and the binding affinities of p23 replacement variants and point mutated variants in (B).

4 Conclusions

4.1 Hsp90 Monomer-Dimer equilibrium

Hsp90 forms tail to tail associated dimers. The kinetic of subunit exchange indicates that the adjustment of the equilibrium is fast compared to the ATP turn over. A K_D of 30 nM using a relative amplitude analysis was found which agrees nice with the K_D obtained from analytical size exclusion experiments. Dissociation could also be monitored using a sensitive fluorescence detection system in AUC experiments. Micromolar concentrations of Hsp90 are found in the cell, suggesting that the monomer is of very low abundance in the cytosol. The rapid subunit exchange reactions of Hsp90 enabled the formation of heterocomplexes that unravelled interesting features of trans-activation of the N-terminal domains. Interestingly, the AMP-PNP-bound Hsp90 does not dissociate in a detectable concentration range indicating that indeed the N-terminal domains bind to each other forming a very stable dimer. For ATPγS, decelerated subunit exchange rates are observed. The dissociation kinetics of the Hsp90-ATPgS complex match nicely to the rate of the ATPγS hydrolysis obtained from the global fit. This confirms the finding that the closed state is not dissociating and that hydrolysis mediated reopening of Hsp90 is required for the dissociation. Using the fluorescence AUC setup, we found that indeed addition of AMP-PNP and ATPγS prevent disassembly completely. These data confirm that ATP is tightly trapped on the pathway coinciding with a strong association of the Hsp90 subunits.

4.2 Hsp90 conformations

During the ATPase cycle, Hsp90 undergoes large conformational changes involving an elongated form in the nucleotide-free state and a closed form in the ATP-bound form (Shiau et al, 2006; Ali et al, 2006). Open and closed forms of Hsp90, which can be generated by adding AMP-PNP, show large differences in their frictional

coefficient in AUC analysis, leading to an increase in sedimentation of the closed state by 1 S. The second N-terminal dimerisation site induces a counter clockwise twist of the Hsp90 subunits and causes a significant compaction of the molecule in solution. EM analysis of these conformations can be confirmed by these findings (Southworth and Agard, 2008). The structural impression of the nucleotide-free from suggests that Hsp90 might be remarkably flexible and adjustable to the requirements of the substrate in this state. The reaction from the open to the closed state was analysed in detail using the established FRET setup after mixing using ATPγS.

4.3 Kinetic model of the Hsp90 cycle

The FRET analysis revealed complex kinetics for the conformational changes induced by ATPγS which could not be explained by the current model for the Hsp90 cycle (Weikl et al, 2000). Binding of nucleotides to the N-terminal domain are fast events which seem to be independent of the subsequent conformational changes (Leskovar et al, 2008; Frey et al, 2007; Weikl et al, 2000). In the previous model, a single step from the open to the closed conformation was suggested (Weikl et al, 2000). The kinetic study revealed that two intermediates are required to explain the complex kinetic behaviour (**Figure 69**). As depicted, the first intermediate (I1) is formed after fast binding of ATP to the N-terminal domain and might play a critical role to sense the γ-Phosphate of ATP at the active site. For GHKL ATPases the γ-Phosphate points outward from the N-terminal domain that is required to anchor the AMP moiety (Prodromou et al, 1997a). Thus, recognition of this particular phosphate is achieved by other parts than the initial binding site. The ATP-lid is presumably involved in this reaction which closes over the bound ATP. Rearrangement of the lid might lead to a displacement of the first N-terminal β-strand to prepare N-terminal dimerisation and the domain swap with the N-terminal domain of the trans-subunit. The details of the I1 structure remain speculative, although it seems that it might partially form even without the trans N-terminal domain (**Figure 31**). The structure of I1 has to be considered open with a closed lid in the N-terminal domain. The helix bound to the lid before is now set free to

facilitate N-N contacts (I2) (Richter et al, 2006). High FRET assignments for I2 in the global fitting suggest that large rearrangement occurred going from I1 to I2. This reaction is seems faster than the closure of the lid as suggested by the rate constants and presumably should have a frictional element. Interestingly, the ATPase activity is indeed inhibited in viscous solvents (Klaus Richter personal communication). The step from I1 to I2 is a likely candidate for the inhibiting effect. We thus considered I2

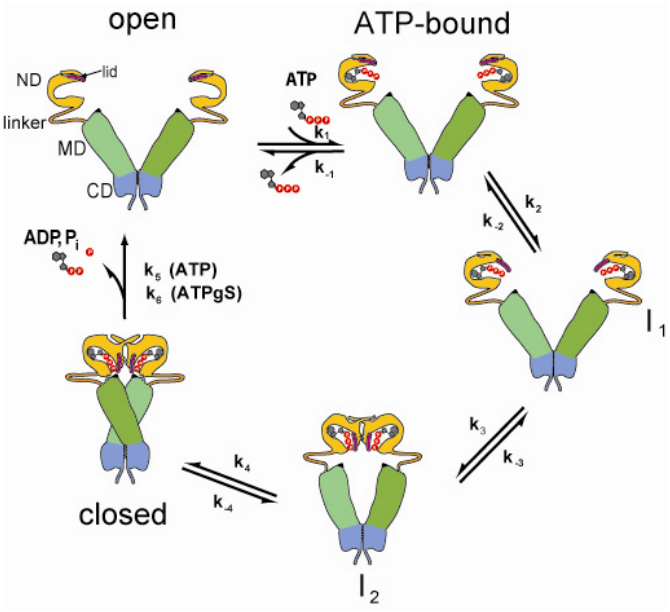

Figure 69: Model of the Hsp90 cycle based on the kinetic model from the FRET analysis. Five states were required to fit the data. The states are the apo-state or open state, the initial ATP-bound form without rearrangements, intermediate state 1 with a closed lid, intermediate state 2 with dimerised N-terminal domains and the final closed state ready to hydrolyse the bound ATP.

to be N-terminally dimerised. The reaction from I2 to the closed conformation likely involves repositioning of the M-domain to the N-terminal domain to form the ATP hydrolysing conformation. The rate constants of this reaction step tell that it is irreversible committing the bound nucleotide for hydrolysis. This particular closed state also is completely resistant to dissociation. When chasing the complex with unlabelled Hsp90, the open state is required to monitor subunit exchange. Thus, when the closed state is formed using the nucleotide AMP-PNP which cannot be

hydrolysed, subunit exchange is not observed. When stabilising the closed state using ATPγS, the hydrolysis rate of ATPγS can be measured directly as it is rate-limiting for the subunit exchange. The reaction from the closed conformation back to the open Hsp90 was considered to occur in a single step. Intermediates in that reaction have been implicated from ADP binding experiments to apo-Hsp90. It was suggested that ADP stabilizes another compact state distinct from the closed conformation (Southworth and Agard, 2008). Kinetics of yeast Hsp90 do not identify an intermediate for the reopening of Hsp90. Also incubating Hsp90 with ADP does not induce a structural change that neither can be detected with our FRET system nor it is detected by AUC experiments. These findings however do not fully exclude a post hydrolysis state. As the model represents a kinetic model intermediate states of Hsp90 with ADP or Pi bound were not considered. Reopening and release of products sets Hsp90 back to its initial conformation.

4.4 How Co-chaperones influence the conformational cycle

The picture of the conformational changes emerged from data excluding any co-factors of the Hsp90 system. In eukaryotic cells, however many co-chaperones exist that are thought to regulate the Hsp90 cycle (Richter et al, 2005). Some inhibit or activate the Hsp90 ATPase (Richter et al, 2003; Panaretou et al, 2002). It has been shown that also substrate proteins can affect the ATPase activity (McLaughlin et al, 2002). The ATPase activity is coupled to conformational changes and the microscopic effect of each co-chaperone or substrate on the Hsp90 conformation can lead to an effect on the ATPase. The description of the cycle is therefore a prerequisite to understand the functions of the co-chaperones involved in substrate maturation.

The established substrate cycle was worked out for SHRs maturing in reticulocyte lysate in which four different substrate complexes could be identified which differ in their co-chaperone composition. First, the substrate is associated with Hsp70 and becomes transferred to Hsp90 that is recruited via Hop which can interact with Hsp70 and Hsp90 simultaneously (Pratt et al, 2006). If transfer occurred, Hop is

exchanged in an intermediate Hsp90 complex for PPIase co-chaperones containing TPR domains. Then p23 binds to the complex which is thought to stabilize the substrate.

4.4.1 Hop/Sti1

Hop shows high affinity to Hsp90. Nucleotide binding remains unaffected although the ATPase activity is potently inhibited in the Sti1 complex. The finding made here that an early conformational change can be inhibited by Sti1 explains why p23 or Sti1 bind mutually exclusive to the chaperone (Richter et al, 2004; Richter et al, 2003). For the efficient suppression of conformational changes in Hsp90, Sti1 presumably needs two binding sites in the chaperone one before the hinge involved in structural changes, the other after this hinge so that Sti1 might function as a bracket preventing structural rearrangements. The high affinity site is the C-terminal tail of Hsp90 to which TPR 1 of Hop binds. The second site is unknown. It is also unclear whether the Sti1 mechanism works via a trans or a cis mechanism, i. e. interacting at the second site with the same (cis) or the other subunit (trans).

4.4.2 PPIases

Binding to Hsp90 takes place via the C-terminal MEEVD motif. Members of this co-chaperone class are cyclophilins and FK506 binding proteins. It is thought that direct interaction takes place between the PPIase domain and the client that is bound to Hsp90. Profound data have been collected for the FKBP52 and FKBP51 proteins involved in the sexual development in mice (Hong et al, 2007; Barent et al, 1998). Knock outs of these proteins show specific defects in the androgen and oestrogen receptor pathways in aggrement with their impact on their maturation which has been analysed in vitro before. PPIases act downstream from substrate transfer from Hsp70 and it has been suggested that the substrate selects for the associated PPIase as their interaction seems to be very dynamic (Graumann and Jungbauer, 2000).

Cpr6 has been analysed as one representative of the class of PPIases. Cpr6 slightly activates the Hsp90 ATPase under low salt conditions (Johnson et al, 2007; Prodromou et al, 1999). A slight modulating activity on the conformational changes could be identified. These findings could be confirmed using ATP which produced no significant change in FRET but supplementation of Cpr6 increased the FRET amplitude for ATP to a detectable level suggesting that Cpr6 stabilizes a high FRET intermediate.

4.4.3 Aha1

For Aha1 it is rather unclear whether it coexists with other co-chaperones in an Hsp90 complex. It promotes conformational changes leading to the closed conformation. How this connects to substrate maturation is largely part of speculations, yet. However, in vivo it could be shown that a mutated form of the CFTR could be rescued when Aha1 is depleted, suggesting that Aha1 might play a role in quality control, membrane protein folding or is involved in substrate release (Wang et al, 2006). We found that Aha1 accelerates formation of the closed ATPase-active conformation. The binding of Aha1 induces structural changes in the Hsp90 dimer. It seems that Aha1 bypasses early intermediates in the pathway that relate to conformational changes surrounding the ATP binding site. Another interesting point is that in the Aha1 complex the Hsp90 dimerisation is stabilized. In principle only 2 possible hypothesis can explain this fact. I) Hsp90 dimerisation is stabilized through dimerisation of its N-terminal domains in a conformation that is stabilised by Aha1 or II) one Aha1 molecule binds to both subunits simultaneously stabilising Hsp90 dimers indirectly.

4.4.4 p23

p23 is the most conformation-sensitive interaction partner of Hsp90 known (Ali et al, 2006; Richter et al, 2004; Johnson and Toft, 1995b). The mice knock out is lethal at

birth because of retarded lung development (Grad et al, 2006). Early studies identified the protein in Hsp90 progesterone receptor complexes where it was suggested to be an essential component for assembly (Johnson et al, 1994). Crystal structural analysis and other data showed that p23 binding requires the closed state of Hsp90 (Ali et al, 2006). p23 binding to Hsp90 presumably inhibits the hydrolysis step or prevents a conformational change (Richter et al, 2004). The N-terminal dimerised state is stabilized by p23 and high FRET intermediates become more populated using ATP in the presents of p23 (Forafonov et al, 2008; Richter et al, 2004).

p23 binding is conformation-sensitive and it was found in Hsp90 client protein complexes, as substrate proteins bound to Hsp90 directly affect p23 binding. Affinity to Hsp90 substrate complexes is increased 7-fold using the p53core domain as a substrate.

Luciferase as a model substrate showed no effect on p23 affinity. CS for which temperature inactivation and aggregation could be prevented by p23 showed stimulation of lower potency compared to the p53core doamain. This suggests that p23 is recruited to the Hsp90 system by the conformation of Hsp90 and the substrate that is bound.

The C-terminal natively unfolded domain of p23 functions as an intrinsic inhibitor for the interaction with Hsp90. Inhibition becomes reliefed if substrate is present.

The binding affinities of all analysed p23 mutants in the presence and absence of p53 are depicted in Figure 68. Truncations of the C-terminal tail show increasing affinity for Hsp90 in the absence of substrate. In a similar way, replacement of the Q/L-rich and the G/M-rich region show higher binding affinity to empty Hsp90. High affinity binding depends on the integrity of the interaction loop. Only the point-mutated proteins loose high affinity binding to Hsp90.

The underling mechanism might involve an entropy transfer to the substrate protein which was shown to transiently interact with the C-tail of p23. Especially the G/M-rich region and the Q/L-rich region participate in binding to the substrate and delay aggregation reactions, an activity that seems to correlate and is a prerequisite for stimulated binding to Hsp90 substrate complexes. The destabilising mutant in the

Hsp90 interaction loop, I117A, indicated that binding relies on the proper conformation of the loop between the last sheets of the protein. CD data suggest that the positive CD signal at 230 nm is a reporter for loop stability and thus can report on the binding activity of the respective p23 protein. Thus p23 is active in sensing substrates that are productively transferred to the Hsp90 system.

Experiments using the FRET assay with CS hint to a cooperative triple complex formation. By this mechanism p23 prevents back transfer to Hsp70 as it should displace Hop/Sti1 from the chaperone.

SHRs have been shown to be in hormone binding active state in the presence of p23. Whether this final complex has a static character or is dynamic in terms of p23 interaction and nucleotide as well as substrate binding is matter of active research.

The studies presented here has addressed key question for understanding the molecular mechanism of Hsp90. My results allowed to reconstitute the conformational cycle and to get a first picture of its regulation by co-chaperones. My data support the view that the major level of regulation is grounded in conformational transitions of Hsp90 that govern the ATPase cycle and essentially orchestrate co-chaperone interactions.

5 Literature

Abbas-Terki,T, Briand,PA, Donze,O, and Picard,D. (**2002**). The Hsp90 co-chaperones Cdc37 and Sti1 interact physically and genetically. *Biol.Chem.* **383**, 1335-1342

Albanese,V, Yam,AY, Baughman,J, Parnot,C, and Frydman,J. (**2006**). Systems analyses reveal two chaperone networks with distinct functions in eukaryotic cells. *Cell* **124**, 75-88

Ali,JA, Jackson,AP, Howells,AJ, and Maxwell,A. (**1993**). The 43-kilodalton N-terminal fragment of the DNA gyrase B protein hydrolyzes ATP and binds coumarin drugs. *Biochemistry* **32**, 2717-2724

Ali,MM, Roe,SM, Vaughan,CK, Meyer,P, Panaretou,B, Piper,PW, Prodromou,C, and Pearl,LH. (**2006**). Crystal structure of an Hsp90-nucleotide-p23/Sba1 closed chaperone complex. *Nature* **440**, 1013-1017

Amaral,MD. (**2004**). CFTR and chaperones: processing and degradation. *J.Mol.Neurosci.* **23**, 41-48

Anfinsen,CB. (**1973**). Principles that govern the folding of protein chains. *Science* **181**, 223-230

Anfinsen,CB, Haber,JE, SELA,M, and WHITE,FH, Jr. (**1961**). The kinetics of formation of native ribonuclease during oxidation of the reduced polypeptide chain. *Proc.Natl.Acad.Sci.U.S.A* **47**, 1309-1314

Appenzeller-Herzog,C and Ellgaard,L. (**2008**). The human PDI family: versatility packed into a single fold. *Biochim.Biophys.Acta* **1783**, 535-548

Baker,MJ, Frazier,AE, Gulbis,JM, and Ryan,MT. (**2007**). Mitochondrial protein-import machinery: correlating structure with function. *Trends Cell Biol.* **17**, 456-464

Ballinger,CA, Connell,P, Wu,Y, Hu,Z, Thompson,LJ, Yin,LY, and Patterson,C. (**1999**). Identification of CHIP, a novel tetratricopeptide repeat-containing protein that interacts with heat shock proteins and negatively regulates chaperone functions. *Mol.Cell Biol.* **19**, 4535-4545

Bandhakavi,S, McCann,RO, Hanna,DE, and Glover,CV. (**2003**). A positive feedback loop between protein kinase CKII and Cdc37 promotes the activity of multiple protein kinases. *J.Biol.Chem.* **278**, 2829-2836

Bardwell,JC and Craig,EA. (**1987**). Eukaryotic Mr 83,000 heat shock protein has a homologue in Escherichia coli. *Proc.Natl.Acad.Sci.U.S.A* **84**, 5177-5181

Barent,RL, Nair,SC, Carr,DC, Ruan,Y, Rimerman,RA, Fulton,J, Zhang,Y, and Smith,DF. (**1998**). Analysis of FKBP51/FKBP52 chimeras and mutants for Hsp90 binding and association with progesterone receptor complexes. *Mol.Endocrinol.* **12**, 342-354

Bharadwaj,S, Ali,A, and Ovsenek,N. (**1999**). Multiple components of the HSP90 chaperone complex function in regulation of heat shock factor 1 In vivo. *Mol.Cell Biol.* **19**, 8033-8041

Blagosklonny,MV. (**2002**). Hsp-90-associated oncoproteins: multiple targets of geldanamycin and its analogs. *Leukemia* **16**, 455-462

Bledsoe,RK, Montana,VG, Stanley,TB, Delves,CJ, Apolito,CJ, McKee,DD, Consler,TG, Parks,DJ, Stewart,EL, Willson,TM, Lambert,MH, Moore,JT, Pearce,KH, and Xu,HE. (**2002**). Crystal structure of the glucocorticoid receptor ligand binding domain reveals a novel mode of receptor dimerization and coactivator recognition. *Cell* **110**, 93-105

Blobel,G. (**2000**). Protein targeting. *Biosci.Rep.* **20**, 303-344

Bohen,SP. (**1998**). Genetic and biochemical analysis of p23 and ansamycin antibiotics in the function of Hsp90-dependent signaling proteins. *Mol.Cell Biol.* **18**, 3330-3339

Bolen,DW and Santoro,MM. (**1988**). Unfolding free energy changes determined by the linear extrapolation method. 2. Incorporation of delta G degrees N-U values in a thermodynamic cycle. *Biochemistry* **27**, 8069-8074

Borkovich,KA, Farrelly,FW, Finkelstein,DB, Taulien,J, and Lindquist,S. (**1989**). hsp82 is an essential protein that is required in higher concentrations for growth of cells at higher temperatures. *Mol.Cell Biol.* **9**, 3919-3930

Bose,S, Weikl,T, Bugl,H, and Buchner,J. (**1996**). Chaperone function of Hsp90-associated proteins. *Science* **274**, 1715-1717

Bossy-Wetzel,E, Schwarzenbacher,R, and Lipton,SA. (**2004**). Molecular pathways to neurodegeneration. *Nat.Med.* **10 Suppl**, S2-S9

Braig,K, Otwinowski,Z, Hegde,R, Boisvert,DC, Joachimiak,A, Horwich,AL, and Sigler,PB. (**1994b**). The crystal structure of the bacterial chaperonin GroEL at 2.8 A. *Nature* **371**, 578-586

Braig,K, Otwinowski,Z, Hegde,R, Boisvert,DC, Joachimiak,A, Horwich,AL, and Sigler,PB. (**1994a**). The crystal structure of the bacterial chaperonin GroEL at 2.8 A. *Nature* **371**, 578-586

Brinker,A, Scheufler,C, Von Der,MF, Fleckenstein,B, Herrmann,C, Jung,G, Moarefi,I, and Hartl,FU. (**2002**). Ligand discrimination by TPR domains. Relevance and selectivity of EEVD-recognition in Hsp70 x Hop x Hsp90 complexes. *J.Biol.Chem.* **277**, 19265-19275

Buchner,J. (**1996**). Supervising the fold: functional principles of molecular chaperones. *FASEB J.* **10**, 10-19

Buchner,J, Grallert,H, and Jakob,U. (**1998**). Analysis of chaperone function using citrate synthase as nonnative substrate protein. *Methods Enzymol.* **290**, 323-338

Bukau,B, Deuerling,E, Pfund,C, and Craig,EA. (**2000**). Getting newly synthesized proteins into shape. *Cell* **101**, 119-122

Bukau,B, Weissman,J, and Horwich,A. (**2006**). Molecular chaperones and protein quality control. *Cell* **125**, 443-451

Butler,JS and Loh,SN. (**2006**). Folding and misfolding mechanisms of the p53 DNA binding domain at physiological temperature. *Protein Sci.* **15**, 2457-2465

Buxbaum,JN. (**2004**). The systemic amyloidoses. *Curr.Opin.Rheumatol.* **16**, 67-75

Caplan,AJ, Mandal,AK, and Theodoraki,MA. (**2007**). Molecular chaperones and protein kinase quality control. *Trends Cell Biol.* **17**, 87-92

Carrello,A, Ingley,E, Minchin,RF, Tsai,S, and Ratajczak,T. (**1999**). The common tetratricopeptide repeat acceptor site for steroid receptor-associated immunophilins and hop is located in the dimerization domain of Hsp90. *J.Biol.Chem.* **274**, 2682-2689

Cashikar,AG, Duennwald,M, and Lindquist,SL. (**2005**). A chaperone pathway in protein disaggregation. Hsp26 alters the nature of protein aggregates to facilitate reactivation by Hsp104. *J.Biol.Chem.* **280**, 23869-23875

Chen,S, Prapapanich,V, Rimerman,RA, Honore,B, and Smith,DF. (**1996**). Interactions of p60, a mediator of progesterone receptor assembly, with heat shock proteins hsp90 and hsp70. *Mol.Endocrinol.* **10**, 682-693

Chen,S and Smith,DF. (**1998**). Hop as an adaptor in the heat shock protein 70 (Hsp70) and hsp90 chaperone machinery. *J.Biol.Chem.* **273**, 35194-35200

Chiosis,G and Tao,H. (**2006**). Purine-scaffold Hsp90 inhibitors. *IDrugs.* **9**, 778-782

Chiosis,G, Timaul,MN, Lucas,B, Munster,PN, Zheng,FF, Sepp-Lorenzino,L, and Rosen,N. (**2001**). A small molecule designed to bind to the adenine nucleotide pocket of Hsp90 causes Her2 degradation and the growth arrest and differentiation of breast cancer cells. *Chem.Biol.* **8**, 289-299

Cintron,NS and Toft,D. (**2006**). Defining the requirements for Hsp40 and Hsp70 in the Hsp90 chaperone pathway. *J.Biol.Chem.* **281**, 26235-26244

Darby,NJ, Freedman,RB, and Creighton,TE. (**1994**). Dissecting the mechanism of protein disulfide isomerase: catalysis of disulfide bond formation in a model peptide. *Biochemistry* **33**, 7937-7947

Dehner,A, Klein,C, Hansen,S, Muller,L, Buchner,J, Schwaiger,M, and Kessler,H. (**2005**). Cooperative binding of p53 to DNA: regulation by protein-protein interactions through a double salt bridge. *Angew.Chem.Int.Ed Engl.* **44**, 5247-5251

Deuerling,E, Patzelt,H, Vorderwulbecke,S, Rauch,T, Kramer,G, Schaffitzel,E, Mogk,A, Schulze-Specking,A, Langen,H, and Bukau,B. (**2003**). Trigger Factor and DnaK possess overlapping substrate pools and binding specificities. *Mol.Microbiol.* **47**, 1317-1328

Dill,KA and Chan,HS. (**1997**). From Levinthal to pathways to funnels. *Nat.Struct.Biol.* **4**, 10-19

Dobson,CM and Karplus,M. (**1999**). The fundamentals of protein folding: bringing together theory and experiment. *Curr.Opin.Struct.Biol.* **9**, 92-101

Dolinski,KJ, Cardenas,ME, and Heitman,J. (**1998**). CNS1 encodes an essential p60/Sti1 homolog in Saccharomyces cerevisiae that suppresses cyclophilin 40 mutations and interacts with Hsp90. *Mol.Cell Biol.* **18**, 7344-7352

Driessen,AJ and Nouwen,N. (**2008**). Protein translocation across the bacterial cytoplasmic membrane. *Annu.Rev.Biochem.* **77**, 643-667

Dutta,R and Inouye,M. (**2000**). GHKL, an emergent ATPase/kinase superfamily. *Trends Biochem.Sci.* **25**, 24-28

Eftink,MR. (**1998**). The use of fluorescence methods to monitor unfolding transitions in proteins. *Biochemistry (Mosc.)* **63**, 276-284

Elad,N, Farr,GW, Clare,DK, Orlova,EV, Horwich,AL, and Saibil,HR. (**2007**). Topologies of a substrate protein bound to the chaperonin GroEL. *Mol.Cell* **26**, 415-426

Fang,Y, Fliss,AE, Rao,J, and Caplan,AJ. (**1998**). SBA1 encodes a yeast hsp90 cochaperone that is homologous to vertebrate p23 proteins. *Mol.Cell Biol.* **18**, 3727-3734

Farr,GW, Fenton,WA, and Horwich,AL. (**2007**). Perturbed ATPase activity and not "close confinement" of substrate in the cis cavity affects rates of folding by tail-multiplied GroEL. *Proc.Natl.Acad.Sci.U.S.A* **104**, 5342-5347

Fasman,GD. (**1996**). Circular Dichroism and the Conformational Analysis of Biomolecules (New York: Plenum Press).

Feige and Buchner. (**2009**). The Role of Disulfide Bonds in Protein Folding and Stability.

Feige,MJ, Walter,S, and Buchner,J. (**2004**). Folding mechanism of the CH2 antibody domain. *J.Mol.Biol.* **344**, 107-118

Felts,SJ, Owen,BA, Nguyen,P, Trepel,J, Donner,DB, and Toft,DO. (**2000**). The hsp90-related protein TRAP1 is a mitochondrial protein with distinct functional properties. *J.Biol.Chem.* **275**, 3305-3312

Fenton,WA and Horwich,AL. (**2003**). Chaperonin-mediated protein folding: fate of substrate polypeptide. *Q.Rev.Biophys.* **36**, 229-256

Ferbitz,L, Maier,T, Patzelt,H, Bukau,B, Deuerling,E, and Ban,N. (**2004**). Trigger factor in complex with the ribosome forms a molecular cradle for nascent proteins. *Nature* **431**, 590-596

Fersht,AR. (**1997**). Structure and Mechanism in Protein Science (Julet, M. R. & Hadler, G. L., Eds.).

Fersht,AR and Daggett,V. (**2002**). Protein folding and unfolding at atomic resolution. *Cell* **108**, 573-582

Finkelstein,DB, Strausberg,S, and McAlister,L. (**1982**). Alterations of transcription during heat shock of Saccharomyces cerevisiae. *J.Biol.Chem.* **257**, 8405-8411

Fischer,G and Aumuller,T. (**2003**). Regulation of peptide bond cis/trans isomerization by enzyme catalysis and its implication in physiological processes. *Rev.Physiol Biochem.Pharmacol.* **148**, 105-150

Fischer,G, Bang,H, and Mech,C. (**1984**). [Determination of enzymatic catalysis for the cis-trans-isomerization of peptide binding in proline-containing peptides]. *Biomed.Biochim.Acta* **43**, 1101-1111

Fischer,G, Wittmann-Liebold,B, Lang,K, Kiefhaber,T, and Schmid,FX. (**1989**). Cyclophilin and peptidyl-prolyl cis-trans isomerase are probably identical proteins. *Nature* **337**, 476-478

Forafonov,F, Toogun,OA, Grad,I, Suslova,E, Freeman,BC, and Picard,D. (**2008**). p23/Sba1p protects against Hsp90 inhibitors independently of its intrinsic chaperone activity. *Mol.Cell Biol.* **28**, 3446-3456

Freedman,RB, Bulleid,NJ, Hawkins,HC, and Paver,JL. (**1989**). Role of protein disulphide-isomerase in the expression of native proteins. *Biochem.Soc.Symp.* **55**, 167-192

Freeman,BC, Toft,DO, and Morimoto,RI. (**1996**). Molecular chaperone machines: chaperone activities of the cyclophilin Cyp-40 and the steroid aporeceptor-associated protein p23. *Science* **274**, 1718-1720

Freeman,BC and Yamamoto,KR. (**2002**). Disassembly of transcriptional regulatory complexes by molecular chaperones. *Science* **296**, 2232-2235

Frey,S, Leskovar,A, Reinstein,J, and Buchner,J. (**2007**). The ATPase cycle of the endoplasmic chaperone Grp94. *J.Biol.Chem.* **282**, 35612-35620

Fukunaga,R and Hunter,T. (**2004**). Identification of MAPK substrates by expression screening with solid-phase phosphorylation. *Methods Mol.Biol.* **250**, 211-236

Funfschilling,U and Rospert,S. (**1999**). Nascent polypeptide-associated complex stimulates protein import into yeast mitochondria. *Mol.Biol.Cell* **10**, 3289-3299

Galla,H. (**1988**). Spektroskopische Mehtoden in der Biochemie.

Gausdal,G, Gjertsen,BT, Fladmark,KE, Demol,H, Vandekerckhove,J, and Doskeland,SO. (**2004**). Caspase-dependent, geldanamycin-enhanced cleavage of co-chaperone p23 in leukemic apoptosis. *Leukemia* **18**, 1989-1996

Gautschi,M, Lilie,H, Funfschilling,U, Mun,A, Ross,S, Lithgow,T, Rucknagel,P, and Rospert,S. (**2001**). RAC, a stable ribosome-associated complex in yeast formed by the DnaK-DnaJ homologs Ssz1p and zuotin. *Proc.Natl.Acad.Sci.U.S.A* **98**, 3762-3767

Genevaux,P, Keppel,F, Schwager,F, Langendijk-Genevaux,PS, Hartl,FU, and Georgopoulos,C. (**2004**). In vivo analysis of the overlapping functions of DnaK and trigger factor. *EMBO Rep.* **5**, 195-200

Gill,SC and von Hippel,PH. (**1989**). Calculation of protein extinction coefficients from amino acid sequence data. *Anal.Biochem.* **182**, 319-326

Gleiter,S and Bardwell,JC. (**2008**). Disulfide bond isomerization in prokaryotes. *Biochim.Biophys.Acta* **1783**, 530-534

Glover,JR and Lindquist,S. (**1998**). Hsp104, Hsp70, and Hsp40: a novel chaperone system that rescues previously aggregated proteins. *Cell* **94**, 73-82

Goebl,M and Yanagida,M. (**1991**). The TPR snap helix: a novel protein repeat motif from mitosis to transcription. *Trends Biochem.Sci.* **16**, 173-177

Golbik,R, Yu,C, Weyher-Stingl,E, Huber,R, Moroder,L, Budisa,N, and Schiene-Fischer,C. (**2005**). Peptidyl prolyl cis/trans-isomerases: comparative reactivities of cyclophilins, FK506-binding proteins, and parvulins with fluorinated oligopeptide and protein substrates. *Biochemistry* **44**, 16026-16034

Grad,I, McKee,TA, Ludwig,SM, Hoyle,GW, Ruiz,P, Wurst,W, Floss,T, Miller,CA, III, and Picard,D. (**2006**). The Hsp90 cochaperone p23 is essential for perinatal survival. *Mol.Cell Biol.* **26**, 8976-8983

Graumann,K and Jungbauer,A. (**2000**). Quantitative assessment of complex formation of nuclear-receptor accessory proteins. *Biochem.J.* **345 Pt 3**, 627-636

Grauschopf,U, Fritz,A, and Glockshuber,R. (**2003**). Mechanism of the electron transfer catalyst DsbB from Escherichia coli. *EMBO J.* **22**, 3503-3513

Grenert,JP, Sullivan,WP, Fadden,P, Haystead,TA, Clark,J, Mimnaugh,E, Krutzsch,H, Ochel,HJ, Schulte,TW, Sausville,E, Neckers,LM, and Toft,DO. (**1997**). The amino-terminal domain of heat shock protein 90 (hsp90) that binds geldanamycin is an ATP/ADP switch domain that regulates hsp90 conformation. *J.Biol.Chem.* **272**, 23843-23850

Gruber,CW, Cemazar,M, Heras,B, Martin,JL, and Craik,DJ. (**2006**). Protein disulfide isomerase: the structure of oxidative folding. *Trends Biochem.Sci.* **31**, 455-464

Gupta,RS. (**1995**). Phylogenetic analysis of the 90 kD heat shock family of protein sequences and an examination of the relationship among animals, plants, and fungi species. *Mol.Biol.Evol.* **12**, 1063-1073

Hainzl,O, Wegele,H, Richter,K, and Buchner,J. (**2004**). Cns1 is an activator of the Ssa1 ATPase activity. *J.Biol.Chem.* **279**, 23267-23273

Hanahan,D. (**1983**). Studies on transformation of Escherichia coli with plasmids. *J.Mol.Biol.* **166**, 557-580

Hartl,FU, Pfanner,N, Nicholson,DW, and Neupert,W. (**1989**). Mitochondrial protein import. *Biochim.Biophys.Acta* **988**, 1-45

Hartl,FU and Hayer-Hartl,M. (**2002**). Molecular Chaperones in the Cytosol: from Nascent Chain to Folded Protein. *Science* **295**, 1852-1858

Haslbeck,M, Franzmann,T, Weinfurtner,D, and Buchner,J. (**2005a**). Some like it hot: the structure and function of small heat-shock proteins. *Nat.Struct.Mol.Biol.* **12**, 842-846

Haslbeck,M, Miess,A, Stromer,T, Walter,S, and Buchner,J. (**2005b**). Disassembling protein aggregates in the yeast cytosol. The cooperation of Hsp26 with Ssa1 and Hsp104. *J.Biol.Chem.* **280**, 23861-23868

Hesse,M. (**1991**). Spektroskopische Methoden in der organischen Chemie.

Holmes,JL, Sharp,SY, Hobbs,S, and Workman,P. (**2008**). Silencing of HSP90 cochaperone AHA1 expression decreases client protein activation and increases

cellular sensitivity to the HSP90 inhibitor 17-allylamino-17-demethoxygeldanamycin. *Cancer Res.* **68**, 1188-1197

Hong,J, Kim,ST, Tranguch,S, Smith,DF, and Dey,SK. (**2007**). Deficiency of co-chaperone immunophilin FKBP52 compromises sperm fertilizing capacity. *Reproduction.* **133**, 395-403

Hutchison,KA, Stancato,LF, Owens-Grillo,JK, Johnson,JL, Krishna,P, Toft,DO, and Pratt,WB. (**1995**). The 23-kDa acidic protein in reticulocyte lysate is the weakly bound component of the hsp foldosome that is required for assembly of the glucocorticoid receptor into a functional heterocomplex with hsp90. *J.Biol.Chem.* **270**, 18841-18847

Jakob,U, Gaestel,M, Engel,K, and Buchner,J. (**1993**). Small heat shock proteins are molecular chaperones. *J.Biol.Chem.* **268**, 1517-1520

Jakob,U, Lilie,H, Meyer,I, and Buchner,J. (**1995**). Transient interaction of Hsp90 with early unfolding intermediates of citrate synthase. Implications for heat shock in vivo. *J.Biol.Chem.* **270**, 7288-7294

Jeong,JY, Johns,J, Sinclair,C, Park,JM, and Rossie,S. (**2003**). Characterization of Saccharomyces cerevisiae protein Ser/Thr phosphatase T1 and comparison to its mammalian homolog PP5. *BMC.Cell Biol.* **4**, 3

Johnson,BD, Schumacher,RJ, Ross,ED, and Toft,DO. (**1998**). Hop modulates Hsp70/Hsp90 interactions in protein folding. *J.Biol.Chem.* **273**, 3679-3686

Johnson,JL, Beito,TG, Krco,CJ, and Toft,DO. (**1994**). Characterization of a novel 23-kilodalton protein of unactive progesterone receptor complexes. *Mol.Cell Biol.* **14**, 1956-1963

Johnson,JL, Halas,A, and Flom,G. (**2007**). Nucleotide-dependent interaction of Saccharomyces cerevisiae Hsp90 with the cochaperone proteins Sti1, Cpr6, and Sba1. *Mol.Cell Biol.* **27**, 768-776

Johnson,JL and Toft,DO. (**1994**). A novel chaperone complex for steroid receptors involving heat shock proteins, immunophilins, and p23. *J.Biol.Chem.* **269**, 24989-24993

Johnson,JL and Toft,DO. (**1995c**). Binding of p23 and hsp90 during assembly with the progesterone receptor. *Mol.Endocrinol.* **9**, 670-678

Johnson,JL and Toft,DO. (**1995b**). Binding of p23 and hsp90 during assembly with the progesterone receptor. *Mol.Endocrinol.* **9**, 670-678

Johnson,JL and Toft,DO. (**1995a**). Binding of p23 and hsp90 during assembly with the progesterone receptor. *Mol.Endocrinol.* **9**, 670-678

Jonda,S, Huber-Wunderlich,M, Glockshuber,R, and Mossner,E. (**1999**). Complementation of DsbA deficiency with secreted thioredoxin variants reveals the crucial role of an efficient dithiol oxidant for catalyzed protein folding in the bacterial periplasm. *EMBO J.* **18**, 3271-3281

Kaiser,CM, Chang,HC, Agashe,VR, Lakshmipathy,SK, Etchells,SA, Hayer-Hartl,M, Hartl,FU, and Barral,JM. (**2006**). Real-time observation of trigger factor function on translating ribosomes. *Nature* **444**, 455-460

Kerner,MJ, Naylor,DJ, Ishihama,Y, Maier,T, Chang,HC, Stines,AP, Georgopoulos,C, Frishman,D, Hayer-Hartl,M, Mann,M, and Hartl,FU. (**2005**). Proteome-wide analysis of chaperonin-dependent protein folding in Escherichia coli. *Cell* **122**, 209-220

Kiefhaber,T, Rudolph,R, Kohler,HH, and Buchner,J. (**1991**). Protein aggregation in vitro and in vivo: a quantitative model of the kinetic competition between folding and aggregation. *Biotechnology (N.Y.)* **9**, 825-829

Kim,J, Nueda,A, Meng,YH, Dynan,WS, and Mivechi,NF. (**1997**). Analysis of the phosphorylation of human heat shock transcription factor-1 by MAP kinase family members. *J.Cell Biochem.* **67**, 43-54

Kimura,Y, Rutherford,SL, Miyata,Y, Yahara,I, Freeman,BC, Yue,L, Morimoto,RI, and Lindquist,S. (**1997**). Cdc37 is a molecular chaperone with specific functions in signal transduction. *Genes Dev.* **11**, 1775-1785

Klappa,P, Hawkins,HC, and Freedman,RB. (**1997**). Interactions between protein disulphide isomerase and peptides. *Eur.J.Biochem.* **248**, 37-42

Klein,C, Planker,E, Diercks,T, Kessler,H, Kunkele,KP, Lang,K, Hansen,S, and Schwaiger,M. (**2001**). NMR spectroscopy reveals the solution dimerization interface of p53 core domains bound to their consensus DNA. *J.Biol.Chem.* **276**, 49020-49027

Knauf,U, Newton,EM, Kyriakis,J, and Kingston,RE. (**1996**). Repression of human heat shock factor 1 activity at control temperature by phosphorylation. *Genes Dev.* **10**, 2782-2793

Komiya,T, Rospert,S, Schatz,G, and Mihara,K. (**1997**). Binding of mitochondrial precursor proteins to the cytoplasmic domains of the import receptors Tom70 and Tom20 is determined by cytoplasmic chaperones. *EMBO J.* **16**, 4267-4275

Lakkaraju,AK, Mary,C, Scherrer,A, Johnson,AE, and Strub,K. (**2008**). SRP keeps polypeptides translocation-competent by slowing translation to match limiting ER-targeting sites. *Cell* **133**, 440-451

Lakowicz,J. (**1999**). Principles of fluorescence spectroscopy. *Academic / Plenum Publisher Second Edition.*

Lee,GJ and Vierling,E. (**2000**). A small heat shock protein cooperates with heat shock protein 70 systems to reactivate a heat-denatured protein. *Plant Physiol* **122**, 189-198

Lee,P, Shabbir,A, Cardozo,C, and Caplan,AJ. (**2004**). Sti1 and Cdc37 can stabilize Hsp90 in chaperone complexes with a protein kinase. *Mol.Biol.Cell* **15**, 1785-1792

Lee,S, Sowa,ME, Watanabe,Yh, Sigler,PB, Chiu,W, Yoshida,M, and Tsai,FTF. (**2003**). The Structure of ClpB: A Molecular Chaperone that Rescues Proteins from an Aggregated State. *Cell* **115**, 229-240

Leskovar,A, Wegele,H, Werbeck,ND, Buchner,J, and Reinstein,J. (**2008**). The ATPase cycle of the mitochondrial Hsp90 analog Trap1. *J.Biol.Chem.* **283**, 11677-11688

Levinthal,C. (**1968**). *J.Chim.Phys.* **65**, 44-45

Lindquist,S and Craig,EA. (**1988**). The heat-shock proteins. *Annu.Rev.Genet.* **22**, 631-677

Loo,MA, Jensen,TJ, Cui,L, Hou,Y, Chang,XB, and Riordan,JR. (**1998**). Perturbation of Hsp90 interaction with nascent CFTR prevents its maturation and accelerates its degradation by the proteasome. *EMBO J.* **17**, 6879-6887

Lorimer,GH. (**1996**). A quantitative assessment of the role of the chaperonin proteins in protein folding in vivo. *FASEB J.* **10**, 5-9

Lotz,GP, Brychzy,A, Heinz,S, and Obermann,WM. (**2008**). A novel HSP90 chaperone complex regulates intracellular vesicle transport. *J.Cell Sci.* **121**, 717-723

Lotz,GP, Lin,H, Harst,A, and Obermann,WM. (**2003**). Aha1 binds to the middle domain of Hsp90, contributes to client protein activation, and stimulates the ATPase activity of the molecular chaperone. *J.Biol.Chem.* **278**, 17228-17235

Lucking,CB and Brice,A. (**2000**). Alpha-synuclein and Parkinson's disease. *Cell Mol.Life Sci.* **57**, 1894-1908

Lum,R, Niggemann,M, and Glover,JR. (**2008**). Peptide and protein binding in the axial channel of Hsp104. Insights into the mechanism of protein unfolding. *J.Biol.Chem.* **283**, 30139-30150

Lum,R, Tkach,JM, Vierling,E, and Glover,JR. (**2004**). Evidence for an unfolding/threading mechanism for protein disaggregation by Saccharomyces cerevisiae Hsp104. *J.Biol.Chem.* **279**, 29139-29146

Maruya,M, Sameshima,M, Nemoto,T, and Yahara,I. (**1999**). Monomer arrangement in HSP90 dimer as determined by decoration with N and C-terminal region specific antibodies. *J.Mol.Biol.* **285**, 903-907

Mathew,A and Morimoto,RI. (**1998**). Role of the heat-shock response in the life and death of proteins. *Ann.N.Y.Acad.Sci.* **851**, 99-111

Matsushima,M, Marquart,M, Jones,TA, Colman,PM, Bartels,K, and Huber,R. (**1978**). Crystal structure of the human Fab fragment Kol and its comparison with the intact Kol molecule. *J.Mol.Biol.* **121**, 441-459

McClellan,AJ, Xia,Y, Deutschbauer,AM, Davis,RW, Gerstein,M, and Frydman,J. (**2007**). Diverse cellular functions of the Hsp90 molecular chaperone uncovered using systems approaches. *Cell* **131**, 121-135

McLaughlin,SH, Smith,HW, and Jackson,SE. (**2002**). Stimulation of the weak ATPase activity of human hsp90 by a client protein. *J.Mol.Biol.* **315**, 787-798

McLaughlin,SH, Ventouras,LA, Lobbezoo,B, and Jackson,SE. (**2004**). Independent ATPase activity of Hsp90 subunits creates a flexible assembly platform. *J.Mol.Biol.* **344**, 813-826

McQuillen,K, Roberts,RB, and Britten,RJ. (**1959**). SYNTHESIS OF NASCENT PROTEIN BY RIBOSOMES IN ESCHERICHIA COLI. *Proc.Natl.Acad.Sci.U.S.A* **45**, 1437-1447

Mesecke,N, Terziyska,N, Kozany,C, Baumann,F, Neupert,W, Hell,K, and Herrmann,JM. (**2005**). A disulfide relay system in the intermembrane space of mitochondria that mediates protein import. *Cell* **121**, 1059-1069

Meyer,P, Prodromou,C, Hu,B, Vaughan,C, Roe,SM, Panaretou,B, Piper,PW, and Pearl,LH. (**2003**). Structural and functional analysis of the middle segment of hsp90: implications for ATP hydrolysis and client protein and cochaperone interactions. *Mol.Cell* **11**, 647-658

Meyer,P, Prodromou,C, Liao,C, Hu,B, Roe,SM, Vaughan,CK, Vlasic,I, Panaretou,B, Piper,PW, and Pearl,LH. (**2004**). Structural basis for recruitment of the ATPase activator Aha1 to the Hsp90 chaperone machinery. *EMBO J.* **23**, 1402-1410

Minami,Y, Kimura,Y, Kawasaki,H, Suzuki,K, and Yahara,I. (**1994**). The carboxy-terminal region of mammalian HSP90 is required for its dimerization and function in vivo. *Mol.Cell Biol.* **14**, 1459-1464

Miyata,Y and Nishida,E. (**2004**). CK2 controls multiple protein kinases by phosphorylating a kinase-targeting molecular chaperone, Cdc37. *Mol.Cell Biol.* **24**, 4065-4074

Mollerup,J and Berchtold,MW. (**2005**). The co-chaperone p23 is degraded by caspases and the proteasome during apoptosis. *FEBS Lett.* **579**, 4187-4192

Morishima,Y, Kanelakis,KC, Silverstein,AM, Dittmar,KD, Estrada,L, and Pratt,WB. (**2000**). The Hsp organizer protein hop enhances the rate of but is not essential for glucocorticoid receptor folding by the multiprotein Hsp90-based chaperone system. *J.Biol.Chem.* **275**, 6894-6900

Muller,L, Schaupp,A, Walerych,D, Wegele,H, and Buchner,J. (**2004**). Hsp90 regulates the activity of wild type p53 under physiological and elevated temperatures. *J.Biol.Chem.* **279**, 48846-48854

Mullis,KB and Faloona,FA. (**1987**). Specific synthesis of DNA in vitro via a polymerase-catalyzed chain reaction. *Methods Enzymol.* **155**, 335-350

Nakai,A, Tanabe,M, Kawazoe,Y, Inazawa,J, Morimoto,RI, and Nagata,K. (**1997**). HSF4, a new member of the human heat shock factor family which lacks properties of a transcriptional activator. *Mol.Cell Biol.* **17**, 469-481

Nathan,DF and Lindquist,S. (**1995**). Mutational analysis of Hsp90 function: interactions with a steroid receptor and a protein kinase. *Mol.Cell Biol.* **15**, 3917-3925

Nathan,DF, Vos,MH, and Lindquist,S. (**1997**). In vivo functions of the Saccharomyces cerevisiae Hsp90 chaperone. *Proc.Natl.Acad.Sci.U.S.A* **94**, 12949-12956

Neckers,L. (**2000**). Effects of geldanamycin and other naturally occurring small molecule antagonists of heat shock protein 90 on HER2 protein expression. *Breast Dis.* **11**, 49-59

Nelson,CJ, Santos-Rosa,H, and Kouzarides,T. (**2006**). Proline isomerization of histone H3 regulates lysine methylation and gene expression. *Cell* **126**, 905-916

Nelson,GM, Prapapanich,V, Carrigan,PE, Roberts,PJ, Riggs,DL, and Smith,DF. (**2004**). The heat shock protein 70 cochaperone hip enhances functional maturation of glucocorticoid receptor. *Mol.Endocrinol.* **18**, 1620-1630

Obermann,WM, Sondermann,H, Russo,AA, Pavletich,NP, and Hartl,FU. (**1998**). In vivo function of Hsp90 is dependent on ATP binding and ATP hydrolysis. *J.Cell Biol.* **143**, 901-910

Oxelmark,E, Knoblauch,R, Arnal,S, Su,LF, Schapira,M, and Garabedian,MJ. (**2003**). Genetic dissection of p23, an Hsp90 cochaperone, reveals a distinct surface involved in estrogen receptor signaling. *J.Biol.Chem.* **278**, 36547-36555

Panaretou,B, Prodromou,C, Roe,SM, O'Brien,R, Ladbury,JE, Piper,PW, and Pearl,LH. (**1998**). ATP binding and hydrolysis are essential to the function of the Hsp90 molecular chaperone in vivo. *EMBO J.* **17**, 4829-4836

Panaretou,B, Siligardi,G, Meyer,P, Maloney,A, Sullivan,JK, Singh,S, Millson,SH, Clarke,PA, Naaby-Hansen,S, Stein,R, Cramer,R, Mollapour,M, Workman,P, Piper,PW, Pearl,LH, and Prodromou,C. (**2002**). Activation of the ATPase activity of hsp90 by the stress-regulated cochaperone aha1. *Mol.Cell* **10**, 1307-1318

Parsell,DA, Kowal,AS, Singer,MA, and Lindquist,S. (**1994**). Protein disaggregation mediated by heat-shock protein Hsp104. *Nature* **372**, 475-478

Parsell,DA and Lindquist,S. (**1994**). *The biology of Heat Shock Proteins and Molecular Chaperones*. 53-84

Patzelt,H, Rudiger,S, Brehmer,D, Kramer,G, Vorderwulbecke,S, Schaffitzel,E, Waitz,A, Hesterkamp,T, Dong,L, Schneider-Mergener,J, Bukau,B, and Deuerling,E. (**2001**). Binding specificity of Escherichia coli trigger factor. *Proc.Natl.Acad.Sci.U.S.A* **98**, 14244-14249

Picard,D. (**2006a**). Chaperoning steroid hormone action. *Trends Endocrinol.Metab* **17**, 229-235

Picard,D. (**2006b**). Intracellular dynamics of the Hsp90 co-chaperone p23 is dictated by Hsp90. *Exp.Cell Res.* **312**, 198-204

Picard,D, Khursheed,B, Garabedian,MJ, Fortin,MG, Lindquist,S, and Yamamoto,KR. (**1990**). Reduced levels of hsp90 compromise steroid receptor action in vivo. *Nature* **348**, 166-168

Picard,D, Suslova,E, and Briand,PA. (**2006**). 2-color photobleaching experiments reveal distinct intracellular dynamics of two components of the Hsp90 complex. *Exp.Cell Res.* **312**, 3949-3958

Pirkl,F and Buchner,J. (**2001**). Functional analysis of the Hsp90-associated human peptidyl prolyl cis/trans isomerases FKBP51, FKBP52 and Cyp40. *J.Mol.Biol.* **308**, 795-806

Pockley,AG. (**2003**). Heat shock proteins as regulators of the immune response. *Lancet* **362**, 469-476

Prapapanich,V, Chen,S, and Smith,DF. (**1998**). Mutation of Hip's carboxy-terminal region inhibits a transitional stage of progesterone receptor assembly. *Mol.Cell Biol.* **18**, 944-952

Pratt,WB, Morishima,Y, Murphy,M, and Harrell,M. (**2006**). Chaperoning of glucocorticoid receptors. *Handb.Exp.Pharmacol.* 111-138

Prodromou,C, Panaretou,B, Chohan,S, Siligardi,G, O'Brien,R, Ladbury,JE, Roe,SM, Piper,PW, and Pearl,LH. (**2000**). The ATPase cycle of Hsp90 drives a molecular

'clamp' via transient dimerization of the N-terminal domains. *EMBO J.* **19**, 4383-4392

Prodromou,C, Roe,SM, O'Brien,R, Ladbury,JE, Piper,PW, and Pearl,LH. (**1997a**). Identification and structural characterization of the ATP/ADP-binding site in the Hsp90 molecular chaperone. *Cell* **90**, 65-75

Prodromou,C, Roe,SM, Piper,PW, and Pearl,LH. (**1997b**). A molecular clamp in the crystal structure of the N-terminal domain of the yeast Hsp90 chaperone. *Nat.Struct.Biol.* **4**, 477-482

Prodromou,C, Siligardi,G, O'Brien,R, Woolfson,DN, Regan,L, Panaretou,B, Ladbury,JE, Piper,PW, and Pearl,LH. (**1999**). Regulation of Hsp90 ATPase activity by tetratricopeptide repeat (TPR)-domain co-chaperones. *EMBO J.* **18**, 754-762

Prusiner,SB. (**1996**). Molecular biology and pathogenesis of prion diseases. *Trends Biochem.Sci.* **21**, 482-487

Rabindran,SK, Giorgi,G, Clos,J, and Wu,C. (**1991**). Molecular cloning and expression of a human heat shock factor, HSF1. *Proc.Natl.Acad.Sci.U.S.A* **88**, 6906-6910

Ramachandran,GN and Sasisekharan,V. (**1968**). Conformation of polypeptides and proteins. *Adv.Protein Chem.* **23**, 283-438

Ranganathan,R, Lu,KP, Hunter,T, and Noel,JP. (**1997**). Structural and Functional Analysis of the Mitotic Rotamase Pin1 Suggests Substrate Recognition Is Phosphorylation Dependent. *Cell* **89**, 875-886

Ratajczak,T and Carrello,A. (**1996**). Cyclophilin 40 (CyP-40), mapping of its hsp90 binding domain and evidence that FKBP52 competes with CyP-40 for hsp90 binding. *J.Biol.Chem.* **271**, 2961-2965

Reddehase,S, Grumbt,B, Neupert,W, and Hell,K. (**2009**). The disulfide relay system of mitochondria is required for the biogenesis of mitochondrial Ccs1 and Sod1. *J.Mol.Biol.* **385**, 331-338

Richter,K, Meinlschmidt,B, and Buchner,J. (**2005**). Hsp90: From dispensable heat shock protein to global player. *Protein Folding Handbook* 768-829

Richter,K, Moser,S, Hagn,F, Friedrich,R, Hainzl,O, Heller,M, Schlee,S, Kessler,H, Reinstein,J, and Buchner,J. (**2006**). Intrinsic inhibition of the Hsp90 ATPase activity. *J.Biol.Chem.* **281**, 11301-11311

Richter,K, Muschler,P, Hainzl,O, and Buchner,J. (**2001**). Coordinated ATP hydrolysis by the Hsp90 dimer. *J.Biol.Chem.* **276**, 33689-33696

Richter,K, Muschler,P, Hainzl,O, Reinstein,J, and Buchner,J. (**2003**). Sti1 is a non-competitive inhibitor of the Hsp90 ATPase. Binding prevents the N-terminal dimerization reaction during the atpase cycle. *J.Biol.Chem.* **278**, 10328-10333

Richter,K, Reinstein,J, and Buchner,J. (**2002**). N-terminal residues regulate the catalytic efficiency of the Hsp90 ATPase cycle. *J.Biol.Chem.* **277**, 44905-44910

Richter,K, Soroka,J, Skalniak,L, Leskovar,A, Hessling,M, Reinstein,J, and Buchner,J. (**2008**). Conserved conformational changes in the ATPase cycle of human Hsp90. *J.Biol.Chem.* **283**, 17757-17765

Richter,K, Walter,S, and Buchner,J. (**2004**). The Co-chaperone Sba1 connects the ATPase reaction of Hsp90 to the progression of the chaperone cycle. *J.Mol.Biol.* **342**, 1403-1413

Rodriguez,F, Arsene-Ploetze,F, Rist,W, Rudiger,S, Schneider-Mergener,J, Mayer,MP, and Bukau,B. (**2008**). Molecular basis for regulation of the heat shock transcription factor sigma32 by the DnaK and DnaJ chaperones. *Mol.Cell* **32**, 347-358

Roe,SM, Ali,MM, Meyer,P, Vaughan,CK, Panaretou,B, Piper,PW, Prodromou,C, and Pearl,LH. (**2004**). The Mechanism of Hsp90 regulation by the protein kinase-specific cochaperone p50(cdc37). *Cell* **116**, 87-98

Rowe J.A. (**2005**). Analytical Ultracentrifugation.

Sambrook,J, Fritsch,EF, and Maniatis,T. (**1989**). Molecular Cloning: A laboratory manual.

Sanchez,Y, Parsell,DA, Taulien,J, Vogel,JL, Craig,EA, and Lindquist,S. (**1993**). Genetic evidence for a functional relationship between Hsp104 and Hsp70. *J.Bacteriol.* **175**, 6484-6491

Santoro,MM and Bolen,DW. (**1988**). Unfolding free energy changes determined by the linear extrapolation method. 1. Unfolding of phenylmethanesulfonyl alpha-chymotrypsin using different denaturants. *Biochemistry* **27**, 8063-8068

Sarge,KD, Murphy,SP, and Morimoto,RI. (**1993**). Activation of heat shock gene transcription by heat shock factor 1 involves oligomerization, acquisition of DNA-binding activity, and nuclear localization and can occur in the absence of stress. *Mol.Cell Biol.* **13**, 1392-1407

Sarge,KD, Park-Sarge,OK, Kirby,JD, Mayo,KE, and Morimoto,RI. (**1994**). Expression of heat shock factor 2 in mouse testis: potential role as a regulator of heat-shock protein gene expression during spermatogenesis. *Biol.Reprod.* **50**, 1334-1343

Sawada,S, Suzuki,G, Kawase,Y, and Takaku,F. (**1987**). Novel immunosuppressive agent, FK506. In vitro effects on the cloned T cell activation. *J.Immunol.* **139**, 1797-1803

Scheufler,C, Brinker,A, Bourenkov,G, Pegoraro,S, Moroder,L, Bartunik,H, Hartl,FU, and Moarefi,I. (**2000**). Structure of TPR domain-peptide complexes: critical elements in the assembly of the Hsp70-Hsp90 multichaperone machine. *Cell* **101**, 199-210

Schmid,FX. (**1998**). Spectral methods of characterizing protein conformation and conformational changes.

Scholz,C, Stoller,G, Zarnt,T, Fischer,G, and Schmid,FX. (**1997**). Cooperation of enzymatic and chaperone functions of trigger factor in the catalysis of protein folding. *EMBO J.* **16**, 54-58

Scroggins,BT, Prince,T, Shao,J, Uma,S, Huang,W, Guo,Y, Yun,BG, Hedman,K, Matts,RL, and Hartson,SD. (**2003**). High affinity binding of Hsp90 is triggered by multiple discrete segments of its kinase clients. *Biochemistry* **42**, 12550-12561

Shao,J, Prince,T, Hartson,SD, and Matts,RL. (**2003**). Phosphorylation of serine 13 is required for the proper function of the Hsp90 co-chaperone, Cdc37. *J.Biol.Chem.* **278**, 38117-38120

Shiau,AK, Harris,SF, Southworth,DR, and Agard,DA. (**2006**). Structural Analysis of E. coli hsp90 reveals dramatic nucleotide-dependent conformational rearrangements. *Cell* **127**, 329-340

Siegert,R, Leroux,MR, Scheufler,C, Hartl,FU, and Moarefi,I. (**2000**). Structure of the molecular chaperone prefoldin: unique interaction of multiple coiled coil tentacles with unfolded proteins. *Cell* **103**, 621-632

Siligardi,G, Hu,B, Panaretou,B, Piper,PW, Pearl,LH, and Prodromou,C. (**2004**). Co-chaperone regulation of conformational switching in the Hsp90 ATPase cycle. *J.Biol.Chem.* **279**, 51989-51998

Siligardi,G, Panaretou,B, Meyer,P, Singh,S, Woolfson,DN, Piper,PW, Pearl,LH, and Prodromou,C. (**2002**). Regulation of Hsp90 ATPase activity by the co-chaperone Cdc37p/p50cdc37. *J.Biol.Chem.* **277**, 20151-20159

Silverstein,AM, Grammatikakis,N, Cochran,BH, Chinkers,M, and Pratt,WB. (**1998**). p50(cdc37) binds directly to the catalytic domain of Raf as well as to a site on hsp90 that is topologically adjacent to the tetratricopeptide repeat binding site. *J.Biol.Chem.* **273**, 20090-20095

Smith,DF. (**1993**). Dynamics of heat shock protein 90-progesterone receptor binding and the disactivation loop model for steroid receptor complexes. *Mol.Endocrinol.* **7**, 1418-1429

Smith,DF, Faber,LE, and Toft,DO. (**1990**). Purification of unactivated progesterone receptor and identification of novel receptor-associated proteins. *J.Biol.Chem.* **265**, 3996-4003

Smith,DF and Toft,DO. (**2008**). Minireview: the intersection of steroid receptors with molecular chaperones: observations and questions. *Mol.Endocrinol.* **22**, 2229-2240

Southworth,DR and Agard,DA. (**2008**). Species-dependent ensembles of conserved conformational states define the Hsp90 chaperone ATPase cycle. *Mol.Cell* **32**, 631-640

Spiess,C, Meyer,AS, Reissmann,S, and Frydman,J. (**2004**). Mechanism of the eukaryotic chaperonin: protein folding in the chamber of secrets. *Trends Cell Biol.* **14**, 598-604

Stepanova,L, Leng,X, Parker,SB, and Harper,JW. (**1996**). Mammalian p50Cdc37 is a protein kinase-targeting subunit of Hsp90 that binds and stabilizes Cdk4. *Genes Dev.* **10**, 1491-1502

Sullivan,WP, Owen,BA, and Toft,DO. (**2002**). The influence of ATP and p23 on the conformation of hsp90. *J.Biol.Chem.* **277**, 45942-45948

Tang,YC, Chang,HC, Chakraborty,K, Hartl,FU, and Hayer-Hartl,M. (**2008**). Essential role of the chaperonin folding compartment in vivo. *EMBO J.* **27**, 1458-1468

Tang,YC, Chang,HC, Roeben,A, Wischnewski,D, Wischnewski,N, Kerner,MJ, Hartl,FU, and Hayer-Hartl,M. (**2006**). Structural features of the GroEL-GroES nano-cage required for rapid folding of encapsulated protein. *Cell* **125**, 903-914

Tesic,M, Marsh,JA, Cullinan,SB, and Gaber,RF. (**2003**). Functional interactions between Hsp90 and the co-chaperones Cns1 and Cpr7 in Saccharomyces cerevisiae. *J.Biol.Chem.* **278**, 32692-32701

Thies,MJ, Mayer,J, Augustine,JG, Frederick,CA, Lilie,H, and Buchner,J. (**1999**). Folding and association of the antibody domain CH3: prolyl isomerization preceeds dimerization. *J.Mol.Biol.* **293**, 67-79

Toogun,OA, Zeiger,W, and Freeman,BC. (**2007**). The p23 molecular chaperone promotes functional telomerase complexes through DNA dissociation. *Proc.Natl.Acad.Sci.U.S.A* **104**, 5765-5770

Truscott,KN, Brandner,K, and Pfanner,N. (**2003**). Mechanisms of protein import into mitochondria. *Curr.Biol.* **13**, R326-R337

Turnbull,EL, Rosser,MF, and Cyr,DM. (**2007**). The role of the UPS in cystic fibrosis. *BMC.Biochem.* **8 Suppl 1**, S11

Vainberg,IE, Lewis,SA, Rommelaere,H, Ampe,C, Vandekerckhove,J, Klein,HL, and Cowan,NJ. (**1998**). Prefoldin, a chaperone that delivers unfolded proteins to cytosolic chaperonin. *Cell* **93**, 863-873

Vaughan,CK, Gohlke,U, Sobott,F, Good,VM, Ali,MM, Prodromou,C, Robinson,CV, Saibil,HR, and Pearl,LH. (**2006**). Structure of an Hsp90-Cdc37-Cdk4 complex. *Mol.Cell* **23**, 697-707

Vendruscolo,M and Dobson,CM. (**2005**). Towards complete descriptions of the free-energy landscapes of proteins. *Philos.Transact.A Math.Phys.Eng Sci.* **363**, 433-450

Wagner,C and Kiefhaber,T. (**1999**). Intermediates can accelerate protein folding. *Proc.Natl.Acad.Sci.U.S.A* **96**, 6716-6721

Walker,GM. (**1998**). Yeast Physiology and Biotechnology.

Walter,P and Blobel,G. (**1982**). Signal recognition particle contains a 7S RNA essential for protein translocation across the endoplasmic reticulum. *Nature* **299**, 691-698

Wandinger,SK, Suhre,MH, Wegele,H, and Buchner,J. (**2006**). The phosphatase Ppt1 is a dedicated regulator of the molecular chaperone Hsp90. *EMBO J.* **25**, 367-376

Wang,X, Venable,J, LaPointe,P, Hutt,DM, Koulov,AV, Coppinger,J, Gurkan,C, Kellner,W, Matteson,J, Plutner,H, Riordan,JR, Kelly,JW, Yates,JR, III, and Balch,WE. (**2006**). Hsp90 cochaperone Aha1 downregulation rescues misfolding of CFTR in cystic fibrosis. *Cell* **127**, 803-815

Ward,BK, Mark,PJ, Ingram,DM, Minchin,RF, and Ratajczak,T. (**1999**). Expression of the estrogen receptor-associated immunophilins, cyclophilin 40 and FKBP52, in breast cancer. *Breast Cancer Res.Treat.* **58**, 267-280

Weaver,AJ, Sullivan,WP, Felts,SJ, Owen,BA, and Toft,DO. (**2000**). Crystal structure and activity of human p23, a heat shock protein 90 co-chaperone. *J.Biol.Chem.* **275**, 23045-23052

Wegele,H, Muschler,P, Bunck,M, Reinstein,J, and Buchner,J. (**2003**). Dissection of the contribution of individual domains to the ATPase mechanism of Hsp90. *J.Biol.Chem.* **278**, 39303-39310

Wegele,H, Wandinger,SK, Schmid,AB, Reinstein,J, and Buchner,J. (**2006**). Substrate transfer from the chaperone Hsp70 to Hsp90. *J.Mol.Biol.* **356**, 802-811

Weikl,T, Abelmann,K, and Buchner,J. (**1999**). An unstructured C-terminal region of the Hsp90 co-chaperone p23 is important for its chaperone function. *J.Mol.Biol.* **293**, 685-691

Weikl,T, Muschler,P, Richter,K, Veit,T, Reinstein,J, and Buchner,J. (**2000**). C-terminal regions of Hsp90 are important for trapping the nucleotide during the ATPase cycle. *J.Mol.Biol.* **303**, 583-592

Whitesell,L and Lindquist,SL. (**2005**). HSP90 and the chaperoning of cancer. *Nat.Rev.Cancer* **5**, 761-772

Whitesell,L, Mimnaugh,EG, De Costa,B, Myers,CE, and Neckers,LM. (**1994**). Inhibition of heat shock protein HSP90-pp60v-src heteroprotein complex formation by benzoquinone ansamycins: essential role for stress proteins in oncogenic transformation. *Proc.Natl.Acad.Sci.U.S.A* **91**, 8324-8328

Wiech,H, Buchner,J, Zimmermann,R, and Jakob,U. (**1992**). Hsp90 chaperones protein folding in vitro. *Nature* **358**, 169-170

Winter,J, Klappa,P, Freedman,RB, Lilie,H, and Rudolph,R. (**2002**). Catalytic activity and chaperone function of human protein-disulfide isomerase are required for the efficient refolding of proinsulin. *J.Biol.Chem.* **277**, 310-317

Young,JC, Hoogenraad,NJ, and Hartl,FU. (**2003**). Molecular chaperones Hsp90 and Hsp70 deliver preproteins to the mitochondrial import receptor Tom70. *Cell* **112**, 41-50

Yura,T. (**1996**). Regulation and conservation of the heat-shock transcription factor sigma32. *Genes Cells* **1**, 277-284

Zhang,M, Windheim,M, Roe,SM, Peggie,M, Cohen,P, Prodromou,C, and Pearl,LH. (**2005**). Chaperoned ubiquitylation--crystal structures of the CHIP U box E3 ubiquitin ligase and a CHIP-Ubc13-Uev1a complex. *Mol.Cell* **20**, 525-538

Zhao,Q, Boschelli,F, Caplan,AJ, and Arndt,KT. (**2004**). Identification of a conserved sequence motif that promotes Cdc37 and cyclin D1 binding to Cdk4. *J.Biol.Chem.* **279**, 12560-12564

Zhao,R, Davey,M, Hsu,YC, Kaplanek,P, Tong,A, Parsons,AB, Krogan,N, Cagney,G, Mai,D, Greenblatt,J, Boone,C, Emili,A, and Houry,WA. (**2005**). Navigating the chaperone network: an integrative map of physical and genetic interactions mediated by the hsp90 chaperone. *Cell* **120**, 715-727

Zou,J, Guo,Y, Guettouche,T, Smith,DF, and Voellmy,R. (**1998a**). Repression of heat shock transcription factor HSF1 activation by HSP90 (HSP90 complex) that forms a stress-sensitive complex with HSF1. *Cell* **94**, 471-480

Zou,J, Salminen,WF, Roberts,SM, and Voellmy,R. (**1998b**). Correlation between glutathione oxidation and trimerization of heat shock factor 1, an early step in stress induction of the Hsp response. *Cell Stress.Chaperones.* **3**, 130-141

6 Acknowledgements

At first I would like to thank Johannes Buchner for letting me work on this very interesting topic and for his confidence. I thank Klaus Richter for fruitful collaborations and discussions till deep night that briefed me at the time. I thank Susanne Hilber for her support, her organising skills and here memorable hospitality. And I thank my friends and colleagues in our group for encouragement and the nice and stimulating working atmosphere. And I would like to thank my family, my girlfriend and especially my parents for their trust in me.

7 Declaration

Hiermit erkläre ich, Martin Heßling, dass ich die vorliegende Arbeit selbständig verfasst und keine anderen als die angegebenen Quellen und Hilfsmittel verwendet habe. Die Arbeit wurde bisher keiner Prüfungskommission vorgelegt. Teile dieser Arbeit wurde in wissenschaftlichen Journalen veröffentlicht.

_____

Martin J. Heßling

München, 26. Januar 2009